

Novel beam-based correction and stabilisation methods for particle accelerators

Lukáš Malina

24th October 2018

Thesis submitted for the degree of Philosophiæ Doctor



© Lukáš Malina, 2018

*Series of dissertations submitted to the
Faculty of Mathematics and Natural Sciences, University of Oslo
No. 2041*

ISSN 1501-7710

All rights reserved. No part of this publication may be
reproduced or transmitted, in any form or by any means, without permission.

Cover: Hanne Baadsgaard Utigard.
Print production: Reprosentralen, University of Oslo.

"Everything should be made as simple as possible, but not simpler."

Albert Einstein

Abstract

Precise control of beam optics and beam stability is of critical importance for machine protection and performance of today's high-energy particle accelerators. For the next generation of accelerators, the tolerances are even tighter. This thesis presents new methods and improved techniques to efficiently identify, measure and correct a range of errors in particle accelerators. Circular and linear accelerators have been studied in parallel. The Circular Large Hadron Collider (LHC) collides mostly protons at energies of 6.5 TeV and European Synchrotron Radiation Facility (ESRF) storage ring accelerates electrons to produce synchrotron light. The Compact Linear Collider (CLIC) will provide electron-positron collisions at centre of mass energies up to 3 TeV. In CLIC, a non-colliding beam, referred to as drive beam, generates RF power to accelerate the main beam.

LHC's optics measurement scheme was improved, also by studying ESRF. This resulted in significantly improved β -function measurement, achieving twice the best-documented precision so far. The optics correction algorithm was improved allowing β -beating in the LHC to systematically reach a level below 1.8% rms. An adiabatic simultaneous 3-dimensional beam excitation, which combines AC-dipoles with RF-frequency modulation, significantly sped up beam optics measurements. The analysis of beam frequency spectra from turn-by-turn data was also made significantly faster, in the LHC by a factor ~ 300 . These results contributed to LHC's excellent performance beyond its designed targets. They also contributed towards its upgrade the High Luminosity LHC.

CLIC has stringent requirements on drive beam stability in terms of beam current, energy and phase. In the CLIC Test Facility 3 (CTF3), a novel algorithm to identify drifts and correlations was developed and applied in a study of drive beam stabilisation. The underlying causes of drifts were found and multiple beam-based feedbacks were developed and commissioned in CTF3, in this way achieving the stability goals. These improvements therefore played a key role in demonstrating the viability of CLIC in terms of drive beam stability.

Contents

Contents	v
Preface	ix
Acknowledgements	xi
Acronyms and Abbreviations	xiii
List of Figures	xv
List of Tables	xvii
1 Introduction	1
2 Beam dynamics	5
2.1 Transverse dynamics	6
2.2 Longitudinal dynamics	9
2.3 Chromatic effects	10
3 Beam measurements	11
3.1 Beam instrumentation	11
3.1.1 Beam position monitors	11
3.1.2 Additional instrumentation	12
3.2 Algebraic and Statistical methods	13
3.2.1 Response Matrix	13
3.2.2 Singular Value Decomposition	13
3.2.3 Iterative Filtering	14
3.3 Static optics measurements	14
3.3.1 Quadrupole scan	15

3.3.2	K-modulation	15
3.3.3	Closest tune approach	16
3.3.4	Orbit response matrix	16
3.3.5	Comparison of static methods	16
3.4	Turn-by-Turn optics measurements with excited beam	16
3.4.1	Excitation	17
3.4.2	Harmonic analysis	19
3.4.3	Measured properties	21
4	Beam correction methods	27
4.1	Local orbit bumps	27
4.2	Global orbit	28
4.3	Local optics	28
4.4	Global optics	29
5	LHC Beam-based Model	33
5.1	Beam-based matching - correcting the model	33
5.1.1	Model orbit matching	34
5.1.2	Model optics matching	34
5.1.3	Orbit and optics matching interleaved	34
5.2	Degeneracy of the model	34
6	Beam stabilisation - continuous correction	37
6.1	Statistical analysis of correlations	37
6.2	Stabilisation concepts	38
6.3	CTF3 drive beam stabilisation	38
7	Summary and outlook	41
7.1	Consequences for HL-LHC	45
7.2	Consequences for CLIC	45
	Bibliography	47

Scientific Publications	I
Paper I: Recent improvements of drive beam stability in CTF3	II
Paper II: Review of LHC on-line model implementation and of its ap- plications	VI
Paper III: LHC optics commissioning: A journey towards 1% optics control	XI
Paper IV: Improving the precision of linear optics measurements based on turn-by-turn beam position monitor data after a pulsed excita- tion in lepton storage rings	XXI
Paper V: Drive beam stabilisation in the CLIC Test Facility 3	XXX
Paper VI: Optics measurements in storage rings based on simultaneous 3-dimensional beam excitation	XXXIX
Paper VII: Performance optimization of turn-by-turn beam position mon- itor data harmonic analysis	XLIV

Preface

This thesis is submitted for the degree of Philosophiæ Doctor at the Department of Physics, Faculty of Mathematics and Natural Sciences, University of Oslo, Norway. It has been funded by CERN Doctoral Student Programme. The thesis is written around seven scientific publications, listed below and appended at the end of this thesis.

1. L. Malina, R. Corsini, D. Gamba, T. Persson and P. Skowroński, “Recent improvements of drive beam stability in CTF3”, in *Proceedings of IPAC’16, Busan, Korea, May 2016*, paper WEPOR007, (2016). [1]
2. T. Persson, J. Coello de Portugal, M. Fjellstrom, L. Malina, G. Roy, P. Skowroński, A. Szczotka and J. Moeskops, “Review of LHC on-line model implementation and of its applications”, in *Proceedings of IPAC’16, Busan, Korea, May 2016*, paper TUPMW030, (2016). [2]
3. T. Persson, F. Carlier, J. Coello de Portugal, A. Garcia-Tabares Valdivieso, A. Langner, E. H. Maclean, L. Malina, P. Skowroński, B. Salvant, R. Tomás and A. C. Garcia Bonilla, “LHC optics commissioning: A journey towards 1% optics control”, *Phys. Rev. Accel. Beams* **20**, 061002 (2017). [3]
4. L. Malina, J. Coello de Portugal, T. Persson, P. K. Skowroński, R. Tomás, A. Franchi and S. M. Liuzzo, “Improving the precision of linear optics measurements based on turn-by-turn beam position monitor data after a pulsed excitation in lepton storage rings”, *Phys. Rev. Accel. Beams* **20**, 082802 (2017). [4]
5. L. Malina, R. Corsini, T. Persson, P. Skowroński and E. Adli, “Drive beam stabilisation in the CLIC Test Facility 3”, *Nucl. Instrum. Methods Phys. Res. A* **894**, 25-32 (2018). [5]

6. L. Malina and J. Coello de Portugal, “Optics measurements in storage rings based on simultaneous 3-dimensional beam excitation”, presented at *IPAC’18, Vancouver, Canada, May 2018*, paper THPAF046, (2018). [6]
7. L. Malina, J. Coello de Portugal, J. Dilly, P.K. Skowroński, R. Tomás and M. Toplis, “Performance optimization of turn-by-turn beam position monitor data harmonic analysis”, presented at *IPAC’18, Vancouver, Canada, May 2018*, paper THPAF045, (2018). [7]

Acknowledgements

Now it comes to probably the hardest part to write, the acknowledgements. Pursuing the PhD takes a significant portion of the time. I have spent this time in a truly cosmopolitan environment at CERN among people who played various roles in my PhD. I have enjoyed the time and learned a lot from them, not only about physics. Unfortunately, I cannot mention everyone explicitly here. I am sure most of you will identify yourselves with shorter text and some more trees left in the mountains.

I would like to express my gratitude to Piotr Skowroński, who offered me to work in the field of particle accelerators. Without him, his pragmatism and guidance, this PhD would have never happened. You have always found time for very fruitful discussions and have had lots of patience, for example, when reading my early paper drafts. The PhD would not even get to the starting line also without my university supervisor Erik Adli and CTF3 team leader Roberto Corsini. I would like to thank Erik for help with organisation of studies and especially with the thesis preparation, during which I often wondered how can you stay so positive. I thank Roberto for help before the start of my PhD and for sharing his immense experience.

I found myself very lucky to work in two great teams, CTF3 and OMC. In CTF3, many different people share the same passion and creativity to run a slightly overlooked test facility. I should mention Tobias Persson and Davide Gamba, who are a couple of years ahead of me in their careers and thankfully still remember solutions of common difficulties. In OMC "owls", who are constantly determined, when commissioning LHC's optics during countless night shifts in CCC. Thank you all for the time spent and discussions in either of control rooms or over coffee. I owe a big thank you to Rogelio Tomás for many discussions and maybe more importantly for his contagious enthusiasm. I would like to thank Jaime Coello de Portugal for great cooperation on our secret projects. I got the opportunity to perform optics measurements in ESRF. I thank Andrea Franchi for his support and

vital comments during the study. Special thanks go to Ewen Maclean, who has over a time carefully proofread my papers and also this thesis.

As life is not only about work, I would like to thank Hanka, who was brave enough to move here with me, supports me throughout this wonderful journey and survived our "a little" adventurous vacations. I would like to thank Javier Barranco, Ana García-Tabarés Valdivieso and Sergey Antipov for making our office indeed the funniest office in the building. Last but not least, I thank all my friends for a great time together.

Acronyms and Abbreviations

ALICE	A Large Ion Collider Experiment
ATLAS	A Toroidal LHC ApparatuS
BBQ	Base Band Tune
BLM	Beam Loss Monitor
BPM	Beam Position Monitor
BPR	Beam Phase Reference
BSRT	Synchrotron Light Monitor
CERN	European Organization for Nuclear Research (originaly Conseil Européen pour la Recherche Nucléaire)
CLIC	Compact Linear Collider
CMS	Compact Muon Solenoid
CTF3	CLIC Test Facility 3
DFS	Dispersion-Free Steering
DOROS	Diode ORbit and Oscillation System
ESRF	European Synchrotron Radiation Facility
HL-LHC	High Luminosity - Large Hadron Collider
IP	Interaction Point
IR	Interaction Region
LEIR	Low Energy Ion Ring
LHC	Large Hadron Collider

LHCb	Large Hadron Collider beauty
Linac	Linear Accelerator
MAD-X	Methodical Accelerator Design
ORM	Orbit Response Matrix
OTM	One Turn Map
PFF	Phase Feed-Forward
RDT	Resonance Driving Term
RF	Radio Frequency
SbS	Segment-by-Segment
SVD	Singular Value Decomposition
TbT	Turn-by-Turn

List of Figures

2.1	Frenet-Serret coordinate system.	6
3.1	The conceptual layout and nomenclature for the parameters close to the IP. The red line represents the β -function, β^* is at the location of IP. The figure is taken from [54].	15
3.2	Sample TbT BPM data of a beam excited by a kicker performing the free coherent betatron oscillation.	18
3.3	Sample TbT BPM data of a beam excited by an AC-dipole performing the driven coherent betatron oscillations (Paper VI). Note the ramp-up and the ramp-down of the oscillation amplitude, which is important to avoid emittance growth [69] (in hadron machines).	19
3.4	Sample TbT data at a dispersive BPM of a beam excited by an AC-dipole when the frequency of RF system has been simultaneously modulated. The beam performs driven coherent betatron oscillations and the beam energy is adiabatically varied (Paper VI).	21
3.5	Sketch of TbT data recomposition for noise floor removal. The decomposition of raw TbT data (in blue) gives full matrices, which are then reduced (in brown edges), as only largest singular values are kept for the recomposition of cleaned TbT data . The figure is taken from Paper VII.	22
3.6	Notation using beam related harmonics H,V(multiples of $Q_x, Q_y, (Q_s)$) is illustrated on horizontal (H) frequency spectrum from TbT BPM data in ESRF storage ring.	23
3.7	Artificial β -beating in the LHC caused by different choice of starting turn (moved by single turns) of a batch of TbT data analysed: before the phase correction - (top), after the phase correction (bottom) - showing significantly lower artificial β -beating.	24

3.8	Envelope of a beam centroid oscillation amplitude (black) after a pulsed excitation by a kicker as a function turn number. The coloured areas represent the dominating bias to linear optics measurements either lattice non-linearities (in red) or noise (in blue). Ideally, the oscillation amplitude is in the white band right after the excitation and stays for a maximal number of turns.	25
4.1	Example of difference of phase advance from propagated measurement using SbS method, before and after local optics correction.	29
4.2	Comparison of β -beating measured in the LHC beam 1 with β^* of 40 cm after global correction in 2015 and in 2016 (Paper III). . . .	31
6.1	Sketch of correlation analysis procedure from Paper V: In the top plot, a time evolution of a beam current signal is shown. In the middle plot, signal's sample correlation coefficients with time over a sliding time window of two different lengths, 200 pulses (black) and 1000 pulses (red), is shown including confidence interval bands. In the bottom plot, the respective $R^2_{non-zero}$ is shown for a given confidence level of the two sets of correlation coefficients.	40
7.1	Applicability overview of methods (in grey rectangles) developed or studied within this work in different accelerator types (coloured ellipses).	44

List of Tables

3.1	Static optics measurement techniques. The meaning of acronyms and symbols follows. C: Calibration or tilt; M: Model; $\bar{\beta}$: Average beta function over a quadrupole; ΔQ_{min} : closest tune approach. . .	17
3.2	Comparison of beam excitation methods: pulsed using a kicker or driven using an AC-Dipole	20
3.3	Overview of TbT-based measurement techniques, most taken from [90]. The meaning of acronyms and symbols follows. C: Calibration or tilt; M: Model.	25
4.1	Global corrections in the LHC using linear response matrix	30
4.2	Rms β -beating and normalised dispersion beating in 2015 and 2016 with the β^* of 40 cm at the two main experiments (ATLAS and CMS), from Paper III.	31

Chapter 1

Introduction

Particle accelerators are being increasingly utilised in a variety of applications. They provide an efficient and often the only method for precise measurements across many scientific fields. This may range from non-destructive imaging helping to understand the palaeolithic human ancestor [8] to particle colliders producing previously unobserved particle species. In 1983 the W -boson was observed [9, 10], followed by observation of the Z -boson [11, 12] at $S\bar{p}\bar{p}S$ collider. In 1995 the top quark was observed [13, 14] at the Tevatron collider. The last missing piece of the Standard Model [15–17], the Higgs Boson was observed in 2012 [18, 19] at Large Hadron Collider (LHC), which is currently operational. More recently, "pentaquarks" were observed [20, 21]. Results obtained by observing the collisions in the LHC will guide the decisions regarding the choice of the next large-scale accelerator project. The possible physics program includes precision measurements of the Higgs boson and top quark properties (mass, spin, width, couplings to other particles, ...), and searches for dark matter [22], supersymmetric particles [23] or hidden dimensions [24].

The three main properties of a future collider are the particle type that it collides, the beam energy and its luminosity. Typically, hadron (composite particle) colliders are well suited for potential new discoveries, as a broader energy range is probed simultaneously in collisions of partons. On the other hand, the elementary (to our current knowledge) leptons are better suited for precise measurements. Charged particles emit synchrotron radiation when being bent (i.e. in a circular accelerator). The associated energy loss is proportional to $(\beta\gamma)^4$ (relativistic factors). A linear electron (-positron) collider is therefore more power efficient compared to similarly sized circular collider, above certain beam energy (hundreds of GeV). The choice of the main properties listed above defines operational

challenges of the collider. In particular, all phenomena to be studied are very rare, hence a large number of collisions are required to study them. This drives the requirements on integrated luminosity (the ratio between the number of a given particle interaction and its cross-section).

For the next generation of high-energy particle colliders being studied, precise control of the beam optics and beam stability is crucial in order to reach the performance required in terms of integrated luminosity. The luminosity rapidly degrades with any deviation from nominal parameters. Even minimal beam losses, for example due to too large beam size or missteering, may lead to severe machine damage. Therefore, novel techniques for sufficient beam control have to be conceived, studied and tested in order to assure safety and performance of these machines. The European Organization for Nuclear Research (originally Conseil Européen pour la Recherche Nucléaire, CERN) is currently studying several options for the next generation of particle colliders, including the Compact Linear Collider (CLIC) [25] and an upgrade to the already operational LHC [26]: called High Luminosity (HL) - LHC.

The LHC is a 27 km long superconducting circular collider that provides proton-proton¹ collisions for four main experiments ATLAS [27], CMS [28], ALICE [29] and LHCb [30]. Two counter-rotating proton beams are injected into the LHC with an energy of 450 GeV. They are then accelerated to 6.5 TeV. The optics parameters are also modified to squeeze the beams transversely in Interaction Points (IPs) before the beams are brought into collision. Colliding beams stay for tens of hours with slowly decreasing intensity until they are dumped. At this point, magnetic fields are ramped down and all settings reset. The amount of collisions is the key figure to optimise even during a single "fill". The optimisation techniques [31] rely on precise beam optics control.

In addition to work performed at the LHC, part of the optics studies reported in this thesis were conducted in European Synchrotron Radiation Facility (ESRF). The ESRF storage ring is a synchrotron-light source: a circular accelerator storing an electron beam in order to produce synchrotron light.

CLIC, a linear collider using normal conducting accelerating cavities, is one of the main candidates to be the next large-scale accelerator facility. It will collide electrons with positrons at centre of mass energies up to 3 TeV in a single IP, with bunch trains arriving 50 times per second. A rich particle physics programme is foreseen [32] during operation of CLIC, which will be constructed in three stages. In CLIC, a two-beam acceleration scheme is utilised. A non-colliding

¹also ion-ion and proton-ion

beam, referred to as the drive beam, generates Radio Frequency (RF) power to accelerate the main colliding beam with a gradient of 100 MV/m. At CERN, the CLIC Test Facility 3 (CTF3), described in Paper V and [33], was built to demonstrate the feasibility of CLIC two-beam acceleration scheme, CLIC specific technology and overall function of drive beam complex. This includes fulfilling stringent requirements on drive beam stability in terms of beam current, energy and phase.

The aim of this PhD study is to develop and experimentally verify tools that improve further the quality of the beams at the CTF3 and the LHC. First, possible improvements to the measurements of the beam optics parameters [34, 35] of all kind are considered (phase advance, β -function, dispersion, coupling and chromatic coupling). Second, correction algorithms are studied and implemented in the suitable manner as operational tools in the control system. Analysis applications and improved models are developed to support the machine setup, as well as the reproducibility and stability of the beams. A study performed in the ESRF storage ring, a machine with highly non-linear optics and equipped with precise Beam Position Monitors (BPMs), was a fruitful addition to this work. By studying both circular (LHC and ESRF) and linear (CLIC and CTF3) accelerators in parallel, the various operational challenges of both types of machine are treated, itself an important factor when determining the feasibility of a next-generation particle collider.

Chapter 2 gives a brief overview of beam dynamics, defining the terms used later in this work. The starting point of every correction is a measurement, and Chapter 3 introduces the beam instrumentation and diagnostics used along with the applied algebraic and statistical methods. A review of optics measurement techniques is presented. Most of the "static" methods are applicable to both linear and circular accelerators. A significant part of the development was targeted towards methods utilising Turn-by-Turn (TbT) BPM data of a beam coherently oscillating around the closed orbit. Beam corrections, both local and global, used to correct the measured orbit or optics, are treated in Chapter 4. In chapter 5, the beam corrections are applied in "reverse order" in order to create an accelerator model a more realistic image of the real accelerator. This way, more accurate models are provided. Chapter 6 describes the full work-flow of beam stabilisation. It starts with the identification of correlations among signals. Various stabilisation concepts are discussed and applied in the stabilisation of the CTF3 drive beam, which is described together with its implications for CLIC.

Chapter 2

Beam dynamics

In this chapter, a brief overview of beam dynamics is presented, mainly for the definition of the terms used later in this work. A more thorough beam dynamics description can be found, for example, in [36].

The particle interaction rate when two beams collide is defined as:

$$R = \mathcal{L}\sigma_{int} \quad (2.1)$$

where σ_{int} is the cross-section of a given particle interaction and \mathcal{L} is luminosity. Luminosity is a property of the beam and the main controllable parameter for a given type and energy of colliding particles. The luminosity of a collider having two beams with the same transverse beam sizes σ_x, σ_y and number of particles in a bunch n_p colliding head on is:

$$\mathcal{L} = f_r \frac{n_p^2 n_b}{4\pi\sigma_x\sigma_y} \mathcal{H}, \quad (2.2)$$

where f_r is the revolution frequency in circular colliders or the repetition frequency of bunch trains in linear colliders, n_b is number of colliding bunches and \mathcal{H} is a geometric factor. Collisions typically occur at a symmetry point, where beam sizes are minimised, in order to maximise the luminosity.

In accelerator beam dynamics, a Frenet-Serret coordinate system is employed with the ideal orbit as a reference. A particle accelerator's orbit is generally not straight. Horizontal resp. vertical position in the transverse plane is noted x resp. y , as shown in Figure 2.1. Longitudinal position along the lattice is noted s .

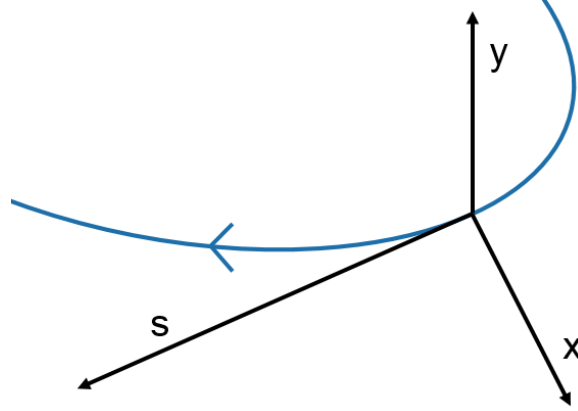


Figure 2.1: Frenet-Serret coordinate system.

2.1 Transverse dynamics

A position-angle phase space is utilised (x, x') . Distribution of particles in a Gaussian beam is described by a covariance matrix (matrix of second order moments), that is parametrised in beam dynamics as:

$$\begin{bmatrix} \langle x^2 \rangle & \langle xx' \rangle \\ \langle xx' \rangle & \langle x'^2 \rangle \end{bmatrix} = \epsilon_{rms} \begin{bmatrix} \beta(s) & -\alpha(s) \\ -\alpha(s) & \gamma(s) \end{bmatrix}, \quad (2.3)$$

where ϵ_{rms} is a rms beam emittance and α , β and γ are Twiss parameters. A similar relation is defined in the vertical plane. Emittance is an area of the phase space, usually corresponding to 1σ of the distribution. Transverse beam size is defined as $\sigma_x = \sqrt{\langle x^2 \rangle} = \sqrt{\epsilon_{rms}\beta}$.

With only linear forces $K(s)$, a particle's equation of motion takes form of Hill's equation [37]

$$x''(s) + K(s)x(s) = 0 \quad (2.4)$$

with following solution:

$$x(s) = C_1 \sqrt{\beta(s)} \cos(\phi(s) - \phi_0) + C_2 \sqrt{\beta(s)} \sin(\phi(s) - \phi_0) \quad (2.5)$$

$$x'(s) = C_1 \left(\frac{1}{2\sqrt{\beta(s)}} \beta'(s) \cos(\phi(s) - \phi_0) - \frac{\sin(\phi(s) - \phi_0)}{\sqrt{\beta(s)}} \right) \quad (2.6)$$

$$+ C_2 \left(\frac{1}{2\sqrt{\beta(s)}} \beta'(s) \sin(\phi(s) - \phi_0) + \frac{\cos(\phi(s) - \phi_0)}{\sqrt{\beta(s)}} \right), \quad (2.7)$$

where

$$\phi(s) = \int_0^s \frac{dt}{\beta(s)}. \quad (2.8)$$

Constants C_1 and C_2 can be found from initial conditions at $s = 0$ m.

Here $\gamma x^2 + 2\alpha x x' + \beta x'^2$, called action $2J$, is an integral of motion and is conserved. A transport matrix transforms the initial state phase space at location i to the final state at the location f . For (x, x') phase space it is:

$$\begin{bmatrix} x \\ x' \end{bmatrix}_f = \begin{bmatrix} R_{11} & R_{12} \\ R_{21} & R_{22} \end{bmatrix}_{fi} \begin{bmatrix} x \\ x' \end{bmatrix}_i, \quad (2.9)$$

where the Matrix \mathbf{R}_{fi} can be expressed using Eq. (2.7) in terms of optical functions at the initial and the final locations:

$$\mathbf{R}_{fi} = \begin{bmatrix} \sqrt{\frac{\beta_f}{\beta_i}} (\cos \phi_{fi} + \alpha_i \sin \phi_{fi}) & \sqrt{\beta_f \beta_i} \sin \phi_{fi} \\ \frac{\alpha_i - \alpha_f}{\sqrt{\beta_f \beta_i}} \cos \phi_{fi} - \frac{1 + \alpha_f \alpha_i}{\sqrt{\beta_f \beta_i}} \sin \phi_{fi} & \sqrt{\frac{\beta_i}{\beta_f}} (\cos \phi_{fi} - \alpha_f \sin \phi_{fi}) \end{bmatrix}, \quad (2.10)$$

where ϕ_{fi} is the phase advance between the initial and the final location. The solution of Hill's equation depends on initial conditions, therefore parameters of a beam at given location are functions of the initial Twiss parameters.

In circular accelerators, $K(s)$ is periodic by definition. If a solution of Hill's equation exists, then it is unique and periodic. If the initial and the final locations are equal, the optical functions are also equal and a One Turn Map (OTM) \mathbf{R}_{OTM} can be defined as follows:

$$\mathbf{R}_{OTM} = \begin{bmatrix} \cos \phi + \alpha \sin \phi & \beta \sin \phi \\ -\frac{1 + \alpha^2}{\beta} \sin \phi & \cos \phi - \alpha \sin \phi \end{bmatrix}, \quad (2.11)$$

where ϕ is phase advance over one turn and the Twiss parameters are functions of longitudinal location s around the ring¹. In circular accelerators, a phase advance over one turn divided by 2π is called betatron tune:

$$Q = \frac{1}{2\pi} \oint \frac{ds}{\beta(s)} \quad (2.12)$$

For description of the general non-linear case, magnetic forces are described

¹This is important for beam injection into periodic accelerators. The optical functions of injected beam needs to be "matched" to optical functions of periodic lattice at injection location, otherwise emittance will increase.

by the multipole expansion of transverse magnetic field noted as:

$$B_y + iB_x = \sum_n (b_n + ia_n) (x + iy)^{n-1}, \quad (2.13)$$

where a_n and b_n are skew and normal magnetic multipole components of order $n \in \{1, 2, \dots\}$. For an off-axis orbit x , resp. y , is replaced by $x - x_0$, resp. $y - y_0$. Consequently, the beam experiences lower order magnetic fields, as functions of offsets x_0 or y_0 , termed "feed-down".

In modern beam dynamics the equations of motion are derived using Hamilton equations [38, 39]. A Hamiltonian describing particle's motion including higher order terms is as follows:

$$H = \frac{p_x^2}{2} + \frac{p_y^2}{2} + \frac{K(s)x^2}{2} + \frac{K(s)y^2}{2} + H_p, \quad (2.14)$$

where $p_{x,y}$ is transverse momentum and H_p is contribution due to higher order magnetic fields

$$H_p = \sum_{n>2} \text{Re} \left[(b_n + ia_n) \frac{(x + iy)^n}{n!} \right]. \quad (2.15)$$

Using the following solution of unperturbed motion

$$x, y = \sqrt{2J_{x,y}\beta_{x,y}} \cos(\phi_{x,y} - \phi_{x0,y0}) \quad (2.16)$$

the Hamiltonian can be expanded

$$H_p = \sum_{j+k+l+m>2} h_{jklm} (2J_x)^{\frac{j+k}{2}} (2J_y)^{\frac{l+m}{2}} e^{i[(j-k)(\phi_x - \phi_{x0}) + (l-m)(\phi_y - \phi_{y0})]}. \quad (2.17)$$

Hamiltonian coefficients h_{jklm} are proportional to multipole strengths along the ring. The j, k, l and m coefficients correspond to powers of action in the horizontal and vertical plane, respectively. For detailed derivation of h_{jklm} coefficients, see for example [39]. Observable Resonance Driving Terms (RDTs) f_{jklm} , in this work used in coupling measurements, relate to coefficients h_{jklm} as follows:

$$f_{jklm} = \frac{h_{jklm}}{1 - e^{2\pi i[(j-k)Q_x + (l-m)Q_y]}} \quad (2.18)$$

Higher order terms perturb the linear behaviour described above. Any imperfec-

tion leads to a resonant behaviour, when

$$(j - k)Q_x + (l - m)Q_y = p \quad j, k, l, m, p \in \mathbb{Z}, \quad (2.19)$$

because any perturbation adds up constructively turn by turn. Cumulative deviation from the ideal orbit leads to beam losses. Except for special cases (such as where this behaviour is used for extraction [40]) rational tunes with small denominator are to be avoided. RDTs contribute to specific frequencies in the beam frequency spectrum:

$H(1 - j + k, m - l)$, when $j \neq 0$, and $V(k - j, 1 - l + m)$, when $l \neq 0$, where H and V stand for horizontal and vertical spectra. In parentheses multiplicative factors of fractional horizontal and vertical tunes are shown, defining the resonant frequency.

The transverse coupling resonance, where $Q_x + Q_y = p$ resp. $Q_x - Q_y = p$, is usually named the sum resonance resp. the difference resonance. Amplitude of betatron coupling represented by the difference and sum resonance driving terms is as follows [38]:

$$|f_{1001}| = \frac{1}{2} \sqrt{\frac{H(0, 1)V(1, 0)}{H(1, 0)V(0, 1)}}, \quad |f_{1010}| = \frac{1}{2} \sqrt{\frac{H(0, -1)V(-1, 0)}{H(1, 0)V(0, 1)}}. \quad (2.20)$$

2.2 Longitudinal dynamics

There are two main operations performed on a beam longitudinally: acceleration and bunching. Particles are accelerated to high energies using alternating voltage. In order to accelerate only in phase with alternating voltage, the beam is bunched. Bunching is performed by velocity modulation at low energy. Low energy longitudinal dynamics is not treated in this work because it deals with ultra-relativistic particle beams. A voltage "seen" by a particle depends on its time of arrival. In a stable condition, this leads to a periodic longitudinal motion around the centre of a bunch, called synchrotron motion. Synchrotron tune Q_s is defined similarly to betatron tune - as number of oscillations per turn. Typically, Q_s ranges from 0.0001 to 0.01, which compares to betatron tunes from 2 to 100.

2.3 Chromatic effects

This section summarises coupling between longitudinal and transverse planes. Particles with different momenta are bent differently, therefore particle position depends on its energy. This is described by horizontal dispersion, which relates beam horizontal position and momentum:

$$D_x = \frac{\Delta x}{\Delta p}, \quad (2.21)$$

where Δp is the relative deviation from the beam reference momentum. Vertical dispersion is defined similarly. Normalised dispersion $D_x/\sqrt{\beta_x}$ [41] is often used instead because it provides measurements which are independent of BPM calibration. Energy deviations of particles also change focusing. Dependence of betatron tune on beam momentum is called chromaticity:

$$Q' = \frac{\Delta Q}{\Delta p}, \quad (2.22)$$

The Chromatic W-function [42] describes how the β -function depends on momentum:

$$W = \frac{1}{2} \cdot \sqrt{\left(\frac{\Delta\beta}{\beta \cdot \Delta p}\right)^2 + \left(\frac{\Delta\alpha}{\Delta p} - \frac{\alpha \cdot \Delta\beta}{\beta \cdot \Delta p}\right)^2}, \quad (2.23)$$

where α, β are the Twiss parameters.

Chromatic coupling denotes the change to sum and/or difference linear coupling resonances (f_{1010}, f_{1001}) with relative beam momentum.

$$\chi_{1001,1010} = \frac{\Delta f_{1001,1010}}{\Delta p}. \quad (2.24)$$

If energy deviates from the reference, e.g. due to energy spread, the W-function introduces β -beating and chromatic coupling introduces transverse coupling.

Chapter 3

Beam measurements

Naturally, the starting point of every correction is a measurement. This chapter briefly introduces beam instrumentation and basic measurements such as beam current, position or phase. Later, the applied algebraic and statistical methods are described. Static optics measurements, where the beam stays on the closed orbit, are then introduced. Finally, measurements where the beam coherently oscillates around the closed orbit are described.

3.1 Beam instrumentation

This section presents a brief overview of beam instrumentation and basic diagnostics, mainly defining the terms used later in this work.

3.1.1 Beam position monitors

BPMs measure beam current (intensity) and position. This can be measured directly, for example, as a sum and a relative difference of signals on electrode pairs. BPMs are usually composed of two or four electrodes, however BPMs with six or even eight electrodes have also been developed [43,44]. BPMs are one of the most important devices to determine the lattice optics properties. BPM non-linearities and other possible flaws are preprocessed and are not taken into account in this work. In the CTF3 drive beam, different types of BPMs [45] with bandwidths of 96 MHz and 192 MHz are used. In beam stabilisation studies, multiple types of inductive BPMs are utilised. Their typical resolutions of average current along the beam pulse range from 1-2 mA (~ 4 A and 1 μ s long pulse) in the linac to few tens of mA (~ 20 A and 100 ns long pulse). The resolutions were estimated from

Singular Value Decomposition (SVD). Electrostatic BPMs in the buncher, which are prone to charging effects, are not used in beam stabilisation studies. The LHC is equipped with two types of BPMs [26] able to acquire TbT data. First, button BPMs with position resolution of about $100\text{ }\mu\text{m}$ are used in the arcs. Second, strip-line BPMs installed in LHC's Interaction Regions (IRs) have a typical position resolution of about $250\text{ }\mu\text{m}$. Resolutions in TbT mode are estimated also using SVD (see Section 3.2.2). Several BPMs are equipped with more sensitive electronics called Diode ORbit and Oscillation System (DOROS) [46]. They are used for betatron coupling measurements and corrections [47]. The BPMs of the ESRF storage ring are described in Paper IV, with the estimated position resolution below $10\text{ }\mu\text{m}$ in TbT mode.

3.1.2 Additional instrumentation

In the study of CTF3 the following measurements are used:

- relative beam phase (time of arrival) is measured by mixing a signal from a wave-guide with reference RF. Such a device is called Beam Phase Reference (BPR) and provides also a relative measurement of longitudinal bunch length.
- RF power is measured in the beginning and at the exit of accelerating travelling wave structures. Beam loading is measured with resolution of typically $\sim 100\text{ kW}$ for signals of tens of MW.
- Beam profile and size is measured with beam screens intercepting the beam. They can estimate the beam energy spread when placed at a location with known non-zero dispersion. Their typical resolution is in the range of a fraction of mm.

In the optics measurements in the LHC, the following measurements are utilised:

- Transverse beam profiles are measured by Synchrotron Light Monitors (BSRTs). It is used as a relative measure of beam emittance.
- Beam losses are detected by Beam Loss Monitors (BLMs), this information is used to maximise the beam oscillation amplitude, and therefore signal to noise ratio, while keeping the beam losses acceptable.

- Base Band Tune (BBQ) - diode peak detector electronic processing of BPM signals yielding precise betatron tune measurement is essential to keep the tune constant and to set optics measurement parameters.

3.2 Algebraic and Statistical methods

This section describes the algebraic and statistical methods used across this thesis work.

3.2.1 Response Matrix

A response matrix is constructed from either a simulated or measured linear response of observables o to a unit change of controllable knobs c (generally represented by the gradient of $\frac{do}{dc}$). A column of a response matrix has a form:

$$\vec{R}_i = \left(\frac{d\vec{o}_1}{dc_i}, \dots, \frac{d\vec{o}_n}{dc_i} \right)^T, \quad (3.1)$$

where o_1, \dots, o_n is a set of observable quantities to be corrected by control knobs c_i . The vector of control knobs correcting the observable has a form:

$$\Delta \vec{c} = -\mathbf{R}^{-1} \cdot \left(\overrightarrow{\Delta o_1}, \dots, \overrightarrow{\Delta o_n} \right) \quad (3.2)$$

If \mathbf{R} is a square matrix of a rank equal to its dimensions, its inversion has a solution. This is often not the case, for example, when the number of observables is not equal to the number of control knobs, and the matrix \mathbf{R} needs to be pseudo-inverted instead. Pseudo-inversion can be performed using SVD and is not exact since an exact solution does not exist.

3.2.2 Singular Value Decomposition

The SVD of a matrix A is as follows

$$A = U \cdot S \cdot V^T, \quad (3.3)$$

where columns of U and V are normalised eigenvectors of $A^T A$ (left-singular vectors) and AA^T (right-singular vectors), respectively. S is a positively definite

diagonal matrix of singular values in decreasing order. The accuracy of SVD together with novel computation procedures is discussed in [48]. The SVD is used for removal of uncorrelated noise between BPMs (several largest singular values are used to recompose the data) and for matrix pseudo-inversion (approximate inversion of non-squared or lower rank matrices).

3.2.3 Iterative Filtering

Most of the measured quantities are assumed to be normally distributed, however in case of failure or an artefact in data processing, outlying values may be produced. Such outliers can significantly bias the results, therefore these values should be removed from the data sample. Finite-sized samples of a normal distribution follow a t-student distribution (parametrised also by a number of degrees of freedom). An iterative cleaning procedure has been developed to remove "tails" which are more populated than in the same-sized normally distributed quantity.

In each iteration, the mean μ and standard deviation σ of values in the data sample are calculated. Values are tested for a hypothesis of belonging to sample of normal distribution given the mean value μ , standard deviation σ and sample size N (t-distribution). The required level of significance in the hypothesis test is a p -value of $1/2N$. The p -value represents the probability of the occurrence of a specific value in a distribution. From a limit on p -value one obtains the maximal distance from the mean value allowed. Values, that are too far from the mean value μ , are removed from the data sample. The algorithm continues with the next iterations until either no more values are removed or a maximal number of iterations is reached.

The algorithm can also operate onto two linearly dependent sets. In such case, a linear fit is performed and the dependency on a second dataset is subtracted in every iteration. This gives a single dataset on which the above-mentioned hypothesis test is performed.

3.3 Static optics measurements

This section gives an overview of various static optics measurement methods used in both linear and circular accelerators. Some of them are utilised to independently cross-check results of the TbT-based measurements that are described in the next section. In some cases, the results are combined, providing a more statistically significant result.

3.3.1 Quadrupole scan

A quadrupole scan reconstructs the transverse phase space parameters from beam profiles [49] measured downstream of the location of interest. Alternatively, the reconstruction utilises fit beam sizes [50]. The beam profiles are measured while varying the strength of "scanned" quadrupole(s) in between the two locations.

3.3.2 K-modulation

K-modulation [51–53] measures the β -function at a magnet from observed betatron tune change upon a quadrupole strength variation

$$\bar{\beta}_{x,y} = \pm 4\pi \frac{\Delta Q}{\Delta K}. \quad (3.4)$$

In the LHC, the measured β -functions at quadrupoles neighbouring the IP are combined to determine and eventually correct β^* and waist ω (Paper III), following the nomenclature shown in Figure 3.1. The afore-mentioned iterative cleaning procedure is employed, namely, to remove outlying data points in a dataset of betatron tune and quadrupole strength.

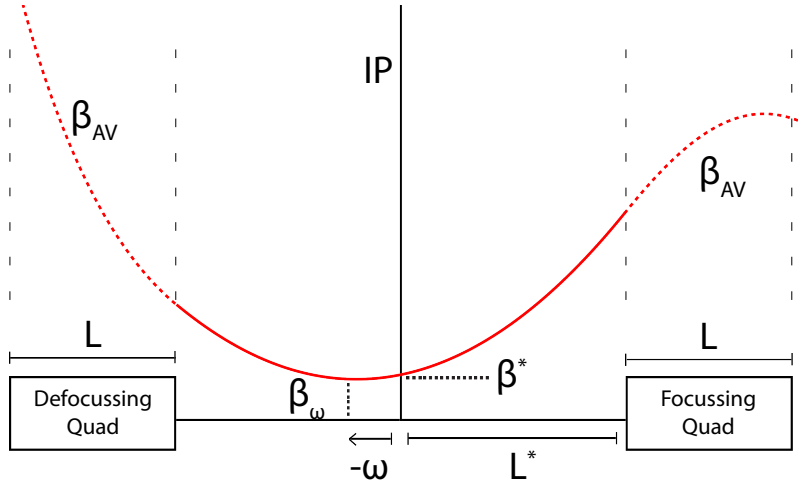


Figure 3.1: The conceptual layout and nomenclature for the parameters close to the IP. The red line represents the β -function, β^* is at the location of IP. The figure is taken from [54].

3.3.3 Closest tune approach

The closest tune approach measures betatron coupling [55] by changing the lattice, such that fractional betatron tunes (horizontal and vertical) are brought closer to each other. The minimal achievable difference between the tunes gives global betatron coupling.

3.3.4 Orbit response matrix

A (closed) orbit distortion can be introduced by a dipole corrector in both linear and circular accelerators. The Orbit Response Matrix (ORM) is measured by individually changing corrector excitation and recording the corresponding orbit shifts from BPM readings [56–59]. The information about magnetic errors in the accelerator lattice can be inferred by a global fit. Precision of β -functions inferred from ORM in the ESRF storage ring has been studied in Paper IV.

A more advanced modification of the ORM method, called phase space painting, is used in CTF3 [60]. Here two correctors are changed simultaneously, such that a nominal (model) ellipse in (x, x') phase space is "painted" at the location of the second orbit corrector. It is advantageous to choose correctors with no active elements in between (only a drift), which reduces possible errors.

3.3.5 Comparison of static methods

An overview of the above-mentioned optics measurement methods is given in Table 3.1. It summarises types of excitation along with observables. Table 3.1 also gives references for various measurements performed, including the possible bias due to calibration, misalignments or model dependency. More importantly, most of these methods are, in principle, applicable to both linear and circular accelerators (with various level of difficulty / impracticality).

3.4 Turn-by-Turn optics measurements with excited beam

This section describes variants how to excite coherent betatron oscillation of a beam, harmonic analysis of acquired TbT BPM data and measurements of different optical parameters. TbT data samples betatron oscillations at a given BPM. Its

Table 3.1: Static optics measurement techniques. The meaning of acronyms and symbols follows. C: Calibration or tilt; M: Model; $\bar{\beta}$: Average beta function over a quadrupole; ΔQ_{min} : closest tune approach.

Excitation	Observable	Parameter	Depends on	Refs
Orbit corrector	Beam position	ϕ, β	C	[60, 61]
		any parameter	C & M	[56–59]
		Arc Action	C & M	[62]
Quadrupole gradient	Tune	β	C	[51–53]
		ΔQ_{min}	-	[55]
	Beam size	β, ϵ	C & M	[49, 50]

reading is

$$x, y(n, s) = \sqrt{2J_{x,y}\beta_{x,y}(s)} \cos(2\pi Q_{x,y}n + \phi_{x,y}(s) + \phi_{x0,y0}) , \quad (3.5)$$

where n is the turn number, s is longitudinal location, $J_{x,y}$ is an action and $\phi_{x0,y0}$ is the initial phase.

3.4.1 Excitation

In order to induce coherent betatron oscillations around closed orbit two options can be used: pulsed excitation by a kicker¹ or driven oscillation by an AC-dipole [64]. In the pulsed excitation case, the beam decoheres [65], because of chromaticity and transverse non-linearities. This damps the amplitude of observed beam centroid motion, and thus limits the spectral resolution. A sample of TbT BPM data after a pulsed excitation is shown in Figure 3.2. Moreover, the decoherence after a pulsed excitation leads to transverse emittance blow-up. In lepton machines the beam emittance can be quickly restored by radiation damping, this is not the case for hadrons as they are heavier and emit less synchrotron radiation. Hadron beam radiation damping is negligible and emittance blow-up is irreversible (at reasonable operational time scale), which leads to a need of re-injection.

Both limitations (decoherence and emittance blow-up) can be overcome by

¹in special cases injection oscillations can be observed, for example in [63].

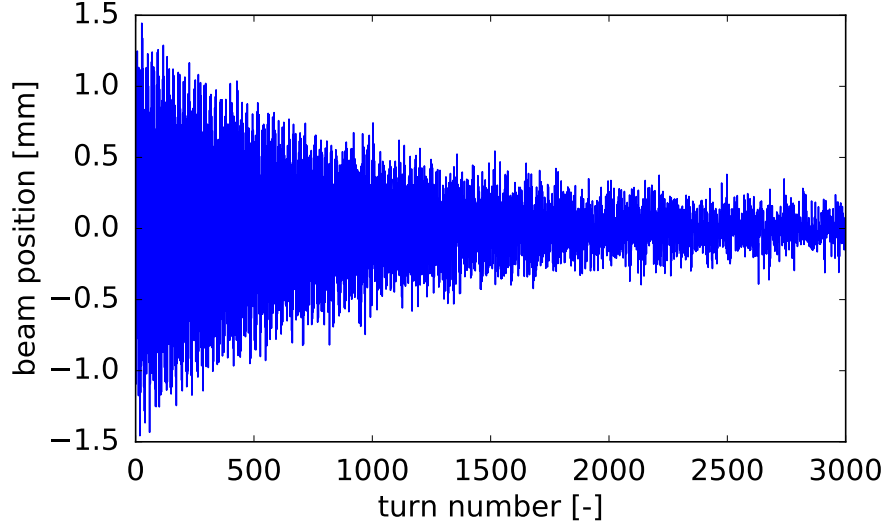


Figure 3.2: Sample TbT BPM data of a beam excited by a kicker performing the free coherent betatron oscillation.

utilizing an AC-dipole to drive the betatron oscillation [64, 66].² Driven oscillation can be adiabatically ramped up and later ramped down again [69] as shown in Figure 3.3, this way maintaining a constant amplitude of betatron motion and avoiding the emittance blow-up. On the other hand, the device is complex and a systematic effect perturbs the lattice under study, which is equivalent (to first order) to a quadrupole at the location of AC-dipole [70–72]. This effect has to be later subtracted in the analysis.

Many lattice optics needed to be commissioned in the LHC (corrected within tight tolerances). This was achieved using an AC-dipole [73, 74] and (Paper IV) in a very short time. This would not be possible with single kicks, which would require frequent re-injection and ramping down and up of the magnetic fields, which is a more than one-hour long operation in the LHC’s superconducting magnets. The AC-dipole excitation is also applicable in studies of collective effects or non-linear dynamics [75–77]. A comparison of pulsed and driven beam excitation is shown in Table 3.2.

In order to measure chromatic properties, such as dispersion, W-function or chromatic coupling, the lattice optics is measured at multiple beam energies. This

²In lepton machines, the speed of decoherence can be partially mitigated by use of special optics with low chromaticity and amplitude detuning (Paper IV) and [67, 68]. This holds for hadron machines as well, however, it is not practical since the beam remains blown-up after the kick anyway.

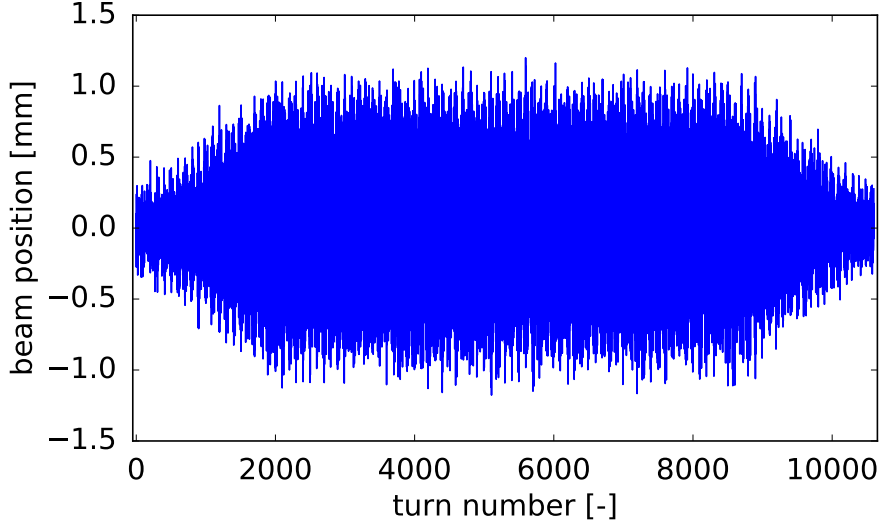


Figure 3.3: Sample TbT BPM data of a beam excited by an AC-dipole performing the driven coherent betatron oscillations (Paper VI). Note the ramp-up and the ramp-down of the oscillation amplitude, which is important to avoid emittance growth [69] (in hadron machines).

procedure is time-consuming. That is why a faster optics measurement method based on simultaneous 3-dimensional beam excitation has been developed within this work and experimentally demonstrated in the LHC (Paper VI). This method allows measurement of linear beam optics simultaneously with chromatic properties. The key element of this method is a fast RF-frequency modulation (providing adiabatic beam energy variation) at the same time as excitation by AC-dipoles. Figure 3.4 shows a sample of TbT data from a dispersive BPM during 3D excitation. Such beam excitation deteriorates neither the beam quality nor the precision of linear optics measurement.

3.4.2 Harmonic analysis

Once TbT BPM data of excited beam is acquired, it is analysed to extract betatron tune spectral lines and other harmonics. In order to improve analysis precision and accuracy, faulty BPMs need to be removed from the data and the data needs to be cleaned of noise. This is done by methods [79–81] based on SVD. Later the harmonic analysis [82–84] is performed.

A new framework (Paper VII) has been developed within this work together with Jaime Coello de Portugal. This framework seamlessly encapsulates data

Table 3.2: Comparison of beam excitation methods: pulsed using a kicker or driven using an AC-Dipole

Pulsed Excitation with kicker	Driven oscillation with AC-dipole
Easy to operate	Driven oscillation (more complex)
No cancelation needed	Need to cancel the effect on the optics quadrupole to the first order [70]
Decoherence limits useful number of turns	No decoherence
Emittance growth limits number of measurements without re-injection	No significant emittance growth [78]

reading, cleaning based on simple cuts, cleaning based on SVD [80] and harmonic analysis [84] using an interpolated Fourier transformation [85]. The "noise floor" removal based on SVD is performed by keeping only a few largest singular modes for later analysis, as shown in Figure 3.5.

We summarise the harmonic analysis, including the novel methods developed within this work, in Paper VII. Their core is a harmonic analysis performed on decomposed TbT data. In this way the accuracy is improved in case of a large number of turns or noisy signal. In terms of CPU time, such analysis is up to 300 times faster compared to BPM-by-BPM harmonic analysis on LHC datasets (Paper VII). Independently of the chosen harmonic analysis the TbT data are approximated by the sum of (typically) 300 strongest harmonics $h \sum_{j=0}^{299} h_j$, shown in Figure 3.6.

It needs to be stressed, that damped oscillations modify the initial phase of the main spectral line [86]. This is relevant for optics measurements based on pulsed beam excitation, where the beam decoheres. In such a case, the optics measurement is biased by choice of the first turn of a batch of TbT data analysed. This introduces a systematic error of about 1% or more in β -function measurement. Correction of phase content was one of the key points needed to improve the precision of β -function measurement in ESRF Paper IV. It is also necessary to impose the same measured betatron tune at all BPMs, otherwise, a phase error is introduced and the above-mentioned correction may not work. Application of phase correction to LHC optics measurements based on pulsed excitation is shown in Figure 3.7.

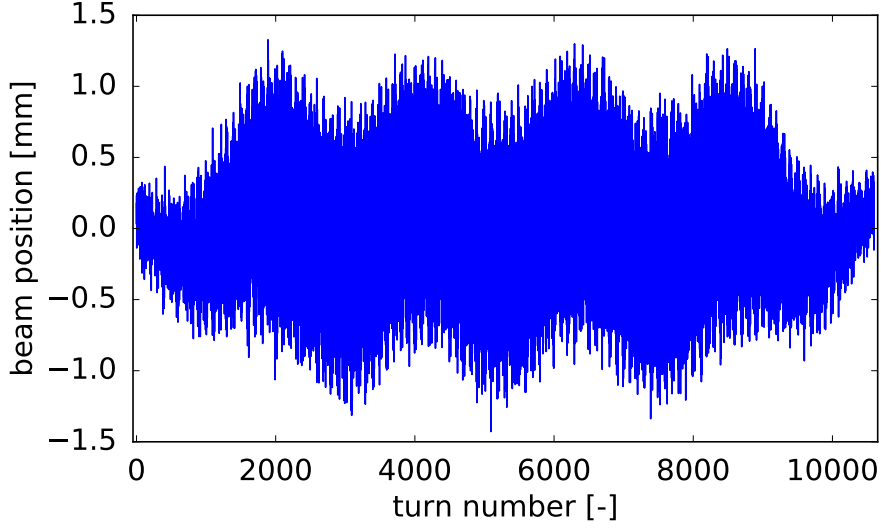


Figure 3.4: Sample TbT data at a dispersive BPM of a beam excited by an AC-dipole when the frequency of RF system has been simultaneously modulated. The beam performs driven coherent betatron oscillations and the beam energy is adiabatically varied (Paper VI).

3.4.3 Measured properties

Optical properties measured from TbT BPM data are described here, i.e. how they are related to spectral lines found in TbT BPM data.

The phase advance between pairs of BPMs is measured as the difference between initial phases of betatron tune lines (H(1,0) in the horizontal plane and V(0,1) in the vertical plane).

The pairs of measured phase advances ϕ_{ij} (from BPM i to BPM j) and ϕ_{ik} (from BPM i to BPM k) can be used to infer β -function at BPM No. i [87] (β from phase):

$$\beta_i = \frac{\cot \phi_{ij} - \cot \phi_{ik}}{\cot \phi_{ij,mod} - \cot \phi_{ik,mod}} \beta_{i,mod}, \quad (3.6)$$

where subscript *mod* refers to model values. This method is BPM calibration independent, however it diverges for phase advances close to π and its multiples. A more complex extension of this method utilizing weighted average from multiple BPM triplets in β -function calculation was developed [88], the so called N-BPM method. The β -function can also be calculated from amplitudes A of betatron tune lines, which are proportional to $\sqrt{\beta}$, as seen from Eq. (3.5), with $\sqrt{2J}$ being

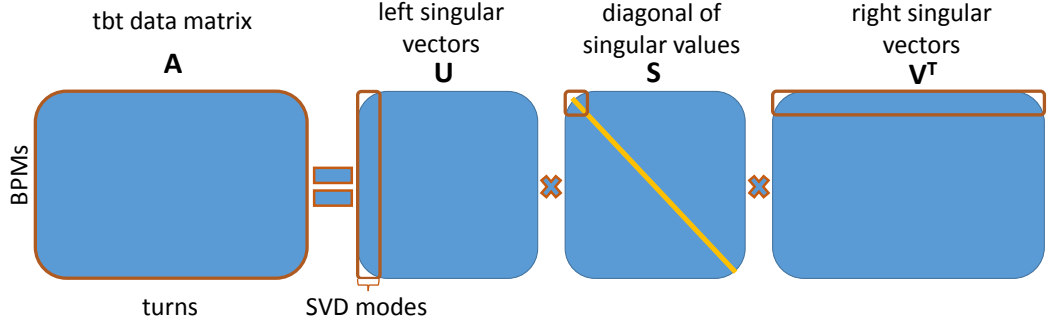


Figure 3.5: Sketch of TbT data recomposition for noise floor removal. The decomposition of raw TbT data (in blue) gives full matrices, which are then reduced (in brown edges), as only largest singular values are kept for the recomposition of cleaned TbT data . The figure is taken from Paper VII.

global factor common to all BPMs:

$$\beta_i = \frac{A_i^2}{2J}, \quad (3.7)$$

where the action is calculated as:

$$2J = \left\langle \frac{A^2}{\beta_{mod}} \right\rangle \quad (3.8)$$

The β from amplitude is biased by relative BPM calibration errors among different BPMs, unlike the action calculation which can be biased by absolute BPM calibration errors as well.

BPM calibration errors can be measured in special optics setups, usually called "alignment" or "ballistic", where the magnets are de-powered in sections of interest.

The amplitude of betatron coupling represented by the difference and sum resonance driving terms can be measured as given by Eq. (2.20). In more complex case of driven motion, calculation of coupling amplitude and phase is described, for example, in [89].

The chromatic properties described in Section 2.3 are usually calculated as a fit from spectra measured at different beam energies. Dispersion is obtained from Eq. (2.21) using measured closed orbit, i.e. amplitude of the H(0,0) spectral line. The normalised dispersion can be obtained in a similar manner, not influenced by BPM gain errors. Alternatively, the horizontal normalised dispersion is measured as a ratio of amplitudes of H(1,0) and H(0,0,1) spectral lines based on 3D beam

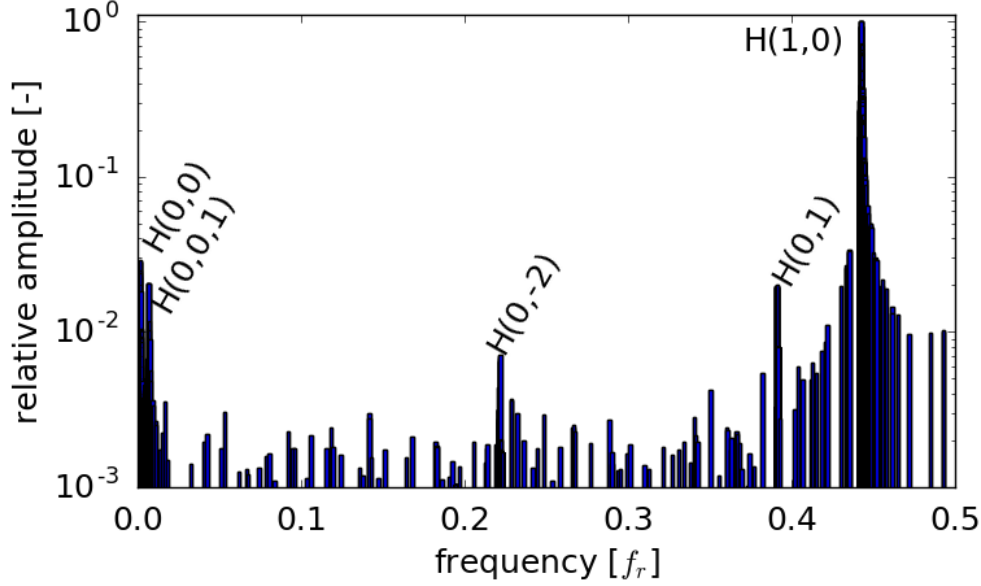


Figure 3.6: Notation using beam related harmonics H, V (multiples of $Q_x, Q_y, (Q_s)$) is illustrated on horizontal (H) frequency spectrum from TbT BPM data in ESRF storage ring.

excitation Paper VI. The sign of dispersion is inferred from the phase of $H(0,0,1)$ and the global scaling factor is obtained by comparison to model values.

W-function and chromatic coupling are fitted employing Eqs. (2.23) and (2.24). Alternatively, synchro-betatron spectral lines measured after 3D beam excitation can potentially be used, however, the analysis is still in an early stage of development. Table 3.3 summarises different TbT measurement techniques.

The precision of β -function measurement from amplitude and from N-BPM methods after pulsed excitation was improved (Paper IV). Part of the improvement can be attributed to optimised measurement and analysis parameters, such as kick amplitude and a number of analysed turns, as summarised in Figure 3.8. Red background colour stands for too high transverse oscillation amplitudes leading to perturbation due to lattice non-linearities. Blue background stands for too low transverse oscillation amplitudes yielding poor signal to noise ratio. Ideally, the oscillation amplitude is in the white band right after the excitation and stays for a maximal number of turns. This can be achieved by low-decoherence optics or by AC-dipole excitation which does not suffer from decoherence. The β -function measurement precision of 0.4 % was achieved in both planes from the N-BPM

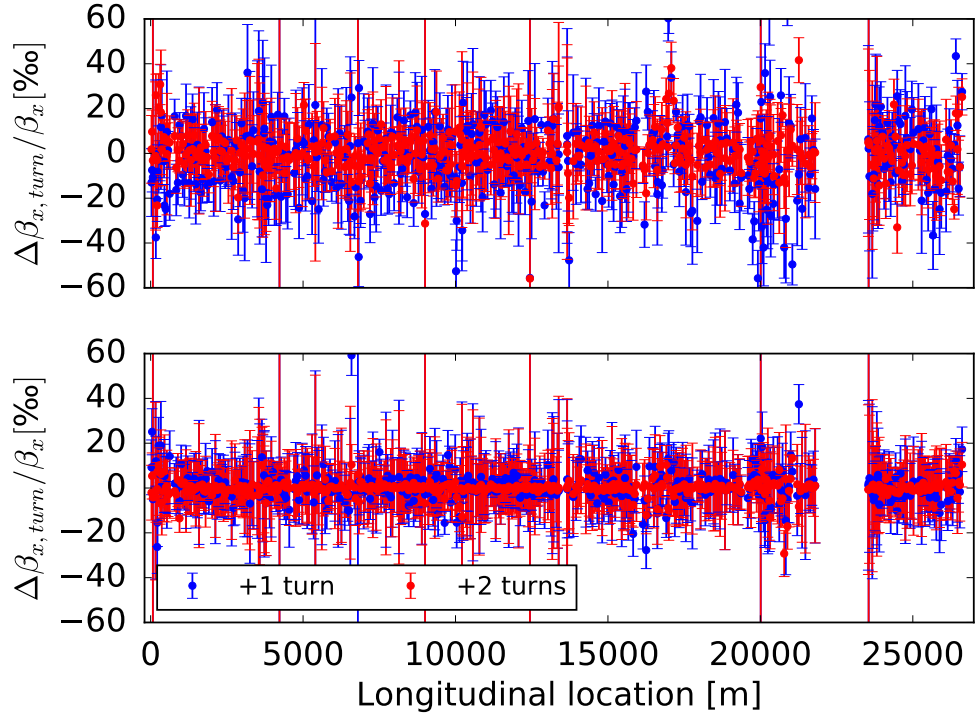


Figure 3.7: Artificial β -beating in the LHC caused by different choice of starting turn (moved by single turns) of a batch of TbT data analysed: before the phase correction - (top), after the phase correction (bottom) - showing significantly lower artificial β -beating.

method and in one plane from ORM method, utilising the low-decoherence optics.

Table 3.3: Overview of TbT-based measurement techniques, most taken from [90]. The meaning of acronyms and symbols follows. C: Calibration or tilt; M: Model.

Excitation	Parameter	Depends on	Refs
Betatron oscillation, free or forced	ϕ	-	[52, 74, 91, 92]
	β from ϕ	M	[79, 87, 88, 93]
	β from amplitude	C & M	[38, 94, 95]
	Action	C & M	[71, 72, 96]
	Coupling	C	[89, 97–100]
	BPM calibration	C & M	[101]
+ RF freq	$D_x/\sqrt{\beta_x}$	M	[41] and Paper VI
	Chromatic coupling	C	[102, 103]

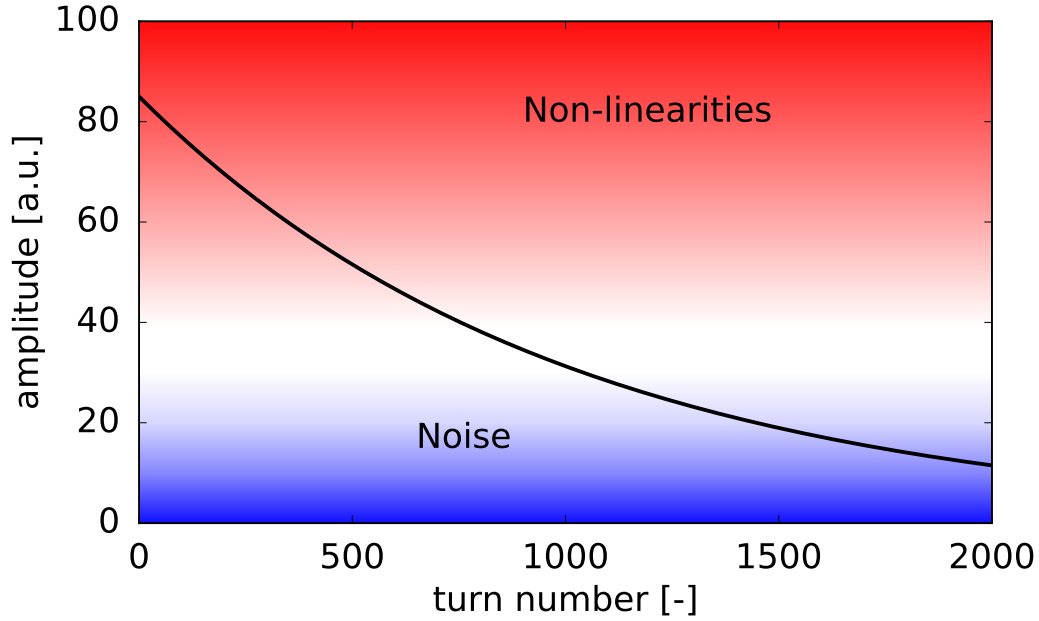


Figure 3.8: Envelope of a beam centroid oscillation amplitude (black) after a pulsed excitation by a kicker as a function turn number. The coloured areas represent the dominating bias to linear optics measurements either lattice non-linearities (in red) or noise (in blue). Ideally, the oscillation amplitude is in the white band right after the excitation and stays for a maximal number of turns.

Chapter 4

Beam correction methods

In this chapter, various beam correction methods are introduced. The principle of orbit corrections and local orbit bumps are described in Section 4.1, followed by global orbit correction techniques in Section 4.2. The optics corrections used in the LHC are also split between local and global corrections (Section 4.3, Section 4.4 respectively). Local corrections can be used independently of accelerator topology in a segment of an accelerator treated as a line.

4.1 Local orbit bumps

The orbit offset Δx_i at a given location i caused by a dipole kick θ_c is as follows:

$$\Delta x_i = \sqrt{\beta_{x,i}\beta_{x,c}} \sin(\phi_{x,i} - \phi_{x,c})\theta_c, \quad (4.1)$$

where the dipole kick θ_c is upstream of the location i . The orbit offset depends on β -functions at both the location of interest and the location of the dipole kick, as well as on betatron phase advance between them. This is the principle of ORM measurements described in Section 3.3.4. Similarly change of angle $\Delta x'_i$ is expressed:

$$\Delta x'_i = \sqrt{\frac{\beta_{x,i}}{\beta_{x,c}}} \cos(\phi_{x,i} - \phi_{x,c})\theta_c, \quad (4.2)$$

The orbit x_i can be corrected "locally" by reverting the kick (angle) θ_c , though this is not always possible. The two equations above can be used to calculate local orbit corrections (bumps) using multiple orbit correctors. The locality of a bump is achieved by imposing no orbit change everywhere but between the correctors.

The simplest case, a so-called π -bump, uses a second orbit corrector at phase advance of multiples of π from the first one to compensate the angle.

Any deviation of β -functions or phase advances leads to "non-closure" of the bump, thus "leaking" of the orbit deviation downstream. Non-linear elements or beam acceleration inside the bump (as well as BPM gain errors) also lead to the bump's non-closure, unless they are taken into account. Orbit bumps at non-linear elements can be introduced on purpose, for example, to correct the linear optics via feed-down at sextupole magnets [38, 104]. The amplitude of global (non-closed) orbit bumps in circular accelerator is also a function of betatron tune.

4.2 Global orbit

Often it is not clear how to pair correctors and BPMs for 1-to-1 orbit corrections (Eq. (4.1)). In such case, a response matrix (Eq. (3.1)) is employed to calculate a correction (Eq. (3.2)). Such an approach is still called 1-to-1 correction, even in cases where numbers of correctors and BPMs differ and SVD is used in inversion of the response matrix. In linear accelerators, it is important to limit emittance growth due to spurious dispersion, which is introduced by the beam not passing through centre of quadrupoles, i.e. when BPMs are misaligned with respect to quadrupoles. Dispersion-Free Steering (DFS) [105] reduces the dispersion by minimising the energy dependence of beam orbit. Due to measurement noise leading to unstable solutions, DFS is usually performed weighted together with 1-to-1 steering [106].

4.3 Local optics

In LHC IRs, where β -functions reach very large values (up to 10km) and the magnets are very powerful, non-conformities in the magnetic field have a much stronger effect on the beam compared to all the other locations. In principle, measured optics quantities at a location outside of IR are propagated through the model lattice as it would be a line, called Segment-by-Segment (SbS) method. Such propagation of measured values is compared to the model values. The lattice errors are calculated by matching a simulation to the measurement. Figure 4.1 shows the deviations of measured phase advance from model before and after local optics correction.

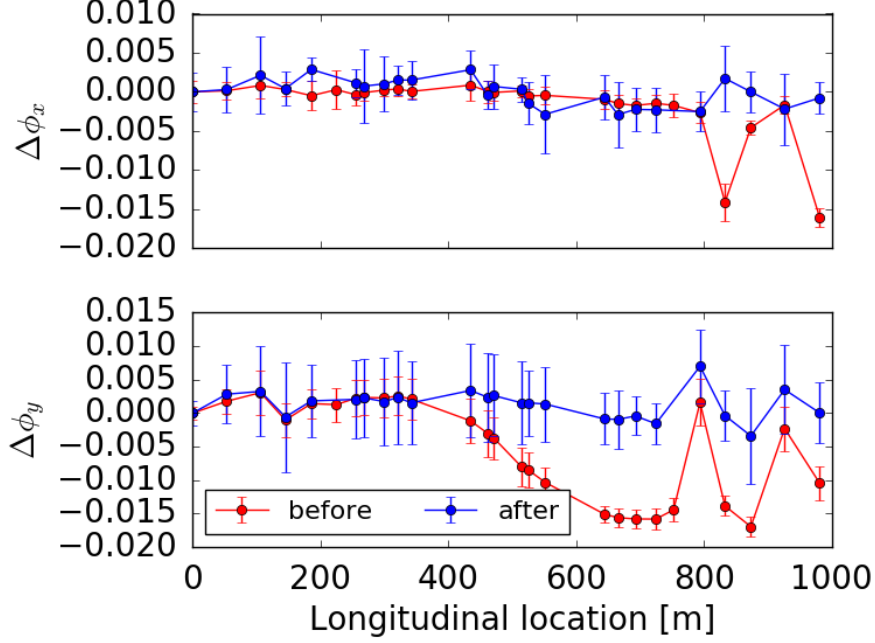


Figure 4.1: Example of difference of phase advance from propagated measurement using SbS method, before and after local optics correction.

4.4 Global optics

Global corrections are usually based on a linear response matrix (Eq. (3.1)) obtained from a model (potentially analytical). The vector of control knobs c_i correcting observable quantities o_1, \dots, o_n is given by Eq. (3.2). The response matrix is pseudo-inverted using SVD. In the following, it is important that not all singular values are represented in the pseudo-inversion. Therefore both observables and control knobs (potentially with different physical dimensions) should have a common measure, in which calculation is performed. A column of the response matrix and the correction are as follows:

$$\vec{R}_i = \left(\frac{\sqrt{w_{o_1}}}{\vec{\sigma}_{o_1}} \cdot \frac{d\vec{o}_1}{dc_i}, \dots, \frac{\sqrt{w_{o_n}}}{\vec{\sigma}_{o_n}} \cdot \frac{d\vec{o}_n}{dc_i} \right)^T \quad (4.3)$$

$$\Delta \vec{c} = -\mathbf{R}^{-1} \cdot \left(\frac{\sqrt{w_{o_1}}}{\vec{\sigma}_{o_1}} \cdot \Delta \vec{o}_1, \dots, \frac{\sqrt{w_{o_n}}}{\vec{\sigma}_{o_n}} \cdot \Delta \vec{o}_n \right), \quad (4.4)$$

where w_o are quantity specific weights and σ_o are measurement uncertainties. The division by vectors of measurement uncertainties is performed in piece-wise manner. For simplicity, normalisation of control-knob measure was omitted here. Table 4.1 shows different types of global optics corrections routinely performed in the LHC. They are defined by sets of observable quantities and the control knobs.

Table 4.1: Global corrections in the LHC using linear response matrix

observable quantities to correct	control knobs
$\Delta\phi_{x,y}, \Delta\beta_{x,y}/\beta_{x,y}, \Delta(D_x/\sqrt{\beta_x})$ and $Q_{x,y}$	quadrupole circuits horizontal orbit at sextupoles
$Re(f_{1001,1010}), Im(f_{1001,1010})$ and D_y	skew quadrupole circuits
$\frac{\Delta Re(f_{1001,1010})}{\Delta p}$ and $\frac{\Delta Im(f_{1001,1010})}{\Delta p}$	skew sextupole circuits

For the most common correction, which uses normal quadrupoles, inclusion of weights based on measurement errors and also physical-quantity specific weights is of greater benefit to optics correction than use of normalised measure (K1L - integrated quadrupole strength) of control knobs. Moreover, physical-quantity specific weights allowed to mitigate luminosity imbalance between ATLAS and CMS via precise correction of β^* s. The correction of β^* s, represented by β -functions measured from K-modulation of quadrupoles neighbouring IPs, is incorporated into the response matrix approach, which had not previously been the case. Even though using K1L as measure of quadrupole strength improves the optics correction, it is obviously only an effective correction as it may assign relatively large corrections to small magnets. When aiming to find sources of errors, a correction algorithm should include actual circuit strength as an observable.

The improved global correction algorithm was deployed in 2016 and yielded a significant improvement to optics quality that year (Paper III). Figure 4.2 shows β -beating in the LHC beam 1 with $\beta^* = 40$ cm after global correction in 2015 and in 2016 (Paper III). A comparison of beam 2 β -beating, along with normalised dispersion beating of both beams in both years can be found in Paper III. Table 4.2 summarises the global correction results. Overall progress in LHC optics commissioning methods is also reported in Paper III and [107]. The most challenging optics commissioned so far in the LHC has $\beta^* = 25$ cm [108].

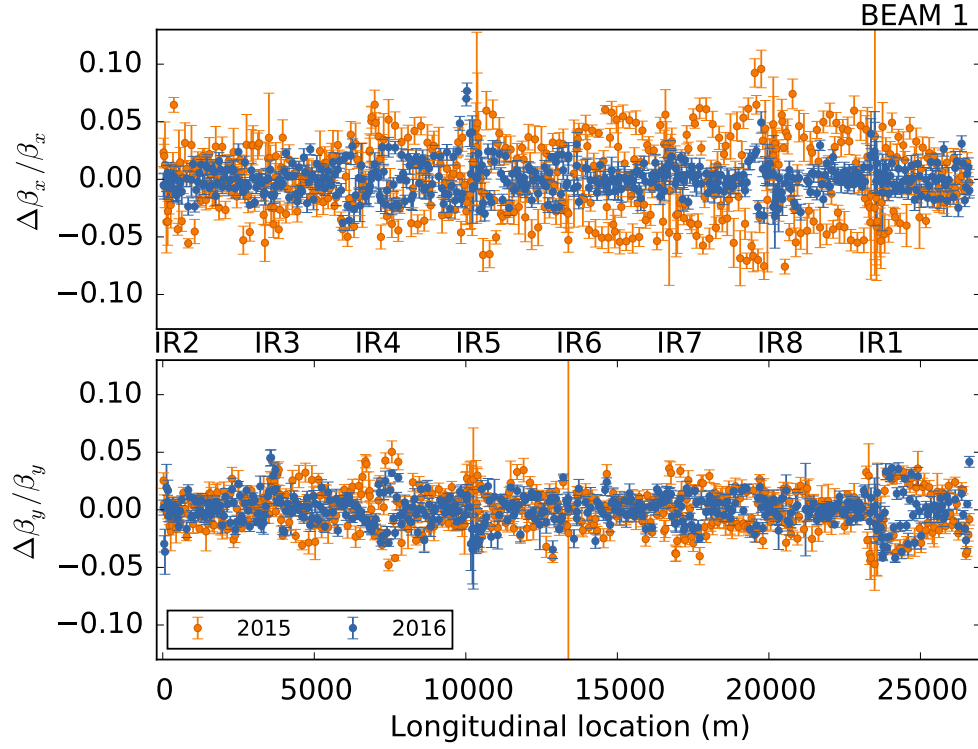


Figure 4.2: Comparison of β -beating measured in the LHC beam 1 with β^* of 40 cm after global correction in 2015 and in 2016 (Paper III).

Table 4.2: Rms β -beating and normalised dispersion beating in 2015 and 2016 with the β^* of 40 cm at the two main experiments (ATLAS and CMS), from Paper III.

Quantity	2015		2016	
	Beam 1	Beam 2	Beam 1	Beam 2
$\frac{\Delta\beta_x}{\beta} [\%]$	3.18	4.24	1.42	1.79
$\frac{\Delta\beta_y}{\beta} [\%]$	1.69	2.07	1.35	1.42
$\frac{\Delta D_x}{\sqrt{\beta_x}} [\sqrt{m}]$	0.0078	0.0113	0.0052	0.0062

Chapter 5

LHC Beam-based Model

This chapter describes the LHC beam-based model. Accurate modelling of a particle accelerator is crucial for its efficient and safe exploitation. It allows for rapid setup and optimisation of its performance. By predicting with good precision the beam dynamics and its evolution upon parameter changes, beam manipulations can be made in a safe manner. Additionally, there are many measurements that rely on the model predictions. For example, the LHC wire scanner emittance measurements rely on the model value of the β -functions, which is a source of a major uncertainty [109]. The beam size error of corrected optics will likely be increased in HL-LHC as the optics configuration will be more challenging and consequently the correction schemes pushed to the limit.

The modelling of beam orbit and lattice optics, using the beam as a diagnostic tool, is described in Section 5.1. This chapter builds upon Chapter 4, the correction methods are used in "reversed order", i.e. not correcting the real accelerator to match its model, but making the model a more realistic image of the accelerator.

5.1 Beam-based matching - correcting the model

Once the beam optics are measured, they are implemented into the LHC lattice model. In general, this is done employing "virtual" magnet elements, which are introduced in the model, even where there is no corresponding magnet in the real accelerator.

5.1.1 Model orbit matching

In Paper II, correction of the model orbit towards the measurement has been improved. Any unrealistically large (far from the reference) orbit measurements are filtered out. Additional virtual correctors were attached to some of the dipoles inside the interaction regions. Some of the position measurements may be missing or filtered out, which leaves a number of consecutive virtual correctors without measurements in between them. The extra virtual correctors (without neighbouring position measurement) are not used for orbit correction performed in Methodical Accelerator Design (MAD-X). This scheme was successfully verified, reaching a 0.1 mm deviations from measured orbit.

5.1.2 Model optics matching

In order to correct the lattice model towards the optics measurement (Paper II), a sign of global optics correction (Eq. (4.4)) is inverted. The optics is measured with a precision of about 1% (β -functions). The peak β -beating in the LHC is about 5% (supposed to reach up to 20% in HL-LHC). The matching reproduces the β -functions within 1% accuracy, which significantly reduces the errors coming from the lattice model. Samples of studies, profiting from the utilisation of beam-based model, are mentioned in Paper II.

5.1.3 Orbit and optics matching interleaved

Due to feed-down effects the orbit and the optics matching influences each other. For example, a dipole kick from misaligned quadrupole changes as a function of its strength. For this reason, usually, three iterations of the two corrections are interleaved. This also addresses the lattice non-linearities as the target for next iteration of optics correction is calculated in MAD-X. Unlike linear response matrix, MAD-X simulation accounts for the non-linearities. The iterative approach (without orbit correction), is currently used also in global optics correction algorithm.

5.2 Degeneracy of the model

The integer betatron tunes in the LHC are large (~ 60). From the Eq. (4.1) it follows, that there are many locations where the same orbit distortion can ori-

ginate. Similarly, quadrupole and higher order errors originating from different locations may have the same effects. Moreover, feed-down effects are difficult to distinguish from the lower order errors as they behave the same way. Some of the lattice errors were identified [101, 104], however the LHC beam-based model is still an effective model, i.e. the corrections do not necessarily correspond to the actual error sources. Systematic errors could be identified by combining multiple measurements of different lattice optics.

While the LHC beam-based model accurately matches the β -functions and orbit, the predictive power of the model in terms of other parameters needs to be verified. For the HL-LHC, a predictive model may be essential to tackle the operational challenges of optics configurations pushed to the limit, for example, non-linear optics corrections.

Chapter 6

Beam stabilisation - continuous correction

This chapter discusses beam stabilisation, starting with an algorithm to find correlations among signals (Section 6.1). Once a useful correlation and a correction strategy are found, a feedback can be constructed (Section 6.2). These stabilisation concepts were applied in Papers I and V. In Section 6.3, the stabilisation of the CTF3 drive beam is described together with implications the successful demonstration has for CLIC.

6.1 Statistical analysis of correlations

An algorithm to identify statistically significant correlations among signals has been developed (Paper V). A new measure $R^2_{non-zero}$ is defined, which is positive if the correlation coefficient is inconsistent with zero at chosen confidence level, as shown in Figure 6.1. When $R^2_{non-zero} > 0$, it has similar properties as the coefficient of determination R^2 (correlation coefficient squared). R^2 is often used as a measure of fit quality. Most importantly, it denotes a (minimal) fraction of a signal variance that can be explained by the other signal. For example, $R^2_{non-zero} = 0.6$ means that 60% of signal variance can be explained by the correlation. This is very efficient for filtering of candidate correlations. It is also independent of accelerator type and signal units.

When considering any correlation identified using the method above, it needs to be kept in mind that noise cannot be explained by the correlation. Noise therefore reduces the maximal $R^2_{non-zero}$. When a statistically significant correlation

between two signals is found, the underlying process should be understood to avoid spurious correlation.

6.2 Stabilisation concepts

This section builds upon Chapter 4 and discusses methods used in Papers I and V. Different approaches to parameter deviations, that are not constant in time and are thus impractical with regard to manual correction, are discussed. The correlation between the observable quantity and a control knob is assumed to be found and understood. In practice, both the observable and control knob may correspond to multiple parameters.

In an ideal case, a reference value is set or measured and a response matrix parametrises sufficiently well the behaviour for a typical size of deviation. In such a case, a simple measurement-correction feedback loop can be implemented. Typical free parameters of such feedback loop are integration time and gain, i.e. a number of samples and a correction scaling factor.

In another common case, the observable quantity is being minimised. The response matrix cannot be used in a single step as the correction sign is, a priori, unknown around local extremes of the observable quantity. Measurements at multiple settings of control knob are needed, to perform a general non-linear fit. It needs to be stressed, that "measurement" may also stand for a function of the observable quantity. The process is often linearised using Newton's method, where only two measurements are needed. It is also important that the difference between the two measurements is sufficiently large, such that the performance is not driven by noise, and at the same time is smaller than usual size of deviation to avoid resonant behaviour of the feedback loop. This introduces an additional free parameter, a limit on the difference between the measurement and the reference value, below which a feedback does not act.

6.3 CTF3 drive beam stabilisation

CTF3 was built to demonstrate the CLIC two-beam acceleration scheme [33]. The scheme includes generation of a high current drive beam via the beam multiplication technique, which is then used to produce RF power necessary to accelerate the main beam. One of the main challenges for CLIC and CTF3 is that tight requirements need to be met in terms of drive beam stability [110].

In order to implement stabilisation schemes for a real machine, data monitoring applications are needed. For example, unknown drifts of machine parameters need to be identified. In the CTF3 a watchdog application was developed (Paper I), that shows graphically if all the machine settings and acquisition signals are close enough to the reference. It points out the differences in a logical order on a dedicated fix display. It is typically used together with the *ReferenceMonitor* [111], for optimal and stable operation.

Stability analysis (Section 6.1) showed that beam phase is mostly defined in the injector. The beam phase can be corrected by adjusting the phases of the RF power delivered by the injector klystrons. In the linac, the phases of the RF are adjusted to match the beam loading. In order to control beam current, a grid voltage of the thermionic gun is adjusted.

The stability analysis resulted in fixes and improvements of key pieces of hardware and in the implementation of multiple (mostly beam-based) feedback systems (Papers I and V). These feedbacks systems have proven themselves to be very useful, not only to stabilise the drive beam, but also to aid machine start-ups. After longer breaks in machine operation (for example overnight) RF parameters drifted randomly leading to almost no beam transmission. The feedbacks automatically return the RF parameters to the reference values within few hundreds of pulses. A further technique demonstrated in CTF3 is Phase Feed-Forward (PFF) [112]. This technique is critical for the CLIC accelerator. It utilises beam phase measurements fed forward to fast kickers, which change the beam path length and therefore bunch arrival time.

The drive beam stability, with and without (an early version of) the beam-based feedbacks systems, is compared (Paper I). The average drive beam stability achieved in CTF3 meets the requirements for CLIC in terms beam phase and energy stability (Paper V). It also gives sufficient proof-of-principle for beam current stabilisation, given the differences between CTF3 and CLIC, as discussed in the Conclusions of Paper V.

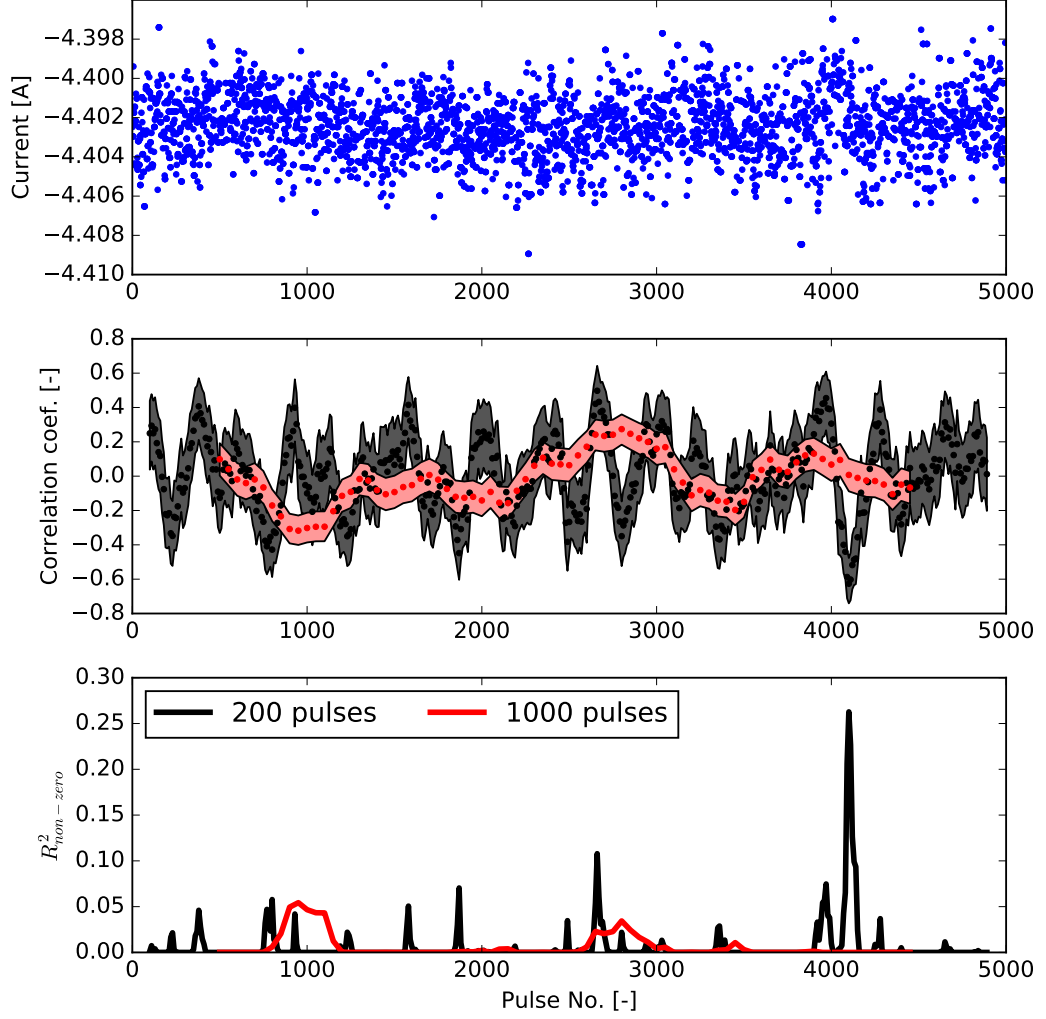


Figure 6.1: Sketch of correlation analysis procedure from Paper V: In the top plot, a time evolution of a beam current signal is shown. In the middle plot, signal's sample correlation coefficients with time over a sliding time window of two different lengths, 200 pulses (black) and 1000 pulses (red), is shown including confidence interval bands. In the bottom plot, the respective $R^2_{non-zero}$ is shown for a given confidence level of the two sets of correlation coefficients.

Chapter 7

Summary and outlook

Precise control of beam optics and beam stability is of critical importance for machine protection and performance of today's particle accelerators. Its importance increases for the next generation of high-energy particle colliders, as technology limits are pushed further. In this dissertation, methods of accelerator performance optimisation at the CTF3, LHC and ESRF have been studied. New techniques have been developed and the performance of existing methods has been improved. The progress has been achieved over a full work-chain ranging from measurements with their analyses, through applied corrections, to modelling and beam stabilisation. Both circular and linear colliders are studied in parallel, having different operational challenges, itself an important factor to determine the feasibility of a next-generation particle collider.

In linear accelerators, every beam measurement or correction is performed with a fresh beam, unlike in a case of circular accelerators, where the beam is stored and can, in principle, be reused. Lattice parameters measured in rings fundamentally differ from the beam parameters measured in linacs, as discussed in Chapter 2. The challenges in linacs are often related to beam energy errors, while in rings challenges arise from transverse resonances caused by repeated passage through imperfections. In linacs, the causality of the measurement and the correction is usually clear, unlike in rings where corrections are often non-local due to large degeneracy. The "static" beam optics measurements methods used in both linear and circular accelerators were reviewed in Section 3.3, followed by a review of measurement methods specific to rings, yet independent of particle type. A thorough comparison of some of the methods can be found in Paper IV.

A new optics measurement technique, where the beam is excited adiabatically in all three spatial dimensions simultaneously (in circular machines using AC-

dipoles combined with RF-frequency modulation), has been invented and successfully demonstrated in Paper VI. This technique significantly speeds up the optics measurements and thus saves precious beam time during LHC commissioning and machine development sessions. The first results prove that added complexity of beam excitation does not deteriorate precision and accuracy relative to previous methods (Paper VI). This technique is becoming a "push the button" operational tool to measure the beam optics.

A new harmonic analysis method has been developed (Paper VII). It analyses the spectra of SVD-decomposed Turn-by-Turn (TbT) data and recomposes the data in the frequency domain only. In the LHC, this reduced the time required for harmonic analysis by a factor ~ 300 . This method also improves the accuracy compared to standard BPM-by-BPM analysis. It is routinely used in optics measurements and in automatic coupling correction, which wouldn't be operationally viable without faster harmonic analysis. In a case where multiple bunches will be excited a global optics correction can be calculated within a minute (providing enough TbT data is recorded), compared to about an hour without these techniques.

The performance of the LHC optics measurement scheme has been studied and compared with an alternative method, Orbit Response Matrix (ORM), in the ESRF storage ring. Unexpected effects revealed the limitations of both methods when applied to the strongly non-linear and quickly damping electron beams of synchrotron light sources. The precision of TbT techniques (N-BPM and Amplitude) was improved by refining the Fourier transform of TbT data with properly chosen excitation amplitude. In the kicker excitation case, the generally worse precision (compared to AC-Dipole excitation) was re-gained by refining the phase advance measurement. The experimental results showed the precision of β -functions was pushed down to 0.4% a factor more than two better than the best previously documented results. An accuracy better than 1% in both in TbT and ORM techniques has been shown in Paper IV.

The optics correction algorithms used in the LHC were improved. This resulted in reduced β -beating after global correction. Optics corrections were found for multiple optics. As well as being used in LHC operation they also served as necessary input for research of systematic optics errors and their modelling. The LHC optics has been successfully commissioned down to a β^* of 0.25 m at 6.5 TeV, which is lower than the design value of 0.55 m at 7 TeV. In the most challenging optical configurations of a high energy hadron collider, an unprecedented control of β -beating below 1.8% rms has been demonstrated. This is important

for the safety of the machine and the control of the luminosity delivered to experiments. These results have been possible due to studies of appropriate weights on the different optics parameters in global corrections, the longer AC-dipole plateau and the N-BPM method (Paper III).

The improvements of the very same correction algorithm described above, also allowed automatic generation of a lattice model that reproduces measured values of orbit and linear optics (Paper II). Simultaneous matching of orbit and linear optics parameters, entangled by feed-down effects, results in an agreement of modelled β -functions to the several ‰ level. These tools were applied to multiple studies, e.g. the impact of the orbit on chromaticity via octupolar feed-down. The knowledge of accurate optics parameters is crucial for a variety of measurements. This is especially important during machine development and commissioning efforts when the beam optics might not have been corrected yet.

All this has contributed to LHC’s excellent performance, which has reached far beyond its design values. Needless to say, the afore-mentioned methods are applicable to circular accelerators in general. Further improvements may still be needed, however, to control the more challenging optics foreseen for LHC’s upgrade, HL-LHC.

Precision particle physics measurement in the era beyond HL-LHC could be conducted, for example, in CLIC. Proving CLIC’s feasibility in terms of drive beam stability is the main focus of Chapter 6 and Paper V.

A novel analysis technique, which allows identification of beam drifts and their sources in a vast amount of signals, has been developed. It shows statistically significant correlations of signals in a sliding time window, visualised as a movie. The algorithm has proven itself to be very effective for the identification of the critical issues for beam stability. It is essential for the understanding of drifts, as well as for the later implementation of feedback systems. Moreover, it was also successfully used in Low Energy Ion Ring (LEIR), proving its independence of accelerator topology and particle type.

Feedback systems to stabilise the CLIC drive beam have been designed and commissioned at CTF3. They act on current from the electron source, phases of klystrons in the injector as well as in linac. In this way the feedback systems can stabilise the drive beam current, phase and energy (Paper V). Such feedback systems can be used in FEL Linacs, which operate similarly to CTF3 Linac. Another system, an online watchdog application has been developed (Paper I) to find any deviations from reference values in the machine as well as their approximate origin. In CTF3, results of this work allowed for efficient use of beam time,

which would be otherwise consumed by near constantly required beam setup and adjustments. Moreover, the feasibility of CLIC drive beam complex, used for the two-beam acceleration technique, has been proven and the a strategy for CLIC drive beam stabilisation has been proposed in Paper V.

An overview of principal applicability of the above-mentioned methods to accelerators of different topologies or particle types is shown in Figure 7.1. Applications to other types of machines may trade off the input effort to adapt a given method to the performance potentially gained. As an example, optics measurements based on 3D beam excitation are very vital for hadron rings with large turn-around time. In principle, they can also be utilised in lepton rings. However, due to much shorter synchrotron radiation damping time in lepton beams, the emittance is quickly recovered without a need for re-injection. In such a case, the time gained is likely not worth of the added complexity. In contrast, the correlation identification framework could be applied to any accelerator with basically no additional effort.

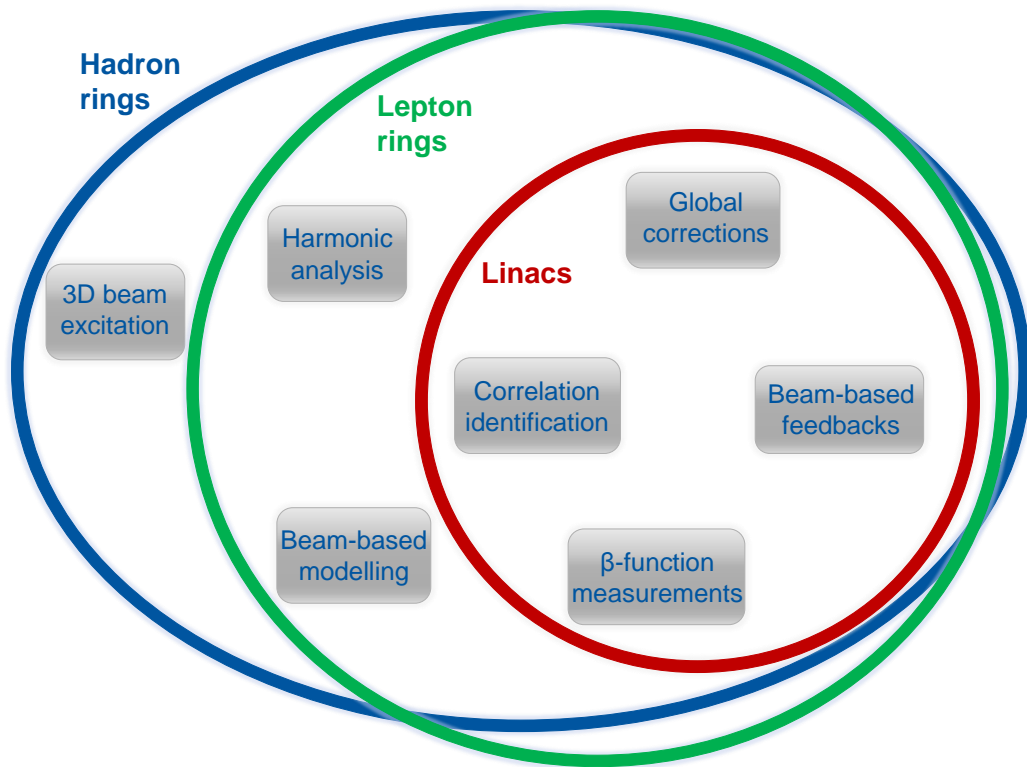


Figure 7.1: Applicability overview of methods (in grey rectangles) developed or studied within this work in different accelerator types (coloured ellipses).

7.1 Consequences for HL-LHC

The methods developed for the LHC will ultimately be used also for HL-LHC. The β^* -levelling optimisation of luminosity delivered to the experiments requires many optical configurations to be commissioned. The methods developed in this thesis will allow for accurate and efficient optics measurements and corrections. Because of more precise optics control the lattice optics can be pushed further towards the tolerances. This as well as faster optics measurement methods, increases the integrated luminosity, a key figure of a particle collider. Nevertheless, some of the challenges for optics measurements in HL-LHC still remain. For example, lack of precision in β^* measurements or the available dynamic aperture for the optics measurement itself in presence of non-linear errors, which will have to be taken into account in correction strategy.

7.2 Consequences for CLIC

In Paper V, the feasibility of CLIC drive beam complex, used for the two-beam acceleration technique, has been proven and a strategy for the CLIC drive beam stabilisation has been proposed. The stabilisation strategy includes the beam-based feedback systems, which were validated in CTF3, a monitoring application as well as a drift analysis framework necessary for beam optimisation. Key beam instrumentation was also identified (for example, beam phase measurement), in order to make the beam stabilisation possible. CLIC will also have circular beam lines, combiner rings in drive beam complex and damping rings for the main beam. The optics measurement and correction developments will be essential for their commissioning. The results of this thesis are likely to improve CLIC beam commissioning and operation throughout the whole machine.

Bibliography

- [1] L. Malina, R. Corsini, D. Gamba, T. Persson, and P. K. Skowronski, Recent improvements in drive beam stability in CTF3, in *Proc. IPAC'16, Busan, Korea, May 2016*, (2016), p. 2677-2679.
- [2] T. Persson, J. Coello de Portugal, M. Fjellstrom, L. Malina, G. Roy, P. Skowronski, A. Szczotka, and J. Moeskops, Review of the LHC online model implementation and of its applications, in *Proc. IPAC'16, Busan, Korea, May 2016*, (2016), p. 1505-1508.
- [3] T. Persson et al., LHC optics commissioning: A journey towards 1% optics control, *Phys. Rev. Accel. Beams* **20**, 061002 (2017).
- [4] L. Malina, J. Coello de Portugal, T. Persson, P. K. Skowroński, R. Tomás, A. Franchi, and S. Liuzzo, Improving the precision of linear optics measurements based on turn-by-turn beam position monitor data after a pulsed excitation in lepton storage rings, *Phys. Rev. Accel. Beams* **20**, 082802 (2017).
- [5] L. Malina, R. Corsini, T. Persson, P. Skowroński, and E. Adli, Drive beam stabilisation in the CLIC Test Facility 3, *Nucl. Instrum. Methods Phys. Res. A* **894**, 25-32 (2018).
- [6] L. Malina and J. Coello de Portugal, Optics measurements in storage rings based on simultaneous 3-dimensional beam excitation, in *Proc. IPAC'18, Vancouver, BC, Canada, May 2018*, (2018), p. 3068-3071.
- [7] L. Malina, J. Coello de Portugal, J. Dilly, P. K. Skowronski, R. Tomás, and M. Toplis, Performance optimization of turn-by-turn beam position monitor data harmonic analysis, in *Proc. IPAC'18, Vancouver, BC, Canada, May 2018*, (2018), p. 3064-3067.

- [8] K. J. Carlson, D. Stout, T. Jashashvili, D. J. de Ruiter, P. Tafforeau, K. Carlson, and L. R. Berger, The Endocast of MH1, *Australopithecus sediba*, *Science* **333**, 1402-1407 (2011).
- [9] G. Arnison et al. (UA1 Collaboration), Experimental observation of isolated large transverse energy electrons with associated missing energy at $\sqrt{s} = 540$ GeV, *Phys. Lett. B* **122**, 103-116 (1983).
- [10] M. Banner et al. (UA2 Collaboration), Observation of single isolated electrons of high transverse momentum in events with missing transverse energy at the CERN $\bar{p}p$ collider, *Phys. Lett. B* **122**, 476-485 (1983).
- [11] G. Arnison et al. (UA1 Collaboration), Experimental observation of lepton pairs of invariant mass around $95 \text{ GeV}/c^2$ at the CERN SPS collider, *Phys. Lett. B* **126**, 398-410 (1983).
- [12] P. Bagnaia et al. (UA2 Collaboration), Evidence for $Z^0 \rightarrow e^+e^-$ at the CERN $\bar{p}p$ collider, *Phys. Lett. B* **129**, 130-140 (1983).
- [13] S. Abachi et al. (D0 Collaboration), Observation of the top quark, *Phys. Rev. Lett.* **74**, 2632 (1995).
- [14] F. Abe et al. (CDF Collaboration), Observation of top quark production in $\bar{p}p$ collisions with the Collider Detector at Fermilab, *Phys. Rev. Lett.* **74**, 2626 (1995).
- [15] S. L. Glashow, Partial-symmetries of weak interactions, *Nucl. Phys.* **22**, 579 (1961).
- [16] A. Salam, J. C. Ward, Electromagnetic and weak interactions, *Phys. Lett.* **13**, 168-171 (1964).
- [17] S. Weinberg, A model of leptons, *Phys. Rev. Lett.* **19**, 1264-1266 (1967).
- [18] G. Aad et al. (ATLAS Collaboration), Observation of a new particle in the search for the Standard Model Higgs boson with the ATLAS detector at the LHC, *Phys. Lett. B* **716**, 1-29 (2012).
- [19] S. Chatrchyan et al. (CMS Collaboration), Observation of a new boson at a mass of 125 GeV with the CMS experiment at the LHC, *Phys. Lett. B* **716**, 30-61 (2012).

- [20] R. Aaij et al. (LHCb Collaboration), Model-independent evidence for $J/\psi p$ contributions to $\Lambda_b^0 \rightarrow J/\psi p K^-$ decays, Phys. Rev. Lett. **117**, 082002 (2016).
- [21] R. Aaij et al. (LHCb Collaboration), Evidence for exotic hadron contributions to $\Lambda_b^0 \rightarrow J/\psi p \pi^-$ decays, Phys. Rev. Lett. **117**, 082003 (2016).
- [22] CERN, Dark matter, <https://home.cern/about/physics/dark-matter>.
- [23] CERN, Supersymmetry, <https://home.cern/about/physics/supersymmetry>.
- [24] CERN, Extra dimensions, gravitons, and tiny black holes, <https://home.cern/about/physics/extra-dimensions-gravitons-and-tiny-black-holes>.
- [25] M. Aichler, P. Burrows, M. Draper, T. Garvey, P. Lebrun, K. Peach, N. Phinney, H. Schmickler, D. Schulte, and N. Toge (Editors), A Multi-TeV linear collider based on CLIC technology: CLIC Conceptual Design Report, Report No. CERN-2012-007, 2012.
- [26] O. S. Brüning, P. Collier, P. Lebrun, S. Myers, R. Ostojic, J. Poole, and P. Proudlock (Editors), LHC Design Report, Report No. CERN-2004-003-V-1, 2004.
- [27] G. Aad et al. (The ATLAS collaboration), The ATLAS Experiment at the CERN Large Hadron Collider, J. Instrum. **3**, S08003 (2008).
- [28] S. Chatrchyan et al. (The CMS Collaboration), The CMS experiment at the CERN LHC, J. Instrum. **3**, S08004 (2008).
- [29] K. Aamond et al. (The ALICE Collaboration), The ALICE experiment at the CERN LHC, J. Instrum. **3**, S08002 (2008).
- [30] A. A. Alves Jr. et al. (The LHCb Collaboration), The LHCb detector at the LHC, J. Instrum. **3**, S08005 (2008).
- [31] M. Hostettler, LHC luminosity performance, Ph.D. thesis, Bern University, 2018.
- [32] CLIC and CLICdp collaborations, Updated baseline for a staged Compact Linear Collider, CERN Yellow Reports: Monographs **2016**, CERN-2016-004 (2016).

- [33] G. Geshonke and A. Ghigo, CTF3 Design Report, Report No. CERN-PS-2002-008-RF, 2002.
- [34] A. W. Chao, K. H. Mess, M. Tigner, and F. Zimmermann, Handbook of Accelerator Physics and Engineering, (World Scientific, Singapore, 2006).
- [35] M. G. Minty and F. Zimmermann, Measurement and control of charged particle beams, (Springer, Berlin, 2003).
- [36] A. Wolski, Beam dynamics in high energy particle accelerators, (Imperial College Press, London, 2014).
- [37] E. D. Courant and H. S. Snyder, Theory of the alternating-gradient synchrotron, *Ann. Phys.* **3**, 1-48 (1958).
- [38] R. Tomás, Direct measurement of resonance driving terms in the Super Proton Synchrotron (SPS) of CERN using beam position monitors, Ph.D. thesis, University of Valencia, 2003.
- [39] A. Franchi, Studies and measurements of linear coupling and nonlinearities in hadron circular accelerators, Ph.D. thesis, Johann Wolfgang Goethe-University, 2006.
- [40] R. Capii and M. Giovannozzi, Multiturn extraction and injection by means of adiabatic capture in stable islands of phase space, *Phys. Rev. ST Accel. Beams* **7**, 024001 (2004).
- [41] R. Calaga, R. Tomás, and F. Zimmermann, BPM calibration independent LHC optics correction, in *Proc. PAC'07, Albuquerque, New Mexico, USA, Jun 2007*, (2007), p. 3693-3695.
- [42] B. W. Montague, Linear optics for improved chromaticity correction, Report No. CERN-LEP-NOTE-165, 1979.
- [43] K. Yanagida, S. Suzuki, and H. Hanaki, Design and beam test of six-electrode BPMs for second-order moment measurement, in *Proc. LINAC'12, Tel-Aviv, Israel, Sep 2012*, (2013), p. 464-466.
- [44] M. Tejima, M. Masuzawa, M. Tobiyama, K. Satoh, S. Hiramatsu, and K. Oide, Special beam position monitor with 8-button electrodes for the KEKB interaction region, in *Proc. EPAC'02, Paris, France, Jun 2002*, (2002), p. 1980-1982.

- [45] L. Soby, CTF3 BPMs : electronics, radiation, operational challenges, in *Proc. IWLC, Geneve, Switzerland, Oct 2010*, (2010).
- [46] J. Olexa, O. Ondracek, Z. Brezovic, and M. Gasior, Prototype system for phase advance measurements of LHC small beam oscillations, Report No. CERN-ACC-NOTE-2013-0038, 2013.
- [47] T. Persson et al., Experience with DOROS BPMs for coupling measurement and correction, in *Proc. IPAC'16, Busan, Korea, May 2016*, (2016), p. 303-305.
- [48] N. Halko, P. G. Martinsson and J. A. Tropp, Finding structure with randomness: Probabilistic algorithms for constructing approximate matrix decompositions, *SIAM Rev.* **53**, 217-288 (2011).
- [49] D. Gamba et al., Transverse beam phase-space measurement experience at CTF3, in *Proc. IPAC'17, Copenhagen, Denmark, May 2017*, (2017), p. 393-396.
- [50] F. Löhl, Measurements of the transverse emittance at the VUV-FEL, Ph.D. thesis, Hamburg University, 2005.
- [51] A. Hofmann and B. Zotter, Measurement of the β -functions in the ISR, Report No. ISR-TH/AH/BZ/amb-Run 641, 1975.
- [52] J. Borer, A. Hofmann, J.-P. Koutchouk, T. Risselada, and B. Zotter, Measurements of betatron phase advance and beta function in the ISR, *IEEE Trans. Nuc. Sci.* **30**, 2406-2408 (1983).
- [53] M. Kuhn, B. Dehning, V. Kain, R. Tomas, G. Trad, and R. Steinhagen, New tools for k-modulation in the LHC, in *Proc. IPAC'14, Dresden, Germany, Jun 2014*, (2014), p. 1024-1026.
- [54] F. Carlier and R. Tomás, Accuracy & Feasibility of the β^* Measurement for LHC and HL-LHC using K-Modulation, *Phys. Rev. Accel. Beams* **20**, 011005 (2017).
- [55] E. C. Raka, Measurement of the linear coupling in the Brookhaven AGS, *IEEE Trans. Nuc. Sci.* **22**, 1938-1940 (1975).

- [56] W. J. Corbett, M. J. Lee, and V. Ziemann, A fast model-calibration procedure for storage rings, in *Proc. PAC'93, Washington, D.C., USA, May 1993*, (1993), p. 108-110.
- [57] J. Safranek, Experimental determination of storage ring optics using orbit response measurements, *Nucl. Instrum. Methods Phys. Res. A* **388**, 27-36 (1997).
- [58] A. Franchi, L. Farvacque, J. Chavanne, F. Ewald, B. Nash, K. Scheidt, and R. Tomás, Vertical emittance reduction and preservation in electron storage rings via resonance driving terms correction, *Phys. Rev. ST Accel. Beams* **14**, 034002 (2011).
- [59] M. Aiba and M. Böge, Local orbit response matrix measurement at SLS, in *Proc. IPAC'15, Richmond, VA, USA, May 2015*, (2015), p. 1713-1715.
- [60] R. Corsini, S. Döbert, W. Farabolini, D. Gamba, T. Lefevre, L. Malina, T. Persson, J. Roberts, P. Skowroński and F. Tecker (editors), CTF3 final report, in preparation.
- [61] A. Morita, H. Koiso, Y. Ohnishi, and K. Oide, Measurement and correction of on- and off-momentum beta functions at KEKB, *Phys. Rev. ST Accel. Beams* **10**, 072801 (2007).
- [62] J. F. Cardona, Linear and non linear studies at RHIC interaction regions and optical design of the rapid cycling medical synchrotron, Ph.D. thesis, State University of New York, 2003.
- [63] M. Aiba et al., First β -beating measurement and optics analysis for the CERN Large Hadron Collider, *Phys. Rev. ST Accel. Beams* **12**, 081002 (2009).
- [64] M. Bai, S. Y. Lee, J. W. Glenn, H. Huang, L. Ratner, T. Roser, M. J. Syphers, and W. van Asselt, Experimental test of coherent betatron resonance excitations, *Phys. Rev. E* **56**, 6002 (1997).
- [65] R. E. Meller, A. W. Chao, J. M. Peterson, S. G. Peggs, and M. Furman, Decoherence of kicked beams, Report No. SSC-N-360, 1987.
- [66] M. Bai et al., Overcoming intrinsic spin resonances with an rf dipole, *Phys. Rev. Lett.* **80**, 4673 (1998).

- [67] A. Langner, G. Benedetti, M. Carlà, U. Iriso, Z. Martí, J. Coello de Portugal, and R. Tomás, Utilizing the N beam position monitor method for turn-by-turn optics measurements, *Phys. Rev. Accel. Beams* **19**, 092803 (2016).
- [68] M. Carlà, G. Benedetti, T. Günzel, U. Iriso and Z. Martí, Local transverse coupling impedance measurements in a synchrotron light source from turn-by-turn acquisitions, *Phys. Rev. Accel. Beams* **19**, 121002 (2016).
- [69] R. Tomás, Adiabaticity of the ramping process of an ac dipole, *Phys. Rev. ST Accel. Beams* **8**, 024401 (2005).
- [70] S. Peggs and C. Tang, Nonlinear diagnostics using an AC Dipole, Report No. RHIC-AP-159, 1998.
- [71] R. Tomás, Normal form of particle motion under the influence of an ac dipole, *Phys. Rev. ST Accel. Beams* **5**, 054001 (2002).
- [72] R. Miyamoto, S. E. Kopp, A. Jansson, and M. J. Syphers, Parametrization of the driven betatron oscillation, *Phys. Rev. ST Accel. Beams* **11**, 084002 (2008).
- [73] R. Tomás, O. Brüning, M. Giovannozzi, P. Hagen, M. Lamont, F. Schmidt, G. Vanbavinckhove, M. Aiba, R. Calaga, and R. Miyamoto, CERN Large Hadron Collider optics model, measurements and corrections, *Phys. Rev. ST Accel. Beams* **13**, 121004 (2010).
- [74] R. Tomás et al., Record low beta beating in the LHC, *Phys. Rev. ST Accel. Beams* **15**, 091001 (2012).
- [75] S. White, E. Maclean, and R. Tomás, Direct amplitude detuning measurement with ac dipole, *Phys. Rev. ST Accel. Beams* **16**, 071002 (2013).
- [76] N. Biancacci and R. Tomás, Using ac dipoles to localize sources of beam coupling impedance, *Phys. Rev. Accel. Beams* **19**, 054001 (2016).
- [77] S. Mönig, E. H. Maclean, T. H. B. Persson, J. Coello de Portugal, A. Langner, R. Tomás, Short term dynamic aperture with ac dipoles, in *Proc. IPAC'16, Busan, Korea, May 2016*, (2016), p. 3496-3499.
- [78] R. Tomás, M. Bai, R. Calaga, W. Fischer, A. Franchi, and G. Rumolo, Measurement of global and local resonance terms, *Phys. Rev. ST Accel. Beams* **8**, 024001 (2005).

- [79] J. Irwin, C. X. Wang, Y. T. Yan, K. L. F. Bane, Y. Cai, F.-J. Decker, M. G. Minty, G. V. Stupakov, and F. Zimmermann, Model-Independent Beam Dynamics Analysis, *Phys. Rev. Lett.* **82**, 1684 (1999).
- [80] R. Calaga and R. Tomás, Statistical analysis of RHIC beam position monitors performance, *Phys. Rev. ST Accel. Beams* **7**, 042801 (2004).
- [81] X. Huang, S. Y. Lee, E. Prebys, and R. Tomlin, Application of independent component analysis to Fermilab Booster, *Phys. Rev. ST Accel. Beams* **8**, 064001 (2005).
- [82] R. Bartolini and F. Schmidt, SUSIX: A computer code for frequency analysis of non-linear betatron motion, Report No. CERN SL-Note-98-017-AP, 1998.
- [83] T. Bach and R. Tomás, Improvements for Optics Measurements and Corrections Software, Report No. CERN-ACC-NOTE-2013-0010, 2013.
- [84] J. Laskar, Frequency analysis for multi-dimensional systems. Global dynamics and diffusion, *Physica D* **67**, 257-281 (1993).
- [85] Ç. Candan, A method for fine resolution frequency estimation from three DFT samples, *IEEE Signal Process. Lett.* **18**, 351-354 (2011).
- [86] W. Guo, S. L. Kramer, F. Willeke, X. Yang, L. Yu, A lattice correction approach through betatron phase advance, in *Proc. IPAC'16, Busan, Korea, May 2016*, (2016), p. 62-64.
- [87] P. Castro-Garcia, Luminosity and beta function measurement at the electron-positron collider ring LEP, Ph.D. thesis, University of Valencia, 1996.
- [88] A. Langner and R. Tomás, Optics measurement algorithms and error analysis for the proton energy frontier, *Phys. Rev. ST Accel. Beams* **18**, 031002 (2015).
- [89] R. Miyamoto, R. Calaga, M. Aiba, R. Tomás, and G. Vanbavinckhove, Measurement of coupling resonance driving terms in the LHC with ac Dipoles, in *Proc. IPAC'11, San Sebastian, Spain, Sep 2011*, (2011), p. 2067-2069.
- [90] R. Tomás, M. Aiba, A. Franchi, and U. Iso, Review of linear optics measurement and correction for charged particle accelerators, *Phys. Rev. Accel. Beams* **20**, 054801 (2017).

- [91] D. Sagan, R. Meller, R. Littauer, and D. Rubin, Betatron phase and coupling measurements at the Cornell Electron/Positron Storage Ring, *Phys. Rev. ST Accel. Beams* **3**, 092801 (2000).
- [92] M. Aiba, M. Böge, J. Chrin, N. Milas, T. Schilcher, and A. Streun, Comparison of linear optics measurement and correction methods at the Swiss Light Source, *Phys. Rev. ST Accel. Beams* **16**, 012802 (2013).
- [93] C. Wang, V. Sajaev, and C.-Y. Yao, Phase advance and β -function measurements using model-independent analysis, *Phys. Rev. ST Accel. Beams* **6**, 104001 (2003).
- [94] X. Shen, S. Y. Lee, M. Bai, S. White, G. Robert-Demolaize, Y. Luo, A. Marusic, and R. Tomás, Application of independent component analysis to ac dipole based optics measurement and correction at the Relativistic Heavy Ion Collider, *Phys. Rev. ST Accel. Beams* **16**, 111001 (2013).
- [95] A. Franchi, Error analysis of linear optics measurements via turn-by-turn beam position data in circular accelerators, *arXiv:1603.00281v3*, (2016).
- [96] J. Cardona, R. Calaga, R. Miyamoto, R. Tomás, and G. Vanbavinckhove, Comparison of the action and phase analysis on LHC orbits with other techniques, in *Proc. IPAC'11, San Sebastian, Spain, May 2011*, (2011), p. 2004-2006.
- [97] A. Franchi, L. Farvacque, F. Ewald, G. LeBec, and K. B. Scheidt, First simultaneous measurement of sextupolar and octupolar resonance driving terms in a circular accelerator from turn-by-turn beam position monitor data, *Phys. Rev. ST Accel. Beams* **17**, 074001 (2014).
- [98] X. Huang, J. Sebek, and D. Martin, Lattice calibration with turn-by-turn BPM data, Report No. SLAC-PUB-15128, 2010.
- [99] T. Persson and R. Tomás, Improved control of the betatron coupling in the Large Hadron Collider, *Phys. Rev. ST Accel. Beams* **17**, 051004 (2014).
- [100] W. Fischer, Robust linear coupling correction with N-turn maps, *Phys. Rev. ST Accel. Beams* **6**, 062801 (2003).
- [101] A. Garcia-Tabares, J. Coello, L. Malina, B. Salvachua, P. Skowronski, M. Solfaroli, R. Tomás, and J. Wenninger, MD test of a ballistic optics, Report No. CERN-ACC-NOTE-2016-0008, 2016.

- [102] T. H. B. Persson, Y. Inntjore Levinsen, R. Tomas, and E. H. Maclean, Chromatic coupling correction in the Large Hadron Collider, *Phys. Rev. ST Accel. Beams* **16**, 081003 (2013).
- [103] Y. Ohnishi, K. Ohmi, H. Koiso, M. Masuzawa, A. Morita, K. Mori, K. Oide, Y. Seimiya, and D. Zhou, Measurement of chromatic X-Y coupling, *Phys. Rev. ST Accel. Beams* **12**, 091002 (2009).
- [104] M. Schenk, S. Fartoukh, K. Li, L. Malina, E. Métral and R. Tomás, MD2190: Q” Stabilization during injection, Report No. CERN-ACC-NOTE-2018-0003, 2018.
- [105] T. O. Raubenheimer and R. D. Ruth, A dispersion-free trajectory correction technique for linear colliders, *Nucl. Instrum. Methods Phys. Res. A* **302**, 191-208 (1991).
- [106] E. Adli, A study of the beam physics in the CLIC drive beam decelerator, Ph.D. thesis, University of Oslo, 2009.
- [107] E. H. Maclean et al., New approach to LHC optics commissioning for the nonlinear era, submitted to *Phys. Rev. Accel. Beams*.
- [108] R. Tomás, private communication.
- [109] M. Kuhn, Emittance preservation at the LHC, Ph.D. thesis, University of Hamburg, 2013.
- [110] D. Schulte et al., Status of the CLIC phase and amplitude stabilisation concept, in *Proc. LINAC’10, Tsukuba, Japan, Nov 2010*, (2010), p. 103-105.
- [111] T. Persson, Fighting beam instabilities at CTF3, Ph.D. thesis, Chalmers University of Technology, 2011.
- [112] J. Roberts, P. Skowronski, P. N. Burrows, G. B. Christian, R. Corsini, A. Ghigo, F. Marcellini, and C. Perry, Stabilization of the arrival time of a relativistic electron beam to the 50 fs level, *Phys. Rev. Accel. Beams* **21**, 011001 (2018).

Scientific Publications

This chapter contains the core articles the author has contributed to during the thesis work. The articles follow in the order as mentioned in the Preface.

Paper I

Recent improvements of drive beam stability in CTF3

RECENT IMPROVEMENTS IN DRIVE BEAM STABILITY IN CTF3

L. Malina¹, R. Corsini, D. Gamba², T. Persson, P.K. Skowroński, CERN, Geneva 23, Switzerland
¹ also at University of Oslo, 0316 Oslo, Norway
² also at JAI, University of Oxford, Oxford OX1 3RH, United Kingdom

Abstract

The proposed Compact Linear Collider (CLIC) uses a high intensity, low energy drive beam producing the RF power to accelerate the low intensity main beam with 100 MeV/m gradient. This scheme puts stringent requirements on drive beam stability in terms of phase, energy and current. Finding and understanding the sources of jitter plays a key role in their mitigation. In this paper, we report on the recent studies in the CLIC Test Facility (CTF3). New jitter and drift sources were identified and adequate beam-based feed-backs were implemented and commissioned. Finally, we present the resulting improvement of drive beam stability.

INTRODUCTION

CTF3 was built to demonstrate the feasibility of the CLIC technology based on the two-beam acceleration concept. This technology imposes strict requirements on drive beam stability, especially in terms of current, energy and phase [1, 2]. The layout of CTF3 is shown in Figure 1.

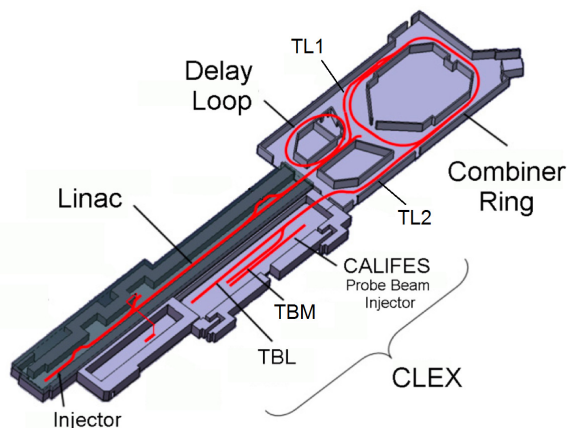


Figure 1: Layout of CTF3

MITIGATION OF DRIFTS

In order to be able to stabilize the beam in a chosen working point any change of the working point itself must be first identified. An online watchdog application has been developed for this purpose. It monitors currents of power supplies driving the magnets, all RF and beam signals and many other high-level inputs. The acquired data are then processed and filtered to highlight the largest differences

of current state of the machine with respect to agreed reference values. Figure 2 shows three continuously updated fixed displays. They present sorted lists of χ^2 s for machine settings, beam-related measurements and various signals grouped by their type and location. The latter is especially helpful to quickly find out in which part of the machine a problem has occurred, since any upstream drift usually provokes all the downstream beam signals to diverge. For practical reasons the locations with no beam presence are omitted. If any further investigation is needed, a dedicated program for data analysis developed for such purpose can be used.

Correlations between signals are searched and studied offline. This permits to identify the sources of either jitter or drift. Once a device is identified, it is first examined, and if it can not be passively stabilized then an appropriate feedback is implemented.

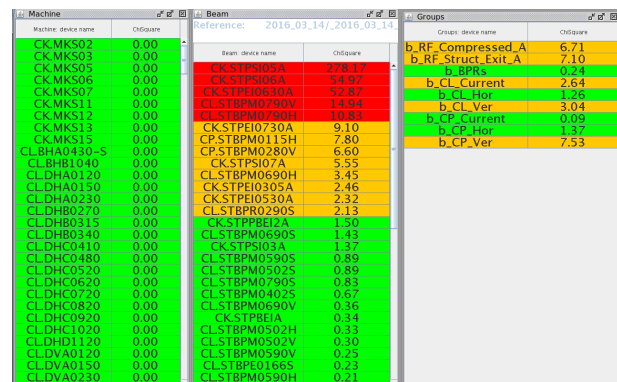


Figure 2: Screen-shot of the watchdog application: left - machine settings, middle - beam and RF measurements and right - devices grouped by location.

BEAM-BASED FEEDBACKS

The CTF3 feedback systems are designed in such a way that their safe operation is ensured. Each feedback does not act unless all the control parameters are within the thresholds defined at the time of commissioning and calibration of the system. Typically, a check is done on the first BPM downstream from the measurement location of the quantity which is being stabilized. Feedbacks follow changes of the beam pulse length and automatically adapt reference ranges. The same feedbacks are used to restore the beam conditions during restart. Nevertheless, reaching the reference working point may be impossible when the output power of one of the two injector klystrons changes dramati-

ically (higher than 1 MW). Attempt to compensate this by adjusting RF phases or gun current may result in significant beam losses. In order to ensure safe operation, a check of injector klystron power was therefore implemented into several feedbacks.

BEAM CURRENT STABILIZATION

In the past years the beam current stability was satisfactory. A feedback system was in place (demonstrating a relative stability of $5 \cdot 10^{-4}$) [3], but was generally not used in operation. Still tests of beam intensity stabilization system were performed. In the middle of the year 2015 the beam current got significantly less stable and affected machine operation. A new feedback system had then to be implemented since the size of drifts was too large for the existing system. The beam current is measured after the injector where the beam becomes fully relativistic and the first high accuracy Beam Position Monitor (BPM) is installed. The feed-back loop is closed on the gun intensity knob, that regulates the grid voltage in the CTF3 thermionic gun.

BEAM PHASE STABILIZATION

The beam phase is predominantly defined by the injector, after which electrons become ultra-relativistic. CTF3 injector can operate in two different modes:

- 3 GHz Beam - only the 3 GHz bunching system and the accelerating cavities are used. They are powered by two klystrons. This mode is typically used during machine start-up and for the experiments that do not require final drive beam intensities above 16 A (e.g. phase feed-forward experiment [4], optics checks and corrections).
- 1.5 GHz Beam - the three additional 1.5 GHz subharmonic bunchers (SHBs) are powered. This is required to operate the delay loop and to achieve the full drive recombination.

Injector Feedback

The Beam Phase Reference monitors (BPR) installed in CTF3 measure the beam phase, but their signal is also proportional to the beam current squared and inversely proportional to the bunch length. Two such devices are installed in the injector, one in the middle of the injector and a second one at its end. Sensitivity analysis showed that the injector feedback work more efficiently if the phases of the klystrons are locked on the phase signal of the upstream BPR and the bunch length signal of the downstream one. This feedback is used for both injector modes. Initially its performance was limited by a noisy beam phase measurement and by 0.36° minimum phase step. Both issues were addressed and eventually fixed during the winter shutdown 2015/2016.

TWT Phase Feedback

For the 1.5 GHz mode an additional feedback was developed in order to stabilize the phases of the traveling wave

tubes (TWTs) that power the SHBs. The system stabilizes the RF power at the exit of SHB cavity in presence of the beam (i.e., beam loading measurement) and the beam phase measured by the upstream BPR. An automatic calibration procedure has been implemented because the proportionality ratios are as well subject to drifts.

BEAM ENERGY STABILIZATION

After implementation of the RF power stabilization system [5], the beam energy stability was improved. Nevertheless, it was found that some beam energy variations remained and caused beam intensity fluctuations through losses. The energy variations are mainly due to slow changes of sensitivity in RF phase and power measurements (e.g. temperature effects), on which the phase loops and the RF power stabilization feed-back rely on, respectively. Second, it must be remembered that any beam current variation affects the acceleration in the fully loaded structures of CTF3.

Loading Feedback

Even though the CTF3 linac is operated in fully loaded mode, for most of the cavities the remaining power at the output port, the loading, is measurable. This strongly depends on the phase between the electron bunches and the accelerating field.

In a first stage, the loading “feedback” was just keeping the remaining power below a given limit or minimizing it as a function of klystron phase. Afterwards a more advanced concept has been developed. The remaining power along the beam pulse (not just the average) is measured and it is stabilized on a reference “trace” while adjusting the appropriate klystron phase. The reference trace is the average of several traces acquired for a short period after the feedback is turned on. The construction of the penalty function is not trivial because simple difference or χ^2 , even in the simplest case, is neither linear nor monotonous as the working point is close to full beam loading. The feedback minimizes a linear combination of χ^2 from the reference measurement (trace along the beam pulse) and the slope of the remaining power along the pulse. By setting a klystron specific free parameter it becomes monotonous function of klystron phase deviation. Loading feedbacks are implemented and commissioned for all the klystrons in Linac and are relatively slow as they operate on scales of minutes rather than seconds. The energy variation is measured as beam position in the first dispersive BPM, with a horizontal dispersion of 60 cm. The relative beam energy variation with and without the beam-based feedbacks is shown in Figure 3.

Energy Flattening Feedback

The residual beam energy variation along the pulse measured at dispersive pickup is usually few times larger than pulse-to-pulse variation. In order to reduce it, energy flattening feedback has been implemented. It modulates the energy gained in the accelerating structures powered by the

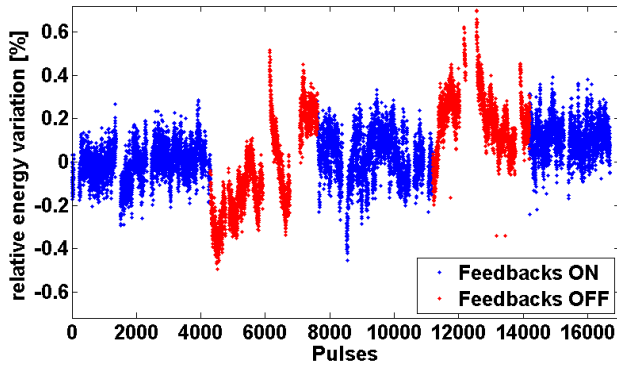


Figure 3: Relative pulse-to-pulse energy variation measured in dispersive pickup with beam-based feedbacks turned on (blue) and off (red).

last linac klystron by programming its waveform generator. The flattening improves the variation along the pulse, nevertheless it has not been fully commissioned for online operation yet.

PRESENT BEAM STABILITY

Presently achieved beam stability is quoted in this section and compared to CTF3 goals. The achieved phase and energy stability over periods of several minutes and several hours is shown in Table 1. Natural energy stability (mean along the pulse) has been improved from 0.22% to 0.12% by improving the gun pulser during the winter shutdown in 2015/2016. Natural phase stability may vary a lot, but usually is about 0.4° at 3 GHz. The current stability from the gun to the dump with a beam multiplication factor 4 is shown in Figure 4. Each blue line stands for a relative current stability over an hour of beam time with beam-based feedbacks running, the red lines stand for the same quantity without beam-based feedbacks. The green dashed line reflects the CTF3 current stability goal.

Table 1: Present Beam Phase and Energy Stability

Time scale	Phase [$^\circ$]	Energy [%]
several minutes	0.15	0.05
several hours	0.24	0.08
CTF3 goal	0.2	0.1

CONCLUSIONS AND OUTLOOK

The CTF3 Drive Beam Stability has been significantly improved in the past years. This was obtained thanks to the new feedbacks presented here, but also because of improved quality and control of the optics [6, 7]. Sources of jitter and drifts were identified and adequate beam-based feedbacks were implemented and commissioned for on-line operation. Some of the CLIC requirements have been reached, the rest is being approached. Additionally, the

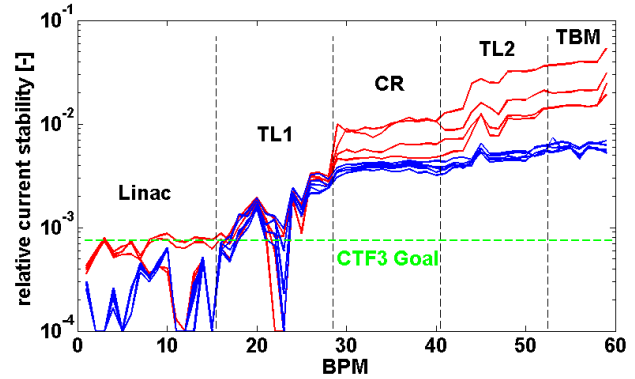


Figure 4: Several sets of relative beam current stability measurement (combination factor 4) along the machine. Each line refer to stability over a period of one hour. In blue; beam-based feedbacks operating, in red: feedbacks turned off.

beam stability is crucial for efficient running of the experiments and beam setup.

ACKNOWLEDGEMENTS

The authors would like to thank all CTF3 operators.

REFERENCES

- [1] G. Geshonke, et al., "CTF3 Design Report", CERN, Geneva, Switzerland, CERN-PS-2002-008-RF, May 2002.
- [2] M. Aichler, et al., "CLIC Conceptual Design Report", CERN, Geneva, Switzerland, CERN-12-007, Oct. 2012.
- [3] A. Dubrovskiy et al., "Review of the Drive Beam Stabilization at CLIC Test Facility CTF3", in *Proc. IPAC'13*, Shanghai, China, May 2013, paper WEPEA069, pp. 2666-2668.
- [4] J. Roberts et al., "Demonstration of CLIC Level Phase Stability Using a High Bandwidth, Low Latency Drive Beam Phase Feedforward System at the CLIC Test Facility CTF3", presented at IPAC'16, Busan, Korea, May 2016, paper WEPOR006, this conference.
- [5] T. Persson and P. Skowronski, "Beam Stability at CTF3", in *Proc. IPAC'12*, New Orleans, Louisiana, USA, May 2012, paper TUPPR032, pp. 1888-1890.
- [6] D. Gamba et al., "Effect and optimization of non-linear chromatic aberration of the CLIC Drive Beam Recombination at CTF3", presented at IPAC'16, Busan, Korea, May 2016, paper THPOR032, this conference.
- [7] P. Skowronski et al., "Status and plans for completion of the experimental program of the CLIC Test Facility CTF3", presented at IPAC'16, Busan, Korea, May 2016, paper TH-PMB046, this conference.

Paper II:

**Review of LHC on-line model implementation and of
its applications**

REVIEW OF LHC ONLINE MODEL IMPLEMENTATION AND OF ITS APPLICATIONS

T. Persson, J. Coello de Portugal, M. Fjellstrom, L. Malina, G. Roy,
P. Skowronski, A. Szczotka, CERN, Geneva, Switzerland
J. Moeskops, RID, Delft, Netherlands

Abstract

The online model of the LHC aims to provide an accurate description of the machine at any given time. In order to do so it extracts the current optics in the machine along with other crucial parameters. It also provides the functionality to match the measured orbit using virtual correctors and the measured beta functions using virtual quadrupoles. In this way an accurate effective model can be created. In order to facilitate the use of the online model a graphical user interface has been developed. In this article we describe the design of the online model and its application in different studies. We give examples of how it has been used to predict the influence of changes before they were applied to the machine.

INTRODUCTION

The modelling plays a fundamental role in the design and operation of modern accelerators. The model is created from the design and measurements of the magnets and the layout of the accelerator. The online model of the LHC aims to create an effective accurate model, which can be used to simulate new settings and effects. The model can also be used for more precise and more realistic simulations compared to the nominal model. It also provides more accurate inputs for model-based measurements and corrections.

The modelling of the optics is done in MAD-X [1]. In order to obtain the additional input a tool has been created to extract parameters that are of interest for the online model. The implementation is done in such a way that it gives the user the possibility to include the desired effects in the modelling with simple commands. The possibility to extract knobs used to correct the machine makes it possible to apply them to the ideal model and observe how the machine would behave without the knob in place.

Figure 1 shows the flow of the online model. The extractor requests the information from a measurement database and from a setting database. It then combines the information and converts it into MAD-X TFS table format, which can be used for the orbit- and β -modelling. All this is then put into a MAD-X description that can be used as is or edited by the user.

EXTRACTOR

In order to create an effective model it is first important to extract all the necessary parameters. There are two groups of parameters that are being extracted. The first group consists of settings, such as the optics in use and settings of selected knobs. These settings are extracted from the LHC Software

Architecture (LSA), which is a high-level layer of the LHC control system [2]. In the LHC, knobs normally refer to a set of magnets that are being changed to adapt, for example, the crossing angles or the transverse coupling. The second group is measurement parameters, such as the tune, energy and orbit. These parameters are stored in a measurement database and are extracted using a Java API. Since different studies need different input it is important to keep the software flexible enough so that the user can include any combination of desired effects. The corrections knobs are in general applied to compensate for the imperfections in order to bring the real machine closer to the ideal one. This also means that extracting all settings of the machine and plugging them into the model will not result in a better model. For example, extracting the settings of all the quadrupoles in the LHC will result in a less accurate β -modelling since the introduced changes are applied to be closer to the nominal model. Instead, a different approach is being used to model the β -functions in the machine. During the commissioning of the LHC the β -functions are measured and we can use these values to create a more accurate model. A similar approach is then implemented for the orbit and both are described in this paper.

ORBIT MODELLING

There are different methods of modelling a specific beam orbit in MAD-X. For the LHC online model, virtual orbit corrector magnets are used for this purpose. A virtual orbit corrector magnet works as a real orbit corrector magnet by applying a momentum kick in the horizontal or vertical plane. These magnets are only included in the model lattice, and not in the real machine. In practice, the virtual correctors will collectively reproduce the effects of misaligned quadrupole magnets and other sources of orbit deviation.

Orbits for the two planes are measured in the machine and are made available to the online model through the model extractor. The orbit is then reconstructed by the orbit correction routine in MAD-X and the corrector strength for each virtual corrector is saved. The saved corrector strengths can then be read back by other MAD-X scripts, to obtain the same measured orbit. As long as there are no major orbit changes in the machine the corrector strengths does not need to be recomputed.

The virtual corrector magnets can in principle be placed anywhere inside the model lattice. For the LHC online model there is one virtual corrector magnet placed at each quadrupole magnet. In this scheme, the corrector strengths needed to reconstruct the measured orbit will mainly esti-

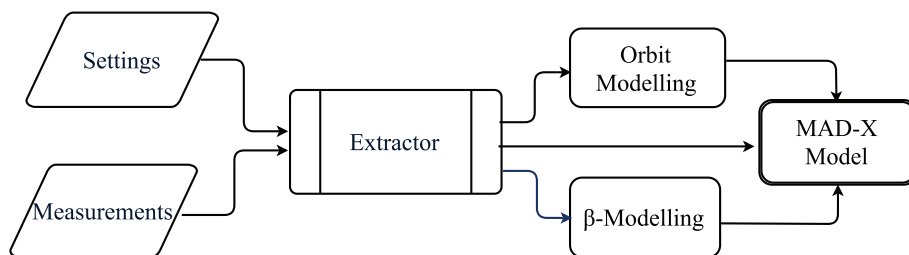


Figure 1: The conceptual flow of the online model.

mate quadrupole magnet misalignment, but also errors of the neighboring main dipoles.

Figure 2 demonstrates the result of reconstructing a measured horizontal orbit. Good results are obtained for the arc sections of the LHC, while less accuracy is obtained for the interaction regions. In part this can be explained by extreme β -function values in these regions as well as less accurate BPM measurements [3]. This can be seen from the erratic behavior of the measured orbit in the upper plot in Figure 2. It is possible to manually disable monitor readings which are believed to be incorrect, in case the monitor has not already been flagged as invalid.

A detailed manual for the virtual corrector scheme implementation in MAD-X, as well as full examples, can be found at the LHC online model web page [4].

BETA MODELLING

The β -matching module is intended to reproduce the measured linear optics. The aim is to create a model where the β -functions are as close as possible to the measured. The measured beta functions are stored in a database. The extractor then retrieves the data when needed for the modelling. In order to model the β -functions it uses thin virtual quadrupoles placed in the middle of real quadrupoles. The strengths of the virtual quadrupoles are calculated using the pseudo-inverted response matrix. The response matrix is created in MAD-X and it contains variations in beta function at each monitor corresponding to a change in the strength of each virtual quadrupole. The method is very similar to what is used to calculate global optics corrections [5]. The accuracy of the method benefits from the newly developed algorithm to reconstruct the β -functions based on N-BPMs [6]. This concept is easily extendable to other types of magnets and could also be used to match for example the transverse coupling using skew quadrupoles.

Typical RMS difference between the obtained model with respect to the measurement is about 0.7% and 0.6% in the horizontal and the vertical plane, respectively. An example of the relative difference between the measured and the matched model is shown in Fig. 3. This is significantly better than the RMS of about 4% between the nominal situation and the measurement. The more precise knowledge of the β -functions are useful both to create a more accurate model

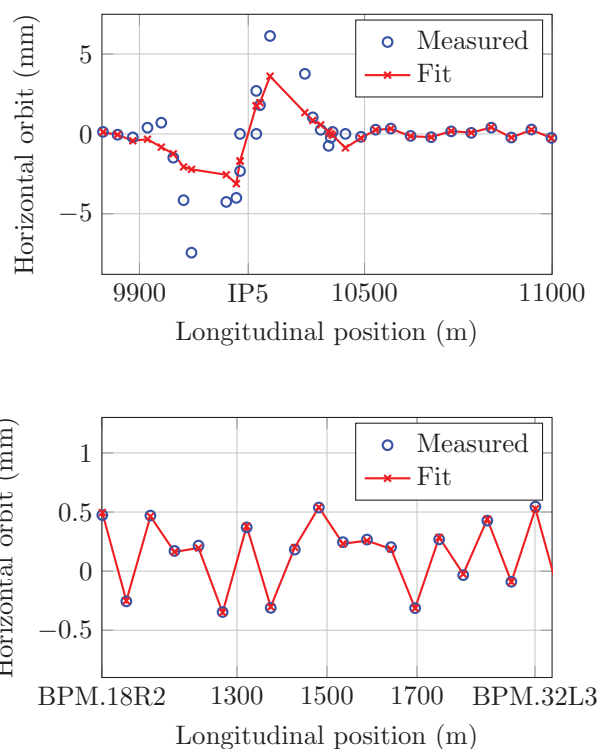


Figure 2: Comparison of the measured and reconstructed orbit for part of one the arcs (below) and around IP5 (above). The x-axis starts from the injection point close to IP2. The beam energy for the measurement was 6.5 TeV and the optics configuration was squeezed optics with a $\beta^* = 80$ cm at IP1 and IP5.

to predict any changes but also to directly extrapolate the measurements to other points in the machine.

USER INTERFACE

There are two main ways of invoking the online model. The first one is through a command line tool, which then creates the model based on the input string and a configuration file. However, in order to facilitate studies, a graphical user interface has also been developed. It provides the user with an easy way to create a model of the machine at given

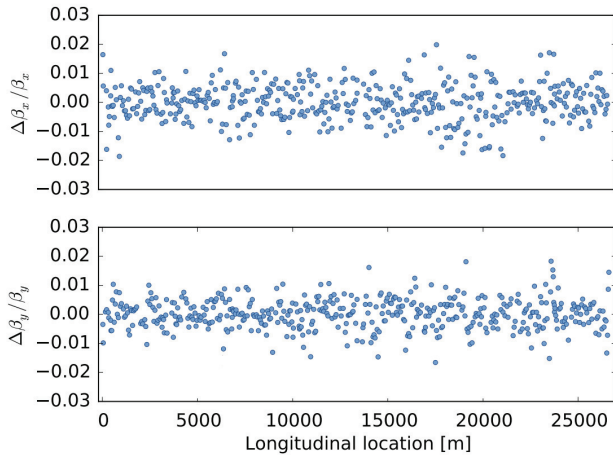


Figure 3: The relative difference between the measured and the matched model. The measurement refers to the optics configuration at flattop in 2015. The x-axis starts from the injection point of Beam 1 close in IP2.

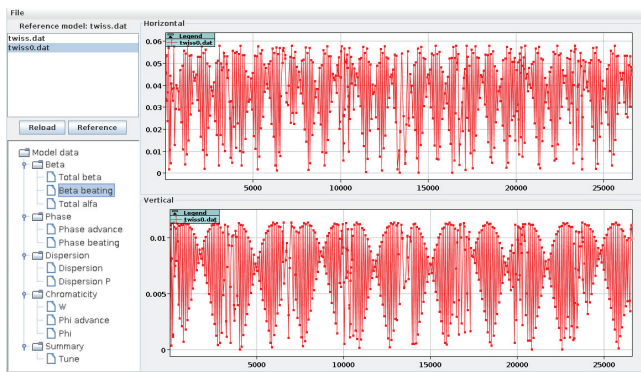


Figure 4: The normalized difference in the β -function between the two models.

time and then include different features, for example orbit matching. The different parameters such as the tunes, β -functions and dispersion are then being displayed and the user can view the differences between a reference model as shown in Fig. 4. When the model is created the user can, for example, vary strengths of magnets and then investigate the impact on the optics. All the MAD-X scripts are output in a folder so they can be run using other scripts to automatize different changes. A detailed description of how to run the GUI and the command line interface can be found in [4].

EXAMPLE STUDY

The online model has been used in several different studies. One of the studies aimed at understanding the influence of the powering of the octupoles on Q' (chromaticity) and Q'' . The machine orbit was reconstructed and the offsets of the magnets were taken into account in the prediction. The octupoles were then set to different strength in the model

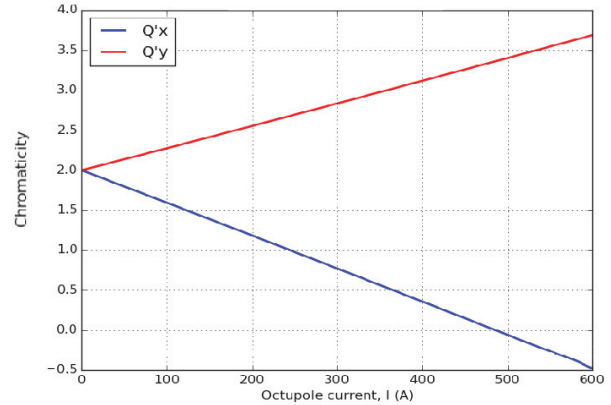


Figure 5: The chromaticity as a function of the powering of the octupoles with the measured orbit reproduced in the model.

and the predicted changes in Q' and Q'' were investigated as shown in Fig. 5 [7].

Another example was during an impedance measurement, that relied on accurate tune determination. During the measurement an orbit change also occurred. The study, with the online model, then aimed to understand if the orbit change together with feed-down could have a large enough effect to cause the observed tune change. The results showed that it was indeed possible and hence, it was not possible to use the measurement to draw conclusions on the impedance.

These are example of typical study which demonstrates the importance of a beam-based model in order to describe the machine more precise and hence interpret the results from a study more accurately.

SUMMARY AND OUTLOOK

The online model has already been used in studies to provide a more accurate description of the machine used to study for example the feed-down on tune and chromaticity. The part of the online model which has been described in this article is part of a larger frame-work of tools. Example of other tools are the aperture meter [8] and the footprint viewer [9]. The possibility to easily extract the settings and measurement from the machine and include them in model creation enables is crucial to create more precise and accurate models. These features will be of increasing importance as the operational parameters of the LHC will entering a more challenging regime.

REFERENCES

- [1] MAD-X web page <http://mad.web.cern.ch/mad/>
- [2] C. Roderick and R. Billen, “The LSA Database to Drive the Accelerator Settings” 12th International Conference On Accelerator And Large Experimental Physics Control Systems, Kobe, Japan (2009).
- [3] K. Fuchsberger and J. Wenninger, “Reference orbit and k-modulation”, LBOC April 2016 <http://lhc-beam-operation-committee.web.cern.ch/lhc-beam-operation-committee/>
- [4] LHC online model web page <http://lhcmode1.web.cern.ch/lhcmode1/>
- [5] R. Tomas et al., “Record low β -beat in the LHC”, Phys. Rev. ST Accel. Beams 15, 091001 (2012).
- [6] A. Langner and R. Tomas, “Optics measurement algorithms and error analysis for the proton energy frontier”, Phys. Rev. ST Accel. Beams 18, 031002 (2015).
- [7] L. Malina et al., “Chromaticity Reprocessing – Fill 3806”, LBOC June 2015 <http://lhc-beam-operation-committee.web.cern.ch/lhc-beam-operation-committee/>
- [8] G.J Müller, “Aperture meter for the Large Hadron Collider”, CERN-ATS-2012-059.
- [9] X. Buffat et al., “The online tune footprint viewer for the LHC”, CERN-ATS-NOTE 2012.

Paper III:

LHC optics commissioning: A journey towards 1% optics control



LHC optics commissioning: A journey towards 1% optics control

T. Persson,^{*} F. Carlier, J. Coello de Portugal, A. Garcia-Tabares Valdivieso, A. Langner,
E. H. Maclean, L. Malina, P. Skowronski, B. Salvant, and R. Tomás
CERN, CH-1211 Geneva, Switzerland

A. C. García Bonilla
Universidad Nacional de Colombia, Bogotá, Colombia
(Received 1 February 2017; published 19 June 2017)

Since 2015 the LHC has been operating at 6.5 TeV. In 2016 the β -functions at the interaction points of ATLAS and CMS were squeezed to 0.4 m. This is below the design $\beta^* = 0.55$ m at 7 TeV, and has been instrumental to surpass the design luminosity of 10^{34} cm⁻² s⁻¹. Achieving a lower than nominal β^* has been possible thanks to the extraordinary performance of the LHC, in which the control of the optics has played a fundamental role. Even though the β -beating for the virgin machine was above 100%, corrections reduced the rms β -beating below 1% at the two main experiments and below 2% rms around the ring. This guarantees a safe operation as well as providing equal amount of luminosity for the two experiments. In this article we describe the recent improvements to the measurement, correction algorithms and technical equipment which allowed this unprecedented control of the optics for a high-energy hadron collider.

DOI: [10.1103/PhysRevAccelBeams.20.061002](https://doi.org/10.1103/PhysRevAccelBeams.20.061002)

I. INTRODUCTION

The 2012 optics commissioning of the LHC reached a new record low β -beating for hadron colliders [1]. Since then, many improvements have been made to equipment, algorithms and analyses to further reduce the errors and uncertainties of the optics measurements and corrections. Improvements to the reconstruction of both β -functions and transverse coupling from turn-by-turn (TbT) data have been made [2,3]. In 2016 dedicated coupling corrections in the LHC brought the closest tune approach to about 2×10^{-4} [4]. This is the lowest level of coupling ever measured in the LHC.

A new online K-modulation application has also been developed, which enables direct measurement of the β^* [5]. It is very important to provide the two main experiments with the same amount of luminosity and hence the same discovery potential [6]. A better understanding of the nonlinear magnetic errors has also been obtained. This includes studies and correction of chromatic coupling [7], nonlinear coupling [8,9], amplitude detuning [10], nonlinear chromaticity [11], and higher order errors in the interaction regions (IRs) [12]. This is an area which will continue to grow in importance as the LHC enters a more challenging regime with an even lower β^* , however the focus of this article is the improvements which enabled the achievement of the 1% control of linear optics in the LHC.

^{*}tobias.persson@cern.ch

Published by the American Physical Society under the terms of the Creative Commons Attribution 4.0 International license. Further distribution of this work must maintain attribution to the author(s) and the published article's title, journal citation, and DOI.

The optics configuration in the LHC is normally referred to by the β^* at the ATLAS and CMS experiments, located in Interaction Point 1 (IP1) and IP5. In 2012 the LHC operated at a β^* of 0.6 m. When the machine was restarted in 2015 this was increased to 0.8 m and in 2016 it was reduced to 0.4 m. This change to the operational configuration makes optics correction even more challenging since the imperfections in the IRs are responsible for a large part of the overall deviation from the design optics [1]. The low β^* is one of the ingredients that has enabled the LHC to reach 1.5×10^{34} cm⁻² s⁻¹ which is 50% above the design value [13,14].

In this paper we describe the changes that have been made since 2012 to obtain an rms β -beating below 1% in the two general purpose and high luminosity experiments. Section II presents the improvements done to the 2015 commissioning and the factors that were limiting the corrections. In 2015 a systematic offset of the longitudinal β -function waist in IP1 and IP5 was discovered which led to a new correction strategy described in Sec. III. The new method incorporated the results from the online K-modulation to further constrain the corrections [5]. Furthermore, the improvements in methods and procedures to obtain the unprecedented low-level β -beating for a high energy collider are described. The result from the optics measurements, after corrections, are presented in Sec. IV. In Sec. V we discuss how the global corrections perform at different configurations and what impact this might have on the foreseen β^* -leveling.

II. 2015 COMMISSIONING

LHC optics commissioning in 2015 took place after more than two years of shutdown, referred to as

Long Shutdown 1 (LS1). The optical configuration featured $\beta^* = 80$ cm at IP1 and IP5. Several improvements were implemented in preparation for this commissioning with the aim to further reduce the error and uncertainty of the optics. A new method to calculate β -functions from the phase advances between beam position monitors (BPMs) had been developed. The previous method used 3 BPMs [15] while the new N-BPM method [3] uses 11 BPMs in the case of the LHC. The BPMs are chosen to have favorable phase advances for the reconstruction of the β -function. This significantly reduces the error bars on the measured β -functions and provides a more accurate estimate of the uncertainty.

The local model used to reconstruct the β -function has also been improved thanks to the ability to read the exact settings of the tune corrector magnets [16,17]. This is important since reconstruction of the β -function relies on the local model.

The AC dipole was upgraded during LS1 to be able to excite the beam for 6600 turns compared to the 2200 before the shutdown. A study of the stability of the AC dipole showed that the horizontal plane for beam 1 had a less stable excitation frequency. Furthermore, an orbit drift disturbing the dispersion measurements is also described in this section. Finally, the measured systematic offset of the β^* -waist in the IPs during 2015 is described.

A. AC dipole performance

The AC dipole creates a coherent betatron oscillation around the closed orbit. This enables beam excitation without emittance increase [18]. The increased length of the TbT data allows investigation of optics stability during one beam excitation. To study potential changes over time the measurement files of 6600 turns were analyzed in parts of 2000 turns each. Noise reduction using the singular value decomposition (SVD) technique [19] was performed for each 2000 turns window separately to avoid additional correlation. This enables the study of the time evolution of observables like the driven and natural tunes in both planes as well as the phase advances between BPMs. Figure 1 shows the evolution of the reconstructed driven tune over time for beam 1 in the horizontal plane. An increase of the driven tune by 10^{-6} can be seen in the horizontal plane for data sets which start from turn number 1000 to 2000. This behavior is not seen in the vertical plane or in any plane for beam 2. It is furthermore visible for different measurement days and different optics. No such behavior is seen for the natural tunes of the machine. Therefore this is assumed to be an artifact produced by imperfection of the AC dipole. Figure 2 shows how the phase advance uncertainty depends on the number of turns analyzed. For the horizontal plane of beam 1, where the measured AC dipole tune unexpectedly changes between turn number 2000 to 3000, the uncertainty on the phase advance also increases with larger numbers of turns analyzed.

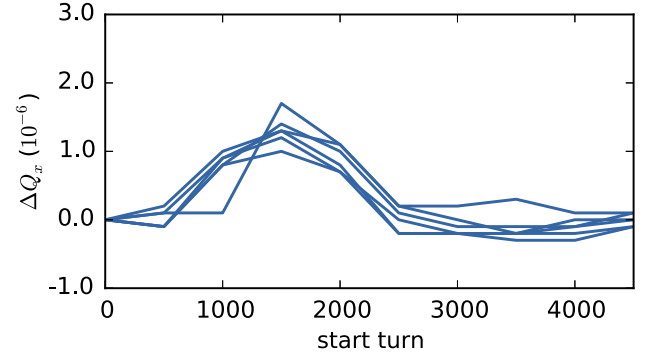


FIG. 1. Measured deviation of the AC dipole horizontal beam 1 tune when 2000 turns out of 6600 were analyzed, starting from different turn numbers. The plot shows six different measurements at a β^* of 80 cm. This bump was not visible for the other plane or beam and has been fixed by replacing the amplifier of the beam 1 AC dipole.

Figure 3 shows the distribution of the phase advance uncertainties for measurements from 2012 (where up to 2200 turns of TbT data were recorded) compared to 2015 (with 6600 turns of TbT data). A rms phase noise below 10^{-3} has been achieved since 2015. The longer TbT data acquisition improves the precision of the measured phase advances. Moreover, a significant difference in the uncertainty is visible for the different planes. This can be attributed to the aforementioned technical issue with the AC dipole in combination of a tendency to excite less in the horizontal plane. This has recently been solved by replacing the amplifier of the beam 1 AC dipole.

B. Orbit drifts

In 2015 orbits were subject to fast drift with periodicity of approximately 8 h [20] due to the movements of the triplet quadrupoles in IP8. This significantly reduced the accuracy of dispersion measurements. This in turn had a negative impact on the performance of the global

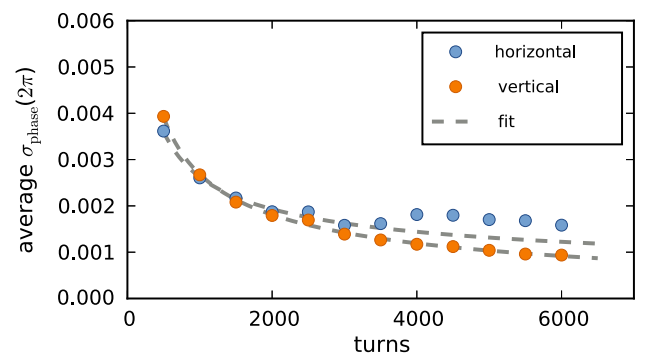


FIG. 2. Average precision of the measured phase advance for different number of turns used in the analysis for beam 1. The fit function is α/\sqrt{x} , and for the horizontal plane only the first five data points were used for the fit.

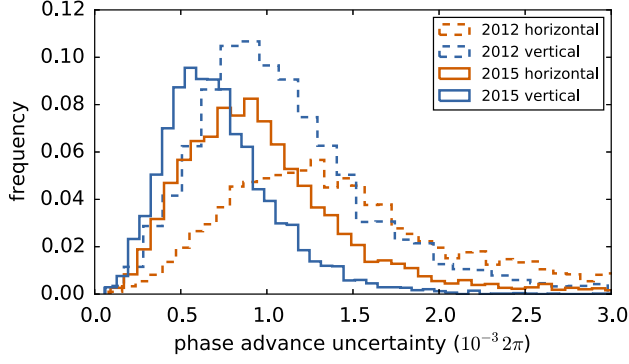


FIG. 3. Uncertainties of the measured betatron phase advances for both beams for optics with $\beta^* = 60$ cm (2012) and $\beta^* = 80$ cm (2015). The y-axis shows the frequency for each level of uncertainty. The total area under each line is normalized to 1.

corrections which correct the β -beating and the normalized dispersion simultaneously [1].

During the 2016 winter shutdown the reason of the movement was traced to cryogenics pressure and temperature regulation and an adequate stabilization system was introduced [20]. These kind of orbit drifts were not observed in 2016.

C. Systematic offset of the β^*

In 2015 it was discovered that there was a systematic offset of the β^* waists in both IP1 and IP5 resulting in an increase of the β^* , causing about 5% luminosity loss [21]. In this article we define the positive waist shift in the direction of the focusing magnet for that plane. Since the two beams travel in opposite direction the direction of positive waist shift will be in opposite physical direction for the two beams in the same plan. This is shown graphically in Fig. 4. The measured β^* and the waist offset measured using K-modulation are shown in Table I. We clearly observe a systematic offset of the waist in the direction of the focusing quadrupole and about 10% β -beating. This was unexpected

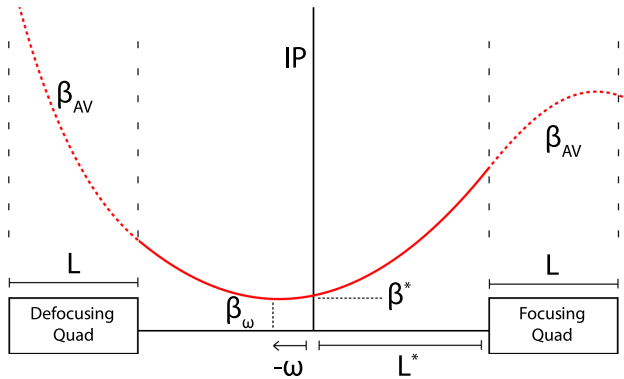


FIG. 4. The conceptual layout and nomenclature for the parameters close to the IP. The read line represents the β -function. The figure is taken from [26].

TABLE I. The measured β^* and waist shift after the final corrections for the 2015 run.

IP	Beam	β_x^* [cm]	β_y^* [cm]	w_x [cm]	w_y [cm]
1	1	88 ± 1	86 ± 1	25 ± 2	23 ± 1
1	2	82 ± 1	83 ± 1	18 ± 2	21 ± 1
5	1	86 ± 1	86 ± 5	22 ± 2	24 ± 9
5	2	87 ± 1	83 ± 2	24 ± 2	16 ± 5

since the estimates of the magnetic errors were unlikely to create such an offset. The assumptions of the gradient uncertainties were based on WISE [22,23], which provides smaller uncertainty values than presented in [24]. In order to estimate whether the measured errors are compatible with the corrections a test of the significance was done. The assumption is that the corrections from 2016 are reproducing the errors. Using this as an input we performed a z-value test [25], which showed that it was less than 4% chance that the errors are following a normal distribution with 0.11% [24] as standard deviation and 0 as mean error. This suggests that the optics errors in the IRs are not well represented by the given rms uncertainty in the triplet quadrupoles. It is possible to propagate the measured β -functions at the BPMs to the IP assuming good knowledge of the model and the size of the imperfections. It was simulated that if quadrupole gradient errors are below 0.04%, as expected in [22], it would result in an accurate estimate of the β^* from the TbT measurement. Offsets of the waist of the β -functions are also important to avoid since it may reduce the available aperture. Furthermore, we also investigated the impact of a longitudinal misalignment of the triplet magnets with an rms of 6 mm. The result shows that the impact is too small to explain the discrepancy.

III. 2016 COMMISSIONING

As described in the previous sections there were several factors limiting optics correction in 2015. In 2016 a regulation of the cryostat was implemented which mitigated the rapid orbit drifts [20]. The problem with the systematic β -function waist offset led to the integration of K-modulation data in optics calculations. K-modulation [5,27] for LHC optics correction is performed using the two most inner magnets close to the IP. This provides a measurement of the β -function in the entire drift space between the magnets. The β -functions which are evaluated at the location of the two most inner BPMs are used for the correction tool. Already during the ion optics commissioning in 2015 additional corrections were performed to mitigate the waist shift [28]. After this experience, the tool for K-modulation measurements was fully automated to obtain the result on-line [26,29], which then could be used in the corrections. The details of this improved procedure and corrections are described in the following sections.

A. Improvements in K-modulation measurements

The K-modulation method has been used to measure the β -functions at the IPs. The average β -functions in the triplet quadrupoles left and right of the IP can be calculated by measuring the tune changes resulting from a gradient modulation in the quadrupole, as described in [26,27,30]. The optics functions are then interpolated towards the IP, thus providing measurements of β^* and the waist.

The online implementation of the K-modulation tool allows for a faster and more accurate measurement of the β^* . Figure 5 shows a typical modulation applied to the quadrupole right of IP1 and the resulting modulated horizontal and vertical tunes in beam 2. The frequency and amplitude of the modulation is generally limited by the quadrupole power converters and the speed of the tune measurement.

K-modulation measurements are performed at injection tunes ($Q_x = 64.28$, $Q_y = 59.31$) which are further away from third order and coupling resonances than the collision tunes ($Q_x = 64.31$, $Q_y = 59.32$).

A cleaning tool has been developed to clean outliers in the tune data online. The domain of acceptance is determined by tracing a parallelogram around the desired data. Figure 6 shows the horizontal tune data for beam 2 obtained after a modulation of the quadrupole left of IP1. The cleaned data, inside the domain of acceptance, is shown in red while the rejected data is shown in blue. This has been a crucial ingredient to efficiently clean the data and obtain accurate results within the time scale of a minute.

The errors in the tune data are determined as a quadrature of the tune precision (2.5×10^{-5}) and the standard deviation resulting from the binning of the base-band-tune (BBQ) [31] data. The binning is necessary due to the lack of synchronization between the tune data and the quadrupole current data. Linear fits of the data provide accurate $\frac{\Delta Q}{\Delta K}$ measurements, as presented in Fig. 6. The typical uncertainty of the fit is between 0.6 m^2 and 1 m^2 . The main variation of the error bar coming from the fit is the quality of the tune measurement.

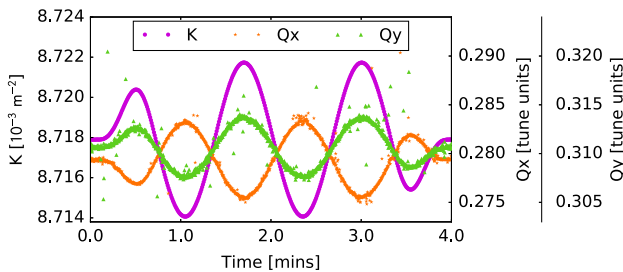


FIG. 5. Horizontal and vertical tune measurements of beam 2 during the gradient modulation of the first quadrupole right of IP1.

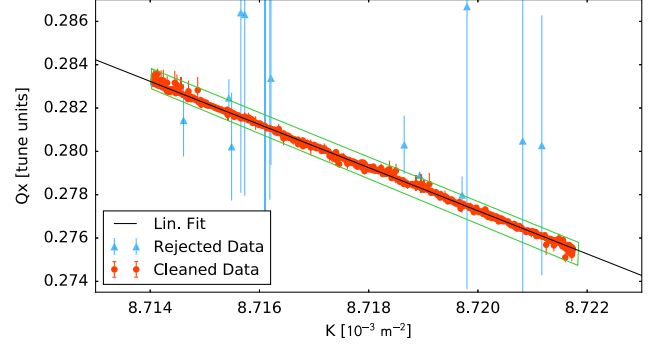


FIG. 6. Linear fit of horizontal tune data for beam 2 with an illustration of the data cleaning process. The rejected data is shown in blue. An online tool is used to specify the domain of acceptance shown in green.

B. Local corrections

Local corrections are applied around the IPs where the magnets are individually powered [1]. The idea is to reconstruct the initial conditions at a location outside the IP and then propagate the optics parameters through the lattice as if it was a beam line. The correction is evaluated for both beams and tested for several optics with larger β^* . Furthermore, since 2016 the β -functions obtained from the K-modulation are also included in the calculation of the local corrections. The upper plot in Fig. 7 shows how corrections calculated in 2015 and 2016 both correct the phase beating. However, in the lower plot of Fig. 7 we observe that it is only the 2016 correction that is able to fit the β -function measured at the two most inner magnets. This illustrates why only the corrections applied in 2016 were able to compensate the waist shift.

In Table II the local corrections for 2012, 2015, and 2016 are shown. The optics errors changed during LS1 which

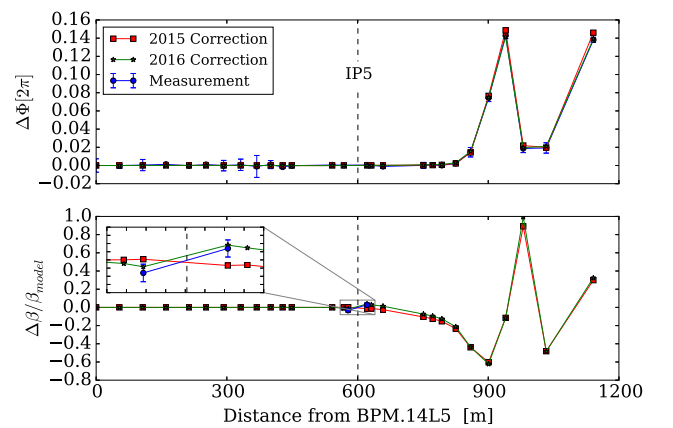


FIG. 7. A comparison between how the 2016 and 2015 corrections would correct the phase error (on top) and the local β -beating (bottom). The red line shows the 2015 correction, the green 2016 and the blue show the measurement. Note that both the lines and points show the deviation from the ideal model.

TABLE II. Local correction strengths from 2012, 2015, and 2016 for (IR) quadrupoles. The circuits of the final focusing quadrupoles are highlighted with a bold font. The powering of the triplets has been $|K_0| = 0.008730 \text{ m}^{-2}$ throughout the years. The polarity indicates if K_0 is positive or negative using the LHC Software Architecture (LSA) convention.

	Circuit	$\Delta k (10^{-5} \text{ m}^{-2})$			Polarity LSA
		2012	2015	2016	
IR1	ktqx1.l1			1.23	–
	ktqx1.r1	1.0		–1.23	+
	ktqx2.l1	1.0	0.35	0.65	+
	ktqx2.r1	–1.4	–0.7	–1.0	–
	ktqx3.l1			1.22	–
	ktqx3.r1			–1.22	+
	kq9.l1b1	1.5			–
IR5	ktqx1.l5		2.0	2.0	–
	ktqx1.r5		–2.0	–2.0	+
	ktqx2.l5	0.7	1.9	0.27	+
	ktqx2.r5	1.05	1.9	1.48	–
	ktqx3.l5			1.49	–
	ktqx3.r5			–1.49	+
	kq4.l5b2	3.80			–

lead to the need for different corrections. This was initially believed to be due to the higher energy, but during a special run at 2.51 TeV in 2015 it was measured that the errors were consistent at the two energies [32]. The sources of the difference between 2012 and 2015 remain unknown, but could derive from longitudinal misalignments or aging of the magnets. The difference in the corrections between 2015 and 2016 derive from the before mentioned correction of the waist shift.

Corrections were also calculated using the Action Phase Jumps method [33,34]. The suggested corrections from this method were similar to the 2015 corrections [35].

In the case of well calibrated BPMs it is possible to reconstruct the β -functions from the amplitude of the oscillations [36,37]. The initial strategy was to use the ballistic optics where the triplets were turned off to calibrate the BPMs and then use them with the new calibrations in the calculation of the local corrections. While the method was not accurate enough to constrain the corrections, it provided important information for debugging the new K-modulation software.

C. Global corrections

Application of the local corrections reduced the β -beating to a peak of about 20%. To reach a lower β -beating a global correction approach is needed. This is required since not all the errors are originating from the IRs. The better corrected optics also provides more margin for other effects such as beam-beam and reduces the luminosity imbalance between the experiments. Global correction in the LHC is

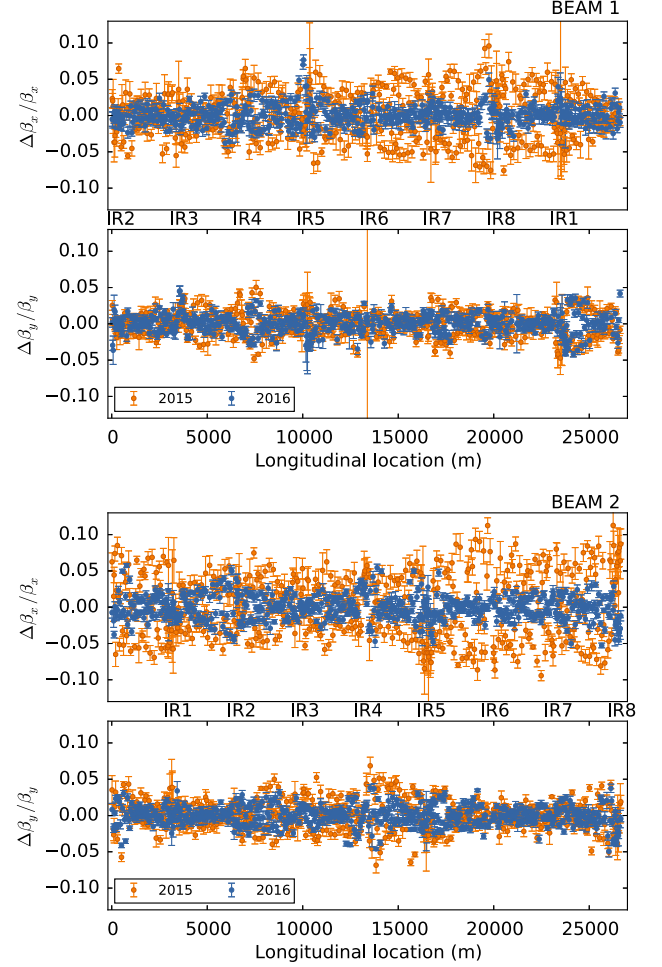


FIG. 8. β -beating at 40 cm β^* for beam 1 (upper) and beam 2 (lower) plot.

based on a response matrix approach. The correction method was improved in 2016 by taking the measurement uncertainties into account as weights. Additionally the quantity specific weights can be specified, i.e., giving a higher weight

TABLE III. Normalized dispersion and min, max and rms of the β -beating (in %) in 2015 and 2016.

	Beam	2015			2016		
		Min	Max	rms	Min	Max	rms
$\frac{\Delta D_x}{\sqrt{\beta_x}} [\sqrt{m}]$	1	–2.2	2.5	0.78	–1.7	1.9	0.52
$\frac{\Delta D_y}{\sqrt{\beta_y}} [\sqrt{m}]$	2	–3.1	2.5	1.13	–1.8	1.6	0.62
$\frac{\Delta \beta_x}{\beta}$	1	–7.6	9.6	3.18	–3.8	7.7	1.42
$\frac{\Delta \beta_y}{\beta}$	1	–4.8	5.0	1.69	–4.2	4.5	1.35
$\frac{\Delta \beta_x}{\beta}$	2	–9.5	11.3	4.24	–5.3	5.8	1.79
$\frac{\Delta \beta_y}{\beta}$	2	–6.8	6.8	2.07	–4.9	3.8	1.42

TABLE IV. The measured β^* before correction, after local correction and after global corrections for the $\beta^* = 40$ cm optics.

	IP 1 β^* [cm]				IP 5 β^* [cm]			
	Beam 1		Beam 2		Beam 1		Beam 2	
	H	V	H	V	H	V	H	V
Before Corr	62.3 \pm 1.2	73.1 \pm 1.0	41.7 \pm 1.3	75.4 \pm 3.0	48.0 \pm 0.8	30.9 \pm 0.1	45.8 \pm 0.2	45.0 \pm 0.8
After Local	41.2 \pm 0.3	40.9 \pm 0.1	36.6 \pm 0.1	40.4 \pm 0.4	35.7 \pm 0.2	40.9 \pm 0.2	40.4 \pm 0.3	40.4 \pm 0.1
After Global	39.8 \pm 0.5	40.1 \pm 0.1	39.8 \pm 0.1	40.1 \pm 0.1	39.9 \pm 0.2	40.1 \pm 0.1	39.5 \pm 0.1	39.6 \pm 0.2

to the β -functions close to the IP than to the phase advance. In every column, the response matrix contains gradients of weighted observables for a change in the model of a quadrupole strength as shown in Eq. (1). The division of two vectors is defined as a vector containing the division of the components with the same index. Quadrupole strength correction, which minimizes the parameters of interest, is obtained through the pseudoinverted response matrix and the measurement vector as shown in Eq. (2). By including results from K-modulation the β -functions at the IP are better corrected, this way minimizing the luminosity imbalance between experiments. In order to find a good trade-off among the observables, corrections are evaluated before they are applied to the machine. The evaluation consists of corrector strengths checks as well as of a prediction of the optics parameters after the correction. This in turn may serve as a figure of merit for the correction weights optimization.

$$\vec{R}_i = \left(\frac{\sqrt{w_{\phi_{x,y}}} \cdot \frac{d\vec{\phi}_{x,y}}{dk_i}}{\vec{\sigma}_{\phi_{x,y}}}, \frac{\sqrt{w_{\beta_{x,y}}} \cdot \frac{d\vec{\beta}_{x,y}}{dk_i}}{\vec{\sigma}_{\beta_{x,y}}}, \frac{\sqrt{w_{ND_x}} \cdot \frac{dND_x}{dk_i}}{\vec{\sigma}_{ND_x}}, \frac{\sqrt{w_Q} \cdot \frac{dQ_{x,y}}{dk_i}}{\vec{\sigma}_{Q_{x,y}}} \right)^T \quad (1)$$

$$\Delta \vec{k} = -\mathbf{R}^{-1} \cdot \left(\sqrt{w_{\phi_{x,y}}} \left(\frac{\Delta \vec{\phi}_{x,y}}{\vec{\sigma}_{\phi_{x,y}}} \right), \sqrt{w_{\beta_{x,y}}} \left(\frac{\Delta \vec{\beta}_{x,y}}{\vec{\sigma}_{\beta_{x,y}}} \right), \sqrt{w_{ND_x}} \left(\frac{\Delta ND_x}{\vec{\sigma}_{ND_x}} \right), \sqrt{w_Q} \left(\frac{\Delta Q_{x,y}}{\vec{\sigma}_{Q_{x,y}}} \right) \right)^T \quad (2)$$

where, $\Delta \vec{k}$ is a vector with the change of k-values, \mathbf{R} is the response matrix composed of the column vectors \vec{R}_i , $w_{\phi_{x,y}}$, $w_{\beta_{x,y}}$, w_{ND_x} , w_Q are the quantity specific weights, $\vec{\phi}$ is a vector containing the phase advances, $\vec{\beta}$ is a vector with the β -functions close to the IPs, $N\vec{D}_x = \frac{\vec{D}_x}{\sqrt{\beta_x}}$ is a vector with the normalized dispersion, $Q_{x,y}$ are the tunes, and $\vec{\sigma}$ are the vectors of the uncertainties of the measurements.

IV. RESULTS

After application of local and global corrections, a final set of measurements with the AC dipole and K-modulation were performed. As a result of the previously mentioned improvements an unprecedented rms β -beating below 2% was achieved in 2016. Figure 8 shows the β -beating for both beams at β^* of 40 cm. The final results have been filtered from malfunctioning BPMs. The filtering was done through removing faulty BPMs using the SVD and removing the BPMs with too high noise levels [38,39]. A small number of BPMs were also removed due to incorrect synchronization of the TbT data. The peak and rms values of the β -beating measured using K-modulation are detailed in Table III. More important than the reduction of the overall β -beating is the improved control at the IP1 and IP5. Table IV shows the measured β^* before and after the different corrections. The final rms β -beating at the IPs is below 1% resulting in an expected luminosity imbalance below 1%. The larger uncertainty in the measurement of the β^* for horizontal beam 1 at IP1 derives from a poor tune measurement. Figure 9 shows a comparison of the average shift of the β^* waist. Table V shows the well corrected waist after the global correction with a maximum deviation of 5.5 cm.

Correction of normalized dispersion was seen to have improved significantly since the problem of orbit drifts were corrected before the 2016 commissioning. The improvements are detailed in Fig. 10 and Table III.

V. BEYOND 2016

The β^* in 2017 is planned to be between 0.33 m and 0.4 m [14]. This will bring the LHC into a regime where the

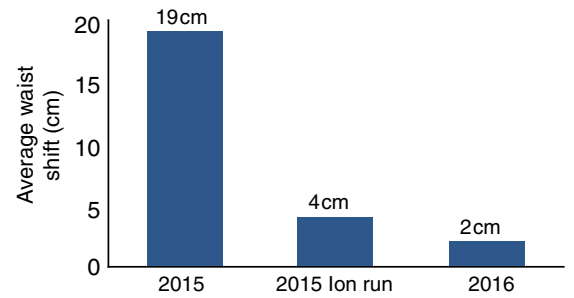
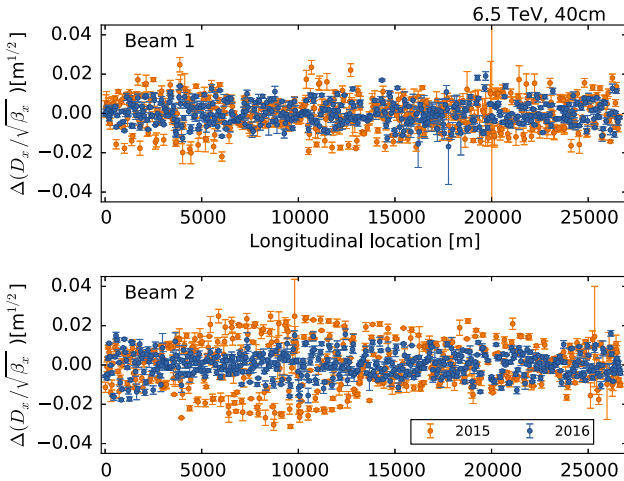
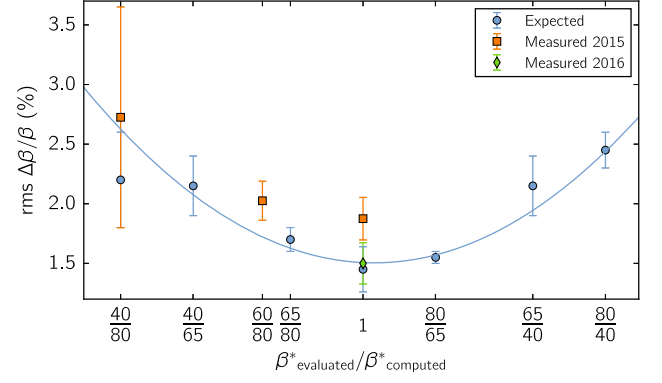


FIG. 9. The average shift of the waist of the β -function at IP1 and IP5 for the $\beta^* = 40$ cm optics.

TABLE V. Measured values of waist offset in IP1 and IP5 after global corrections.

IP	Beam	w_x [cm]	w_y [cm]
1	1	-5.5 ± 1.6	2.3 ± 0.9
1	2	1.7 ± 0.7	0.1 ± 1.1
5	1	3.2 ± 0.9	0.5 ± 0.7
5	2	4.2 ± 0.5	-3.6 ± 1.1

instantaneous luminosity will be limited by the experiments. For a luminosity above $2 \times 10^{34} \text{ cm}^{-2} \text{ s}^{-1}$ pile up in the experiments will be too severe and some type of luminosity leveling will be required [40]. The other limitation on instantaneous luminosity comes from cryogenic power [41]. It is estimated that it can sustain a maximum luminosity of $1.75 \times 10^{34} \text{ cm}^{-2} \text{ s}^{-1}$. While the experiments and the cryostats are not able to cope with too high luminosity the physics program is still interested in maximizing the integrated luminosity. This triggered the idea of having a luminosity leveling using a larger β^* at the beginning of the fill and then decreasing it [42]. In that way the luminosity would stay rather constant throughout the fill. This forces additional constraints on the optics corrections, which would have to be valid for a range of optics. In order to investigate how well the corrections work at different configurations both measurements and simulations were performed. The results are summarized in Fig. 11. It is clearly visible in simulations that a change of β^* of a factor 2 also increases the rms β -beating by about a factor 2. The same trend is observed for the measurements. This demonstrates that the global corrections are working very well for a certain configuration, but are unable to correct effectively a different optics configuration. In order

FIG. 10. Comparison of dispersion beating at β^* of 40 cm between 2015 and 2016.FIG. 11. The rms β -beating when calculating a correction at a certain β^* and applying it at a different. The blue points are based on simulations while the green and orange are based on measurements.

to have a good global corrections for all configurations the errors for all magnets would need to be known, including how they scale with the powering of the magnets. This is currently under investigation and the goal is to identify the errors of the individual magnets. It would also be possible to correct at several different β^* in steps of about 25%.

VI. CONCLUSIONS

The LHC optics has been successfully commissioned down to a β^* of 0.4 m at 6.5 TeV, which is lower than the design value of 0.55 m at 7 TeV. This is the lowest operational β^* used in the LHC and hence the most challenging optical configuration so far. Even so an unprecedented β -beating in a high energy proton collider has been achieved. In particular a control below 1% has been demonstrated for the β^* . This is of importance to provide equal luminosity to the two main experiments. The well-corrected waist is also of importance to provide as much aperture as possible while keeping the β^* at the minimum. These results have only been possible due to the recent improvement in obtaining β -functions on-line from the K-modulation, the incorporation of these results in the local and global corrections, the use of appropriate weights on the different optics parameters, the longer AC dipole plateau, the N-BPM method and the reduction of the orbits drifts from the quadrupole movements.

ACKNOWLEDGMENTS

We greatly thank all LHC Machine Coordinators, Engineers In Charge, and the operation crew for their continuous support during the optics commissioning. The authors also would like to thank Riccardo De Maria and Massimo Giovannozzi for fruitful discussions.

- [1] R. Tomás, R. Calaga, A. Langner, Y.I. Levinsen, E.H. Maclean, T.H.B. Persson, P.K. Skowronski, M. Stzelczyk, G. Vanbavinckhove, and R. Miyamoto, Record low beta-beating in the LHC, *Phys. Rev. ST Accel. Beams* **15**, 091001 (2012).
- [2] T. Persson and R. Tomas, Improved control of the betatron coupling in the Large Hadron Collider, *Phys. Rev. ST Accel. Beams* **17**, 051004 (2014).
- [3] A. Langner and R. Tomas, Optics measurement algorithms and error analysis for the proton energy frontier, *Phys. Rev. ST Accel. Beams* **18**, 031002 (2015).
- [4] E. Maclean, F. Carlier, S. Fartoukh, T. Persson, P. Skowronski, R. Tomás, and D. Wierichs, Report No. CERN-ACC-NOTE-2016-0053.
- [5] M. Khun, V. Kain, A. Langner, and R. Tomás, First k-modulation measurements in the LHC during run 2, in *Proceedings of the International Beam Instrumentation Conference (IBIC), Melbourne, Australia, 2015* (The Australian Synchrotron, Australia, Melbourne, 2015).
- [6] E. Meschi, ATLAS and CMS Luminosity, *129th LHC Machine Committee meeting held on 18 April 2012, CERN, Geneva, Switzerland* (CERN, Geneva, 2012).
- [7] T. H. B. Persson, Y. Inntjore Levinsen, R. Tomás, and E. H. Maclean, Chromatic coupling correction in the Large Hadron Collider, *Phys. Rev. ST Accel. Beams* **16**, 081003 (2013).
- [8] E. H. Maclean, R. Tomás, F. Schmidt, and T. H. B. Persson, Measurement of nonlinear observables in the Large Hadron Collider using kicked beams, *Phys. Rev. ST Accel. Beams* **17**, 081002 (2014).
- [9] R. Tomas, T. H. B. Persson, and E. H. Maclean, Amplitude dependent closest tune approach, *Phys. Rev. Accel. Beams* **19**, 071003 (2016).
- [10] S. White, E. Maclean, and R. Tomás, Amplitude detuning measurement with ac dipole, *Phys. Rev. ST Accel. Beams* **16**, 071002 (2013).
- [11] E. H. Maclean, R. Tomas, F. S. Carlier, A. Langner, L. Malina, T. H. B. Persson, J. Coello de Portugal, P. K. Skowronski, and A. Valdivieso, Report No. CERN-ACC-Note-2016-0013.
- [12] E. H. Maclean, R. Tomás, M. Giovannozzi, and T. H. B. Persson, First measurement and correction of nonlinear errors in the experimental insertions of the CERN Large Hadron Collider, *Phys. Rev. ST Accel. Beams* **18**, 121002 (2015).
- [13] C. Pralavorio, LHC performance reaches new highs, <http://cds.cern.ch/record/2203203> (2016).
- [14] M. Lamont, LHC status and outlook, in *6th HL-LHC Collaboration Meeting, Paris, France* (2016) <https://indico.cern.ch/event/549979/contributions/2257121/attachments/1371133/2079571/LHC-status-HL-Nov16.pdf>.
- [15] P. Castro, J. Borer, A. Burns, G. Morpurgo, and R. Schmidt, Betatron function measurement at LEP using the BOM 1000 turns facility, in *Proceedings of the 15th Particle Accelerator Conference, PAC-1993, Washington, DC, 1993* (IEEE, New York, 1993).
- [16] T. Persson, J. Coello de Portugal, M. Fjellstrom, L. Malina, J. Moeskops, G. Roy, P. Skowronski, and A. Szczotka, Review of the LHC online model implementation and of its applications, in *Proceedings of 7th International Particle Accelerator Conference, Busan, Korea*, edited by C. Petit-Jean-Genaz, D. E. Kim, K. S. Kim, I. S. Ko, K. R. Kim, and V. R. W. Schaa (JACoW, Geneva, Switzerland, 2016).
- [17] J. Coello de Portugal, F. Carlier, A. Langner, T. Persson, P. Skowronski, and R. Tomás, OMC software improvements in 2014, in *Proceedings of the 6th International Particle Accelerator Conference, Richmond, VA*, edited by S. Henderson, E. Akers, T. Satogata, and V. R. W. Schaa (JACoW, Geneva, Switzerland, 2015).
- [18] R. Tomas, A. Franchi, and U. Iriso, Review of Linear Optics Measurement and Correction for Charged Particle Accelerators (to be published).
- [19] R. Calaga and R. Tomás, Statistical analysis of RHIC beam position monitors performance, *Phys. Rev. ST Accel. Beams* **7**, 042801 (2004).
- [20] J. Wenninger, Update on IT movement in IR8, *LBOC Meeting No. 57, CERN, Switzerland, Geneva, 2016*, <https://indico.cern.ch/event/506059/contributions/1184317/>.
- [21] M. Kuhn, Updated results from triplet k-modulation, *LBOC Meeting No. 52*, <https://indico.cern.ch/event/461647/>.
- [22] P. Hagen, M. Giovannozzi, J.-P. Koutchouk, T. Risselada, S. Sanfilippo, E. Todesco, and E. Wildner, WISE: An adaptive simulation of the LHC optics, in *Proceedings of the 10th European Particle Accelerator Conference, Edinburgh, Scotland, 2006* (EPS-AG, Edinburgh, Scotland, 2006).
- [23] P. Hagen P, M. Giovannozzi, J.-P. Koutchouk, T. Risselada, F. Schmidt, E. Todesco, and E. Wildner, WISE: A simulation of the LHC optics including magnet geometrical data, in *Proceedings of the 11th European Particle Accelerator Conference, Genoa, 2008* (EPS-AG, Genoa, Italy, 2008).
- [24] S. Sanfilippo, P. Hagen, J.-P. Koutchouk, M. Giovannozzi, and T. Risselada, Transfer function of the quadrupoles and beta-beating, in *LHC Project Workshop—Chamonix XV* (2006), pp. 151156.
- [25] R. C. Sprinthal, *Basic Statistical Analysis* (Pearson Education, New York, 2011).
- [26] F. Carlier and R. Tomás, Accuracy & feasibility of the β^* measurement for LHC and HL-LHC using K-modulation, *Phys. Rev. Accel. Beams* **20**, 011005 (2017).
- [27] R. Calaga, R. Miyamoto, R. Tomas, and G. Vanbavinckhove, β^* measurement in the LHC based on k-modulation, in *Proceedings of the 2nd International Particle Accelerator Conference, San Sebastián, Spain* (EPS-AG, Spain, 2011).
- [28] T. Persson, β^* corrections strategies, in *LBOC Meeting No. 522015, Geneva, Switzerland*, <https://indico.cern.ch/event/461647/>.
- [29] J. Coello de Portugal, F. Carlier, A. Garcia-Tabares, A. Langner, E. H. Maclean, L. Malina, T. Persson, P. Skowronski, and R. Tomas, Local optics corrections in the HL-LHC IR, in *Proceedings of 7th International Particle Accelerator Conference, Busan, Korea*, edited by C. Petit-Jean-Genaz, D. E. Kim, K. S. Kim, I. S. Ko, K. R. Kim, and V. R. W. Schaa (JACoW, Geneva, Switzerland, 2016).
- [30] M. Kuhn, B. Dehning, V. Kain, R. Tomas, G. Trad, and R. Steinhagen, Technical Report No. CERN-ACC-2014-0159, 2014.

- [31] A. Boccardi, M. Gasior, O. R. Jones, P. Karlsson, and R. J. Steinhausen, First results from the LHC BBQ tune and chromaticity systems, LHC Performance Note 007, 2009.
- [32] L. Malina, Optics errors at 2.51 TeV, in *OMC meeting, CERN, Switzerland, Geneva* https://indico.cern.ch/event/459612/contributions/1973506/attachments/1180972/1709701/Optics_errors_at_2_5TeV.pdf (2015).
- [33] J. F. Cardona and S. G. Peggs, Linear and nonlinear magnetic error measurements using action and phase jump analysis, *Phys. Rev. ST Accel. Beams* **12**, 014002 (2009).
- [34] J. F. Cardona, A. C. Garcia-B, and R. Tomás, Local correction of quadrupole errors at LHC interaction regions using action and phase jump analysis on turn-by-turn beam position data (to be published).
- [35] A. C. García Bonilla, Ph.D. thesis, Universidad Nacional de Colombia, Sede Bogotá, 2015; <http://www.bdigital.unal.edu.co/51630/1/albacarolinagarciaBonilla.2015.pdf>.
- [36] A. Garcia-Tabares, J. Coello, L. Malina, B. Salvachua, P. Skowronski, M. Solfaroli, R. Tomás, and J. Wenninger, Report No. CERN-ACC-NOTE-2016-0008.
- [37] A. Garcia-Tabares Valdivieso, F. Carlier, J. Coello, A. Langner, E. H. Maclean, L. Malina, T. H. B. Persson, P.K. Skowronski, M. Solfaroli, R. Tomás, and J. Wenninger, Optics-measurement-based bpm calibration, in *Proceedings of 7th International Particle Accelerator Conference, Busan, Korea*, edited by C. Petit-Jean-Genaz, D. E. Kim, K. S. Kim, I. S. Ko, K. R. Kim, and V. R. W. Schaa (JACoW, Geneva, Switzerland, 2016).
- [38] A. Garcia, IndiAna Jones and the last calibration, *OMC meeting, CERN, Switzerland, Geneva*, https://indico.cern.ch/event/565942/contributions/2286215/attachments/1329277/1996886/presentation_AGTV_20160831.pdf (2016).
- [39] R. Calaga and R. Tomas, Statistical analysis of RHIC beam position monitors performance, *Phys. Rev. ST Accel. Beams* **7**, 042801 (2004).
- [40] J. Boyd and C. Schwick, Experiments-experience and future, in *7th Evian Workshop, France, 2016* <https://indico.cern.ch/event/578001/contributions/2367027/attachments/1389118/2115414/LPC-Evian2016.pdf>.
- [41] K. Brodzinski, Cryogenics—strategy, unavailability root causes and limitations, in *7th Evian Workshop, France, 2016* https://indico.cern.ch/event/578001/contributions/2366298/attachments/1387785/2112747/2016_Evian_workshop_Cryogenics_final.pdf.
- [42] J. Wenninger and A. A. Gorzawski, Implementation of luminosity leveling by betatron function adjustment at the LHC interaction points, in *Proceedings of the 5th International Particle Accelerator Conference (IPAC 2014) (EPS-AG Dresden, Germany)* (EPS-AG, Dresden, German, 2014).

Paper IV:

**Improving the precision of linear optics measurements
based on turn-by-turn beam position monitor data
after a pulsed excitation in lepton storage rings**

Improving the precision of linear optics measurements based on turn-by-turn beam position monitor data after a pulsed excitation in lepton storage rings

L. Malina*

CERN, Geneva 23, Switzerland and University of Oslo, 0316 Oslo, Norway

J. Coello de Portugal, T. Persson, P. K. Skowroński, and R. Tomás

CERN, Geneva 23, Switzerland

A. Franchi and S. Liuzzo

ESRF, CS 40220, 38043 Grenoble CEDEX 9, France

(Received 24 March 2017; published 4 August 2017)

Beam optics control is of critical importance for machine performance and protection. Nowadays, turn-by-turn (TbT) beam position monitor (BPM) data are increasingly exploited as they allow for fast and simultaneous measurement of various optics quantities. Nevertheless, so far the best documented uncertainty of measured β -functions is of about 10% rms. In this paper we compare the β -functions of the ESRF storage ring measured from two different TbT techniques—the N-BPM and the Amplitude methods—with the ones inferred from a measurement of the orbit response matrix (ORM). We show how to improve the precision of TbT techniques by refining the Fourier transform of TbT data with properly chosen excitation amplitude. The precision of the N-BPM method is further improved by refining the phase advance measurement. This represents a step forward compared to standard TbT measurements. First experimental results showing the precision of β -functions pushed down to 4% both in TbT and ORM techniques are reported and commented.

DOI: [10.1103/PhysRevAccelBeams.20.082802](https://doi.org/10.1103/PhysRevAccelBeams.20.082802)

I. INTRODUCTION

Performance of today's accelerators puts stringent requirements on beam optics control. Moreover, the time spent on optics measurements should be minimized to maximize machine availability. Traditionally, beam optics measurement methods based on the beam closed orbit have been used in synchrotron light sources [1], but the time needed for the measurement could reach several tens of minutes. On the other hand, analysis of turn-by-turn (TbT) beam position monitor (BPM) data allows for simultaneous measurement and correction of various optics quantities as demonstrated in [2–6]. Several beam optics correction methods were compared in [7–9], with typical relative error in the measured β -functions of about 10% rms. In machines requiring a β -beating within 10% [10], it is then necessary to devise optics measurements with better accuracy and precision.

A general analytical study of errors of TbT techniques is reported in [11]. Different linear optics measurement methods applied to the ESRF storage ring were already

compared in [12]. Both works revealed that the key points for a better accuracy are the dependence on the lattice models, as well as by the amplitude of the betatron oscillation vs the BPM resolution and the lattice nonlinearities. In machines with strong nonlinear magnetic elements, such as third-generation and future light sources, the linear analysis of TbT data can be biased by nonlinear terms if the beam excitation is *too large*. In the case of the ESRF storage ring, it is found that amplitudes greater than 1 mm at $\beta_x = 38$ m (action variable, $J_x = 1.3 \times 10^{-8}$ m) are already affected by such terms. In principle lower excitations would be possible by firing the kicker magnet with a weaker current, though the one used at the ESRF storage ring suffers from stability and reproducibility issues at low pulse currents.

We applied two beam optics measurement techniques to TbT data from the ESRF storage ring: the N-BPM method [13] and the Amplitude approach [14]. Both procedures are based on the harmonic analysis of TbT data from all BPMs. The beam is excited in both planes by pulsed magnets (kickers inducing free oscillations). The Amplitude technique evaluates the β -function from the amplitude of the tune spectral line at each BPM and is biased by BPM calibration errors as discussed for example in [15]. The N-BPM method extracts the β -function from the BPM phase advance computed from the phase of the tune line as described in [13]. The β -functions measured with these two

*lukas.malina@cern.ch

Published by the American Physical Society under the terms of the [Creative Commons Attribution 4.0 International](#) license. Further distribution of this work must maintain attribution to the author(s) and the published article's title, journal citation, and DOI.

techniques are compared to those inferred from the measurement and fit of the orbit response matrix (ORM), i.e., of the closed orbit response to a unit change of orbit corrector strengths [16]. The machine model is fitted to reproduce the measured matrix, namely dipole and quadrupole tilts, dipole and quadrupole strength errors, as well as BPM calibration factors. This fit provides an effective model (called the ORM model). The ORM measurement routinely carried out at the ESRF takes about 20 minutes. More generally, the measurement time scales with the length of the storage ring, whereas the one of the TbT techniques is a matter of at most seconds. However, the switch between TbT and orbit modes may require up to twenty minutes, as the ESRF storage ring is equipped with BPM electronics [17], which are not suitable for quick switch between the modes.

In lepton machines synchrotron radiation results in the damping of the TbT transverse motion after a pulsed excitation influencing the analysis of TbT data in two main aspects. First, the evaluation of BPM phase advance, from the phase of the tune spectral line, shows a dependence on the choice of the first turn of the TbT batch of data to be analyzed (even at the level of single turns). A correction to this issue was found in [18]. Second, the natural reduction of the oscillation amplitude over time can be used to obtain a batch of TbT data for the harmonic analysis a few milliseconds after the kicker pulse (strong enough to ensure its stability) with an amplitude sufficiently low to prevent non-linear terms from spoiling the linear analysis of the tune line.

Here we define the terms of: accuracy—the difference to the true value and precision—the spread of the measurements including the known systematic effects. Assuming we have the quantity which has a true value of 1.00, 1.00 ± 0.01 is precise and accurate, 0.90 ± 0.01 is precise, but inaccurate and 1.0 ± 0.1 is imprecise but accurate estimate of the value.

The paper is structured as follows. In Sec. II the measurement setup is outlined, whereas an error analysis of the different measurement techniques based on single-particle simulations of the ESRF storage ring is detailed in Sec. III. Experimental results are eventually discussed and compared in Sec. IV.

II. DEDICATED OPTICS MEASUREMENT

A special sextupole setting was designed and implemented to have both linear chromaticity and amplitude detuning close to zero, resulting in at least several hundred turns of exploitable data for the harmonic analysis.

Optics measurements were performed with transverse oscillation decoherence times of about 740 and 1850 turns in the horizontal and vertical planes, respectively. The synchrotron radiation damping time is about 2500 turns. The fractional betatron tunes were close to nominal values at 0.4414 in the horizontal plane and 0.3899 in the vertical

plane. The measured linear chromaticity was -1.0 and $+0.2$ in the two planes (compared to the operational values of 8 and 13, respectively). 330 bunches with a total current of 7 mA were stored to avoid beam instabilities and position interlocks during the beam excitation. Prior to TbT measurements, linear lattice errors (β -beating, dispersion and coupling) were measured and corrected via ORM analysis reaching typical operational values, i.e. $\sim 5\%$ and $\sim 3\%$ rms β -beating in the two transverse planes and an emittance ratio of $\epsilon_y/\epsilon_x \approx 1\%$. A second ORM was measured and fit to evaluate the β -functions to be used as reference. After that, BPMs were switched to TbT mode and data with maximum amplitude in the range from 0.7 mm ($J_0 = 6.5 \times 10^{-9}$ m) to 1.4 mm ($J_0 = 2.6 \times 10^{-8}$ m) at $\beta = 38$ m were acquired. The beam was excited by kickers located at $\beta_x = 5.1$ m and $\beta_y = 30.5$ m. The time difference between the ORM and TbT measurements was about 3 hours. TbT measurements were repeated for 5 different beam energies (with a $\pm 0.168\%$ span of $\Delta p/p$). For each kicker and energy setting, ten acquisitions were taken.

III. PRECISION AND ERROR ANALYSIS

The performance of a harmonic analysis depends, among other elements, on the number of analyzed turns. Simulations have been carried out in order to evaluate the best number of turns and kicker strength ensuring the highest measurement precision. Single particles with various initial transverse displacements were tracked along the lattice of the ESRF storage ring. The lattice β -functions are shown in Fig. 1. The average horizontal and vertical β -functions are comparable.

BPM noise in TbT mode is estimated from singular value decomposition (SVD)-cleaning [19–21] of measured data. The decomposed TbT data are recomposed using only the 12 largest singular values, this way the noise floor is removed and the data are cleaned. The rms of the

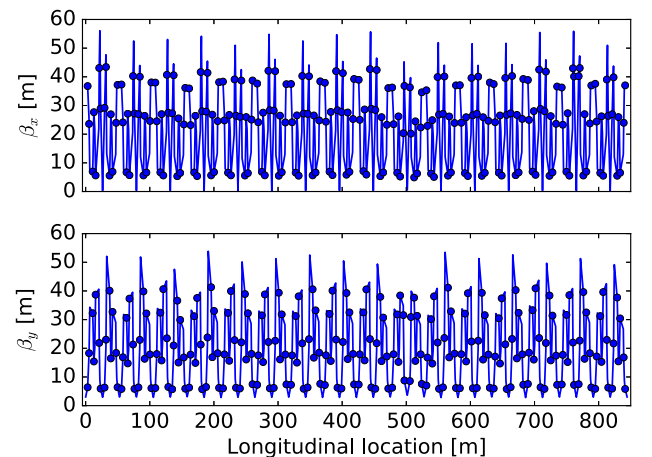


FIG. 1. The lattice β -functions along the ESRF storage ring. The markers refer to BPM positions.

differences between the raw and cleaned data for each BPM provided an average noise of $9.6 \mu\text{m}$ in the horizontal plane and $8.8 \mu\text{m}$ in the vertical plane. This BPM noise was added to the simulated TbT data before being analysed using different numbers of turns with the initial displacement of 0.55 mm (horizontal) and 0.15 mm (vertical) at $\beta_x = 38 \text{ m}$ and $\beta_y = 2.9 \text{ m}$ (initial actions: $J_{x0} = 4.0 \times 10^{-9} \text{ m}$ and $J_{y0} = 3.9 \times 10^{-9} \text{ m}$). Note that the actions of the horizontal and vertical kicks are very similar. The errors of the retrieved BPM phase advance and β -beating as a function of the number of turns are shown in Figs. 2 and 3, respectively. Because the errors disappeared by removing the sextupoles in the simulation it can be concluded that they are dominated by lattice nonlinearities.

As expected from [22], the degradation of the accuracy in evaluation of phase advance and β -function below 1200 turns (blue curves in Figs. 2 and 3) is largely removed when the tune averaged over all BPMs is used to define the tune spectral line (red curves), instead of using the tune peak detected at each single BPM. Therefore in the analysis of experimental data the tune line is forced to be equal to the average tune.

Larger transverse beam excitations modify the content of the tune spectral line, whose amplitude and phase include non-linear terms (proportional to the initial amplitude) stemming from sextupoles in the case of ESRF storage ring [4,11]. Figure 4 shows the artificial β -beating, inferred from the N-BPM method, applied to simulated data with different initial displacements. Up to 45% peak artificial β -beating is observed with an initial amplitude of 4.4 mm at $\beta_x = 38 \text{ m}$ ($J_{x0} = 2.5 \times 10^{-7} \text{ m}$). To decrease the inaccuracy to 2%

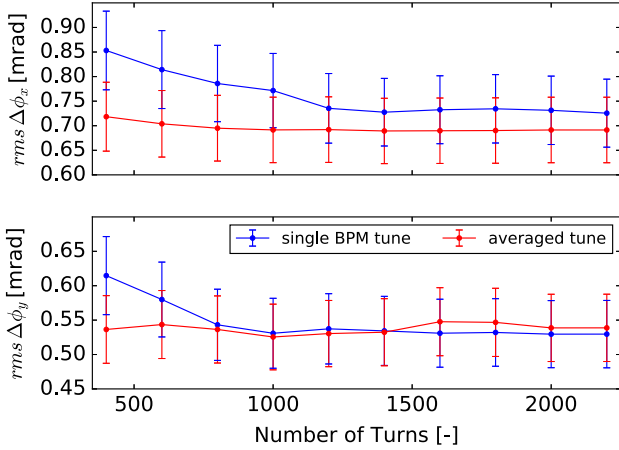


FIG. 2. Simulated rms phase-advance error computed from single-particle simulations of the ESRF storage ring lattice as a function of the number of turns used for the analysis in two cases where the betatron tune is calculated from a single BPMs or averaged over the set of all BPMs (realistic noise has been added to BPM TbT data). The initial displacement of 0.55 mm (horizontal) and 0.15 mm (vertical) at $\beta_x = 38 \text{ m}$ and $\beta_y = 2.9 \text{ m}$ (initial actions: $J_{x0} = 4.0 \times 10^{-9} \text{ m}$ and $J_{y0} = 3.9 \times 10^{-9} \text{ m}$).

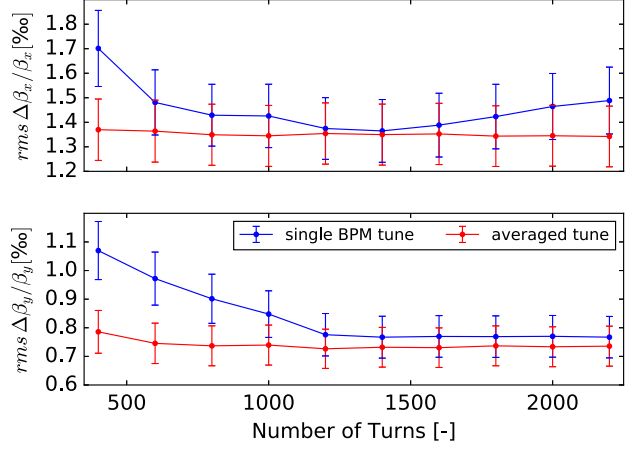


FIG. 3. Simulated rms of artificial β -beating computed by N-BPM from the same single-particle simulations of Fig. 2.

in the measurement of the horizontal β -functions an initial displacement below 0.7 mm (always at $\beta_x = 38 \text{ m}$) is needed, as shown in Fig. 5. The requirement is more relaxed in the vertical plane, for which an initial displacement below 0.17 mm at $\beta_y = 2.9 \text{ m}$, which is equivalent to 0.62 mm at $\beta_y = 38 \text{ m}$ in the horizontal plane, decreases the inaccuracy to 1%. It is factor 2 lower compared to the horizontal plane. As the beam dynamics becomes nonlinear both phase and amplitude of the tune line are perturbed [11]. This may in turn cause a significant disagreement between the two methods at *large* amplitudes, as seen in Fig. 5.

TbT data with the lowest amplitude of the oscillation (0.7 mm) were chosen for the analysis since in this case the linear optics measurements are the least perturbed by amplitude detuning and nonlinearities. Moreover, the natural transverse damping induced by synchrotron radiation has been used to further decrease the systematic effect of

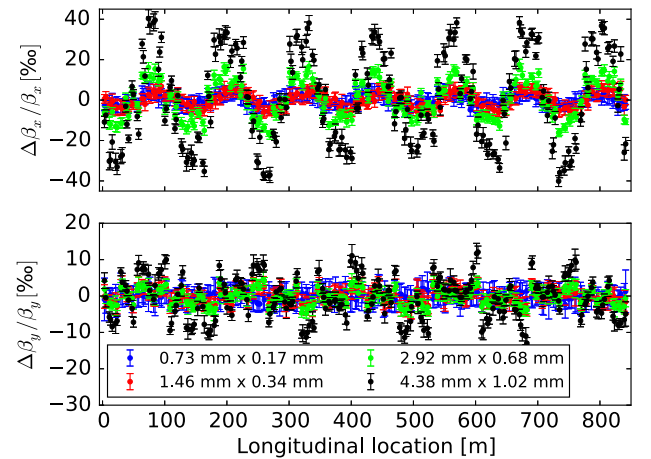


FIG. 4. Simulated artificial β -beating computed by N-BPM from single-particle simulations of the ESRF storage ring lattice at different initial displacements ($\beta_x = 38 \text{ m}$ and $\beta_y = 2.9 \text{ m}$) corresponding to actions from $\sim 5 \times 10^{-9} \text{ m}$ to $\sim 2.5 \times 10^{-7} \text{ m}$.

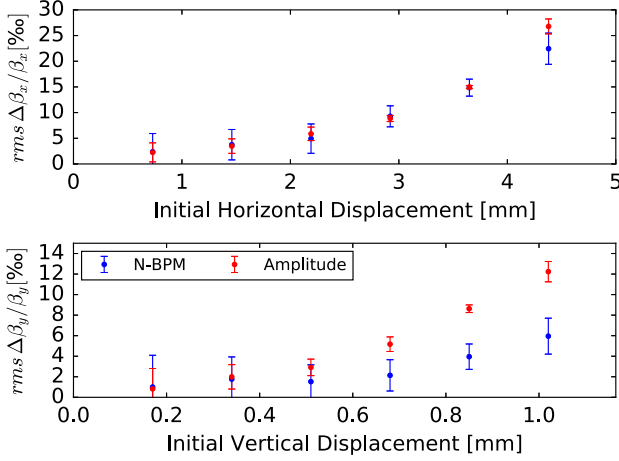


FIG. 5. Simulated rms of artificial β -beating computed by N-BPM and Amplitude methods from the same single-particle simulations with different diagonal initial displacement as in Fig. 4. The error bars refer to the mean (single-BPM) error bars averaged over all BPMs.

sextupoles, in our case by analyzing only a batch of data 200 turns after the kick (for larger kicks longer delay may be needed). Such a shift ensures a maximal transverse oscillation only slightly above 0.5 mm (horizontally, still at $\beta_x = 38$ m) and 0.15 mm (vertically, $\beta_y = 2.9$ m). After the raw data are SVD-cleaned, harmonic analysis is performed using an FFT with frequency interpolation by Jacobsen's method with bias correction [23]. The analyses and errors specific to the TbT methods are described in the following subsections.

A. N-BPM method

The β -function evaluated from the N-BPM method [13] is a weighted average of β -functions obtained from various combinations of BPM triplets, using model transfer matrices in between them. Therefore, uncertainties in the model influence the measurement of β -functions. Ten thousand lattices were simulated, to estimate the resulting systematic error on the β -function calculated from phase advances between a given combination of BPMs. To account for the effects of various sources of error, the estimated misalignments and uncertainties of magnetic properties were added to simulated lattices. The estimated uncertainties were tailored down in order to realistically reproduce the measured rms β -beating. The corresponding estimates of lattice uncertainties are shown in Table I.

The N-BPM method is influenced by phase advance measurement errors, therefore it is sensitive to errors in the synchronization among the BPMs. A phase advance variation has been observed both in simulation and in the measurement, when analysing the TbT data delayed even by a single turn. The variation resulted in rms β -beating up to 10‰ (with a delay of 3 or 4 turns as shown in Fig. 6). This was found to be an effect of the

TABLE I. Estimated Gaussian uncertainties of the ESRF lattice using the ORM inferred model.

Uncertainty	$\sigma_{\text{ORM model}}$
Longitudinal quadrupole misalignment	0.2 mm
Longitudinal BPMs misalignment	0.2 mm
Transverse sextupole misalignment	10 μm
Quadrupole gradient	0.1‰
BPM resolution (horizontal plane)	9.6 μm
BPM resolution (vertical plane)	8.8 μm

transverse damping. In order to refine the phase advance measurement we implemented the phase correction given in [18] for a signal approximated by

$$x_k = Ae^{-\alpha k} \cos(\nu k + \phi + \epsilon), \quad (1)$$

where k , A , and α are the turn number, the amplitude and the damping coefficient. ν , ϕ , and ϵ are the betatron tune, the phase of the tune spectral line and the correction to the phase (all in radians), that is given by

$$\epsilon = \frac{e_1 - e_2}{e_3 - e_4}, \quad (2)$$

where

$$\begin{aligned} e_1 &= \frac{1}{2} \sum_k Ae^{-2\alpha k} \sin 2(\nu k + \phi) \\ e_2 &= \sum_k x_k e^{-\alpha k} \sin(\nu k + \phi) \\ e_3 &= \sum_k x_k e^{-\alpha k} \cos(\nu k + \phi) \\ e_4 &= \sum_k Ae^{-2\alpha k} \cos 2(\nu k + \phi). \end{aligned}$$

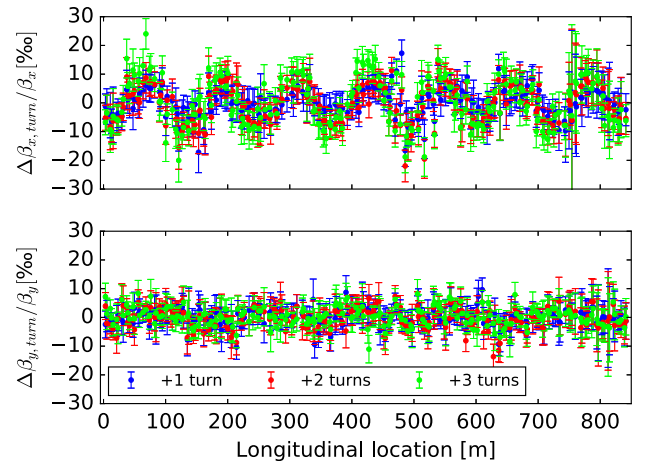


FIG. 6. Measured β -beating when analyzing the TbT data delayed by different number of turns.

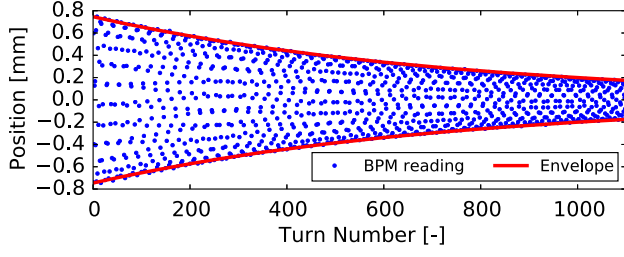


FIG. 7. TbT BPM position readings with estimated exponential envelope.

A robust estimator of the amplitude and damping coefficient has been developed and a sample of TbT data with its estimated exponential envelope is shown in Fig. 7. The correction gives stable results only if the average orbit is subtracted from the data. This improved the robustness of phase advance measurement, resulting in rms β -beating decreased to at most 0.4‰, typically even 0.2‰.

In order to account for the systematic error in the evaluation of the β -beating from nonlinear terms *polluting* the tune spectral line, single-particle simulations were run with initial amplitudes equivalent to those of the measurements. For each amplitude, the resulting artificial β -beating was quantified, as in Fig. 5, and its rms value was included in the systematic error associated to the analysis of experimental data.

B. Amplitude method

The betatron motion at a given BPM is described by Eq. (1). The undamped amplitude of the tune spectral line is

$$A = C\sqrt{2\beta J}, \quad (3)$$

where J is the action (invariant along the ring), while C and β are the BPM gain (≈ 1) and β -function, respectively. All are entangled, as only the product $C\sqrt{\beta J}$ is observable. By assuming BPM gain is the same for all monitors, a way to extract $C\sqrt{J}$ (and hence the β -function at the BPMs) is to impose that model and measured average β -functions be equal, i.e. $K \cdot C^2 \langle \beta^{(\text{meas})} J \rangle = \langle \beta^{(\text{mod})} \rangle$, where K is a global scaling factor. This approach adds in turn two systematic effect, because the average β -function increases with the rms β -beating [11,24] and C changes between BPMs. The BPM calibration errors can be indirectly estimated by comparing the β -functions obtained from N-BPM and Amplitude methods, the former not being affected by these errors.

The dependence of average β -beating on rms β -beating of perturbed lattices with respect to the unperturbed model has been simulated. This turns out to be quadratic (in agreement with [24]), as shown in Fig. 8. The measured β -functions are corrected for this effect of rms β -beating.

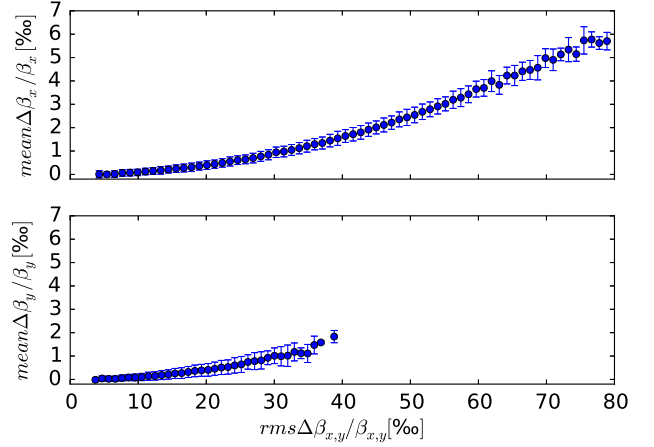


FIG. 8. Average β -beating vs rms β -beating (binned) of perturbed simulated lattices with respect to the unperturbed model of the ESRF storage ring (simulations).

The uncertainty in the simulated average β -beating (for a given rms β -beating) was included in the experimental systematic error, together with the artificial β -function accuracy mentioned above. The error in the analysis of experimental data consists of these systematic errors and statistical errors of β -function measurement.

C. ORM method

To the best of our knowledge, no theoretical study on the accuracy of the ORM method has been published so far. In order to evaluate a systematic error for the ESRF storage ring, numerical simulations have been carried out. Ten different sets of linear lattice errors generating the measured rms β -beating have been created. The ORM analysis has been simulated on those sets and the fitted models have been used to compute ten sets of β -functions at the BPMs. These have been compared to the expected values, yielding an rms uncertainty of about 3‰. The inclusion of the BPM resolution at 10 nm level did not deteriorate that accuracy. In order to estimate the statistical error, we carried out 5 consecutive ORM measurements which resulted in a rms uncertainty of about 5‰ in the horizontal plane and about 2‰ in the vertical plane. This gives the measured β -function precision of 6‰ in horizontal plane and 4‰ in vertical plane.

IV. COMPARISON OF RESULTS

In order to measure the β -functions most precisely, the batch of TbT data 200 turns after the kick with the lowest amplitude was analyzed. In this case the linear optics is the least disturbed by amplitude detuning and non-linearities. The average relative precision of β -functions obtained by different methods is shown in Table II. The N-BPM precision is mainly consisting of the statistical error, and

TABLE II. Relative precision of β -functions obtained by different methods.

Mean relative precision of β s	x [%]	y [%]
N-BPM	4	4
Amplitude	15	12
ORM	6	4

TABLE III. Measured β -beating between different methods.

Rms β -beating	x [%]	y [%]
N-BPM vs Amplitude	17	12
Amplitude vs ORM model	20	13
N-BPM vs ORM model	11	9

remains at the level of 4‰ even if lattice uncertainties are tripled. The precision of the Amplitude method is dominated by BPM gain errors, the contribution of all other sources of error together are less than 5‰.

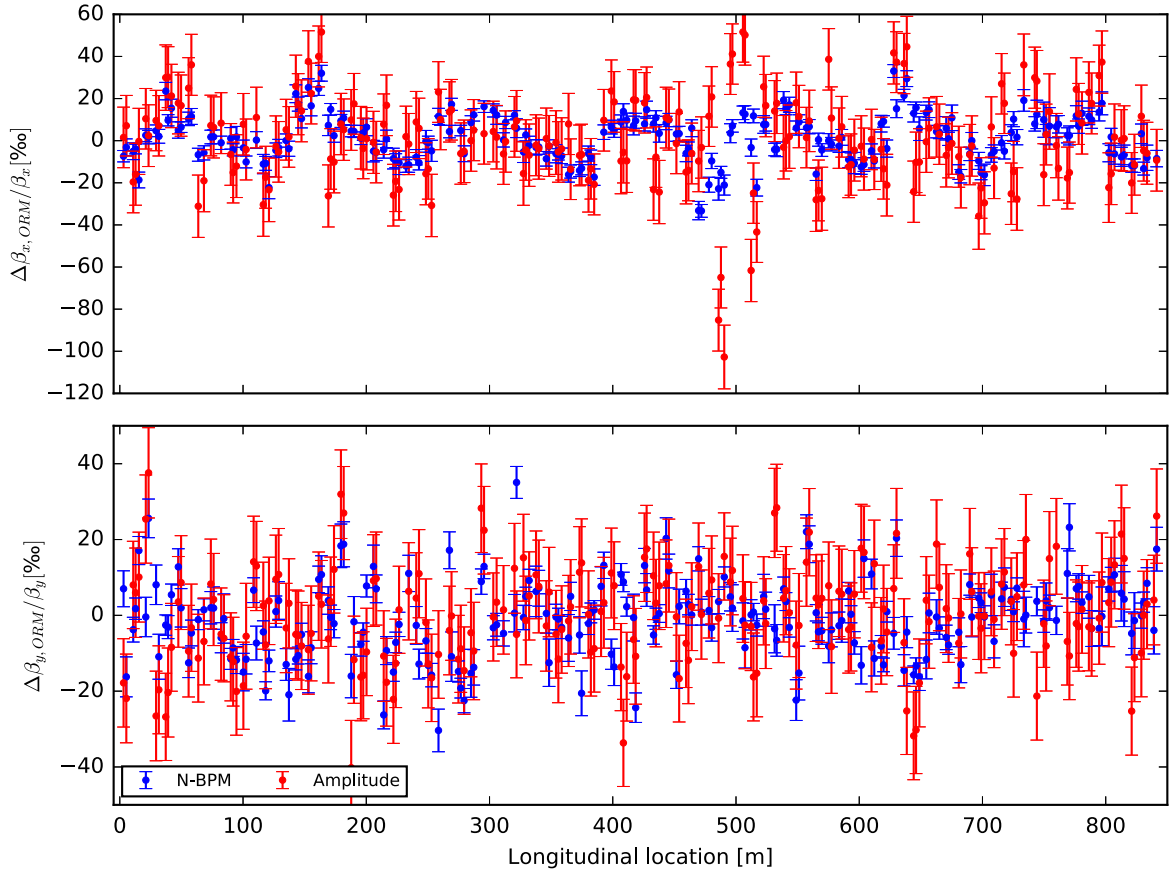
The measured β -beating is shown in Table III and Fig. 9. A drift of the closed orbit of about 15 μm rms was observed between ORM and TbT measurements: simulations suggest that about 5‰ of the difference in the β -beating

between ORM and TbT techniques can be attributed to this orbit drift.

Phase advances between the neighboring BPMs (a more robust observable) were measured from TbT data and compared to those obtained from the ORM model. The difference is shown in Figure 10. The agreement is generally better in horizontal plane. Error bars shown in Fig. 10 are from the TbT measurement only, as there is no estimate of phase advance error inferred from the ORM method.

At a longitudinal location of around 500 m, there is a local insertion optics. A larger than the average discrepancy is visible along that region both in the horizontal β -beating from the Amplitude method (Fig. 9) and in the phase advance beating between TbT measurement and ORM model (Fig. 10). This suggests the existence of local errors not included in the ORM model, in which the phase advances are not fit. The failure of the ORM method to reproduce the lattice errors, has been already observed in [25].

Finally, we compare the normalized dispersion $D/\sqrt{\beta}$, where D stands for dispersion. Normalized dispersion was measured from closed orbit using ORM and from TbT data, their difference shown in Fig. 11. Differences between the two measurements are well within the error bars.

FIG. 9. Measured β -beating with respect to the ORM model.

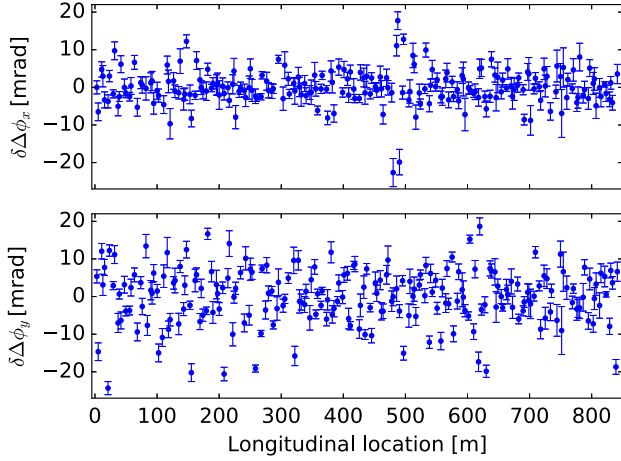


FIG. 10. Measured phase advance beating between neighboring BPMs with respect to the ORM model.

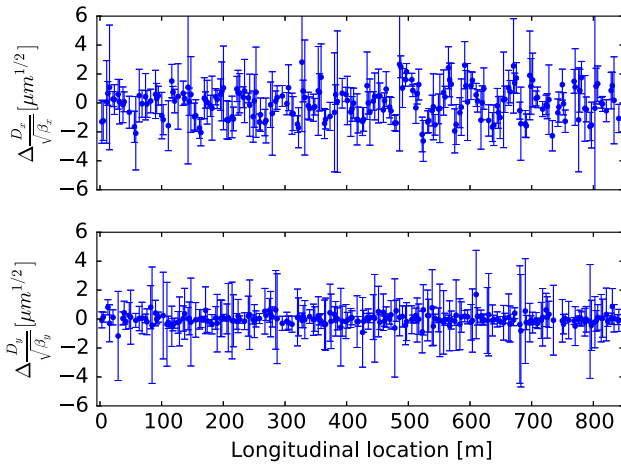


FIG. 11. Difference between measured normalized dispersion obtained from TbT data and from ORM.

V. CONCLUSIONS AND OUTLOOK

Three optics measurement methods were used and their results compared for the ESRF storage ring. A precision of 4‰ for evaluation of β -functions was obtained in both planes by the N-BPM method, as well as in the vertical plane from the ORM method. The horizontal plane from the ORM is slightly worse, reaching a precision of 6‰. The β -beating measured by N-BPM method and ORM are agree to the 10‰ level, which gives an experimental upper limit estimate of the accuracy of the methods. Nevertheless, there is the issue of the time between the two measurements and possible orbit drifts may account for 5‰. The agreement between the Amplitude method and the other two techniques is similar in the vertical plane, but factor 2 worse in the horizontal plane (up to 20‰).

Similar measurements were performed in the ALBA storage ring [9], which has the same BPM hardware and software. The BPM measurement noise at ALBA is about

7 μm [26], most probably due to lower level of mechanical vibrations making the beam more stable. The N-BPM method reached 8‰ precision in the horizontal plane and 6‰ in the vertical plane [26] as defined in the Introduction. By counteracting the effect of oscillation damping and by using smaller kick amplitudes, as it is done here, most probably ALBA measurement precisions could be further improved.

Nevertheless, the 4‰ precision of the N-BPM method is expected to be limited to optics with low decoherence only, while the ORM method performance is less affected for optics with larger chromaticity and amplitude-dependent detuning. The quick decoherence of TbT BPM data can be overcome by replacing pulsed magnets (kickers) as source of excitation with AC-Dipoles [27], or shakers [28]. The beam is excited every turn (undergoing the forced oscillation), this way arbitrary transverse oscillation amplitudes are maintained for arbitrary number of turns independently of the optics. The induced forced oscillation would allow for thousands of exploitable turns at sufficiently low amplitude. The AC-Dipole has a variety of applications [22,29–32], however a detailed systematic study on the interplay between such excitation, radiation damping, and diffusion is still missing. The applicability of such device in the realm of lepton machines still needs to be assessed.

ACKNOWLEDGMENTS

The authors would like thank to the ESRF operators for the preparation of beam, to A. Langner who wrote the N-BPM method analysis software and to L. Farvacque who developed the data acquisition software.

- [1] R. Tomás, M. Aiba, A. Franchi, and U. Iriso, Review of linear optics measurement and correction for charged particle accelerators, *Phys. Rev. Accel. Beams* **20**, 054801 (2017).
- [2] R. Tomás, M. Bai, R. Calaga, W. Fischer, A. Franchi, and G. Rumolo, Measurement of global and local resonance terms, *Phys. Rev. ST Accel. Beams* **8**, 024001 (2005).
- [3] R. Tomás, O. Brüning, M. Giovannozzi, P. Hagen, M. Lamont, F. Schmidt, G. Vanbavinckhove, M. Aiba, R. Calaga, and R. Miyamoto, CERN Large Hadron Collider optics model, measurements and corrections, *Phys. Rev. ST Accel. Beams* **13**, 121004 (2010).
- [4] A. Franchi, L. Farvacque, F. Ewald, G. LeBec, and K. B. Scheidt, First simultaneous measurement of sextupolar and octupolar resonance driving terms in a circular accelerator from turn-by-turn beam position monitor data, *Phys. Rev. ST Accel. Beams* **17**, 074001 (2014).
- [5] A. Langner *et al.*, Developments of the segment-by-segment technique for optics corrections in the LHC, in *Proceedings of IPAC'15, Richmond, USA, 2015* (JACoW, Geneva, Switzerland, 2015), paper MOPJE054.

- [6] X. Yang and X. Huang, Simultaneous linear optics and coupling correction for storage rings with turn-by-turn beam position monitor data, [arXiv:1511.02450v1](#).
- [7] M. Aiba, M. Böge, J. Chrin, N. Milas, T. Schilcher, and A. Streun, Comparison of linear optics measurement and correction methods at the Swiss Light Source, *Phys. Rev. ST Accel. Beams* **16**, 012802 (2013).
- [8] G. Wang *et al.*, Experimental crosscheck of algorithms for magnet lattice correction, in *Proceedings of IPAC'16, Busan, Korea, 2016* (JACoW, Geneva, Switzerland, 2016), paper THPMR008.
- [9] A. Langner, G. Benedetti, M. Carlà, U. Iriso, Z. Martí, J. Coello de Portugal, and R. Tomás, Utilizing the N beam position monitor method for turn-by-turn optics measurements, *Phys. Rev. Accel. Beams* **19**, 092803 (2016).
- [10] Y. Jiao and Z. Duan, Statistical analysis of the limitation of half integer resonances on the available momentum acceptance of the High Energy Photon Source, *Nucl. Instrum. Methods Phys. Res., Sect. A* **841**, 97 (2017).
- [11] A. Franchi, Error analysis of linear optics measurements via turn-by-turn beam position data in circular accelerators, [arXiv:1603.00281v2](#).
- [12] L. Malina *et al.*, Comparison of optics measurements methods in ESRF, in *Proceedings of IPAC'16, Busan, Korea, 2016* (JACoW, Geneva, Switzerland, 2016), paper THPMB045.
- [13] A. Langner and R. Tomás, Optics measurement algorithms and error analysis for the proton energy frontier, *Phys. Rev. ST Accel. Beams* **18**, 031002 (2015).
- [14] J. Borer *et al.*, Harmonic analysis of coherent bunch oscillations in LEP, in *Proceedings of EPAC'92, Berlin, Germany, 1992* (ASF, Berlin, Germany, 1992), p. 1082.
- [15] A. Garcia-Tabares Valdivieso *et al.*, Optics-measurement-based BPM calibration, in *Proceedings of IPAC'16, Busan, Korea, 2016* (JACoW, Geneva, Switzerland, 2016), paper THPMB041.
- [16] W. J. Corbett *et al.*, A fast model-calibration procedure for storage rings, in *Proceedings of the 15th Particle Accelerator Conference, PAC-1993, Washington, DC, 1993* (IEEE, New York, 1993), p. 108.
- [17] B. K. Scheidt and F. Epaud, Installation and commissioning of a complete upgrade of the BPM system for the ESRF storage ring, in *Proceedings of DIPAC09, Basel, Switzerland, 2009*, (JACoW, Basel, Switzerland, 2009), p. 50.
- [18] W. Guo *et al.*, A lattice correction approach through betatron phase advance, in *Proceedings of IPAC'16, Busan, Korea, 2016* (JACoW, Geneva, Switzerland, 2016), paper MOOCB02.
- [19] J. Irwin, C. X. Wang, Y. T. Yan, K. L. F. Bane, Y. Cai, F.-J. Decker, M. G. Minty, G. V. Stupakov, and F. Zimmermann, Model-Independent Beam Dynamics Analysis, *Phys. Rev. Lett.* **82**, 1684 (1999).
- [20] R. Calaga and R. Tomás, Statistical analysis of RHIC beam position monitors performance, *Phys. Rev. ST Accel. Beams* **7**, 042801 (2004).
- [21] X. Huang, S. Y. Lee, E. Prebys, and R. Tomlin, Application of independent component analysis to Fermilab Booster, *Phys. Rev. ST Accel. Beams* **8**, 064001 (2005).
- [22] N. Biancacci and R. Tomás, Using AC dipoles to localize sources of beam coupling impedance, *Phys. Rev. Accel. Beams* **19**, 054001 (2016).
- [23] Ç. Candan, A method for fine resolution frequency estimation from three DFT samples, *IEEE Signal Processing Letters* **18**, 351 (2011).
- [24] R. Calaga, R. Tomás, and F. Zimmermann, BPM calibration independent LHC optics correction, in *Proceedings of the 22nd Particle Accelerator Conference, PAC-2007, Albuquerque, NM* (IEEE, New York, 2007), p. 3693.
- [25] M. Aiba and M. Böge, Local orbit response matrix measurement at SLS, in *Proceedings of IPAC'15, Richmond, USA, May 2015* (JACoW, Geneva, Switzerland, 2015), paper TUPJE044.
- [26] A. Langner (private communication).
- [27] M. Bai, S. Y. Lee, J. W. Glenn, H. Huang, L. Ratner, T. Roser, M. J. Syphers, and W. van Asselt, Experimental test of coherent betatron resonance excitations, *Phys. Rev. E* **56**, 6002 (1997).
- [28] D. Sagan, R. Meller, R. Littauer, and D. Rubin, Betatron phase and coupling measurements at the Cornell Electron/Positron Storage Ring, *Phys. Rev. ST Accel. Beams* **3**, 092801 (2000).
- [29] R. Tomás *et al.*, Record low beta beating in the LHC, *Phys. Rev. ST Accel. Beams* **15**, 091001 (2012).
- [30] S. White, E. Maclean, and R. Tomás, Direct amplitude detuning measurement with AC dipole, *Phys. Rev. ST Accel. Beams* **16**, 071002 (2013).
- [31] T. H. B. Persson, Y. Inntjore Levinsen, R. Tomas, and E. H. Maclean, Chromatic coupling correction in the Large Hadron Collider, *Phys. Rev. ST Accel. Beams* **16**, 081003 (2013).
- [32] S. Mönig *et al.*, Short term dynamic aperture with AC-Dipole DA, in *Proceedings of IPAC'16, Busan, Korea, 2016* (JACoW, Geneva, Switzerland, 2016), paper THPMR044.

Paper V:

Drive beam stabilisation in the CLIC Test Facility 3



Drive beam stabilisation in the CLIC Test Facility 3

L. Malina^{a,b,*}, R. Corsini^a, T. Persson^a, P.K. Skowroński^a, E. Adli^b

^a CERN, Geneva 23, Switzerland

^b University of Oslo, 0316 Oslo, Norway

ARTICLE INFO

Keywords:

CLIC
CLIC test facility
Beam stabilisation
Beam-based feedback
Feedback

ABSTRACT

The proposed Compact Linear Collider (CLIC) uses a high intensity, low energy drive beam to produce the RF power needed to accelerate a lower intensity main beam with 100 MV/m gradient. This scheme puts stringent requirements on drive beam stability in terms of phase, energy and current. The consequent experimental work was carried out in CLIC Test Facility CTF3. In this paper, we present a novel analysis technique in accelerator physics to find beam drifts and their sources in the vast amount of the continuously gathered signals. The instability sources are identified and adequately mitigated either by hardware improvements or by implementation and commissioning of various feedbacks, mostly beam-based. The resulting drive beam stability is of 0.2° @ 3 GHz in phase, 0.08% in relative beam energy and about 0.2% beam current. Finally, we propose a stabilisation concept for CLIC to guarantee the main beam stability.

1. Introduction

The compact linear collider (CLIC) [1] is a proposed particle accelerator, which will possibly take over from Large Hadron Collider (LHC) at the high energy physics frontier after its planned shut down around 2035. CLIC is a linear e^+e^- collider with a centre of mass energy up to 3 TeV. To reach this energy, it will employ a two-beam acceleration scheme [1]. CLIC Test Facility CTF3 [2] is a test facility, which aims to demonstrate the feasibility of CLIC technology by generation of the high current drive beam used for two-beam acceleration and to develop a variety of different CLIC specific equipment.

The two-beam acceleration concept imposes strict requirements on the drive beam stability, in terms of current, energy and phase. The drive beam current stability impacts the stability of the main beam and it is critical for the integrated luminosity. The beam stability goals are defined as the values yielding 1% luminosity loss. The CLIC drive beam stability goals (phase translated to CTF3 machine independent of RF-frequency) are following [3]:

- beam phase of 0.2° at 3 GHz before phase-feed-forward (PFF)
- relative beam energy stability of 1×10^{-3}
- drive beam current stability of 7.5×10^{-4} .

The layout of CTF3 is shown in Fig. 1. A thermionic gun produces 1.3 μ s long pulses of a 5 A continuous electron beam. The injector consists of 3 Sub-Harmonic-Bunching cavities (SHB) operating at 1.5 GHz,

3 GHz pre-buncher, buncher and 2 accelerating structures. The bunch frequency can either be 1.5 GHz or 3 GHz if the SHBs are disabled. It is one of the parameters defining the mode of operation: full factor 8 beam recombination is possible only with a 1.5 GHz beam, while 3 GHz allows only for factor 4. The bunched beam then passes through a magnetic chicane and about 4.3 A is accelerated in the 70 m long linac to the energy of 135 MeV. The acceleration of the beam is done with 3 GHz RF. The power is generated by klystrons delivering 5.5 μ s and 40 MW pulses. Pulse compressors are employed to provide a flat-top of 80 MW and 1.4 μ s. There are 16 accelerating structures operated in fully loaded mode [4]. This gives a high RF to beam efficiency, however, it introduces a strong correlation between the beam current and beam energy. In the delay loop, the beam pulse is converted to four 140 ns pulses of double intensity and bunch spacing by interleaving bunches using transverse RF deflectors. The four pulses are combined into a single one in the combiner ring. The beam is transported towards the experimental area CLEX [2], where it can be sent in the Test Beam Line (TBL), which investigates the effect of deceleration of the drive beam, or in the Two Beam Module (TBM), which experimentally verifies the concept of the two-beam acceleration.

In order to achieve the stringent stability levels needed for present and future machines, complex feed-back systems are usually required [5–9]. In Section 2 we describe the tools and algorithms that allow identification and study of the sources of drifts and jitters during machine operation. Section 3 describes a novel statistical analysis that

* Corresponding author at: CERN, Geneva 23, Switzerland.
E-mail address: lukas.malina@cern.ch (L. Malina).

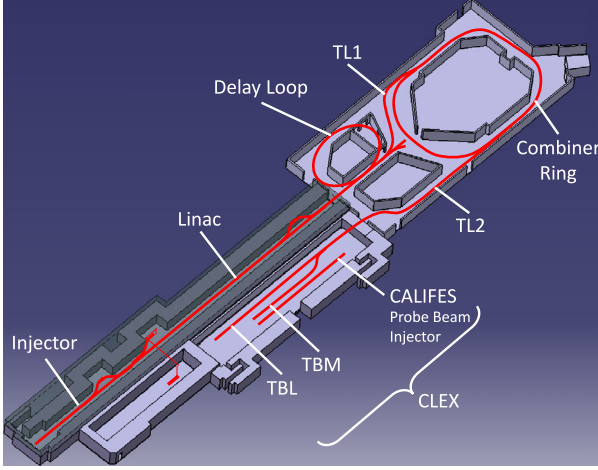


Fig. 1. Layout of CTF3.

allows identification of all relevant drifts within the very large amount of data recorded from hundreds of devices. The analysis leads typically to one of the following outcomes: identification of a particular hardware failure, which needs to be fixed, or to improved understanding of principles governing how to better stabilise the beam using a feedback system. The feedback systems developed for the CTF3 machine are described in detail in Section 4. In Section 5 the resulting beam stability is shown and discussed.

2. Monitoring and operational tools

In this section, we describe the monitoring and operational tools used in the CTF3 machine to identify failures and machine settings changes. In a single beam-pass machine, a change of the initial beam parameters affects all downstream beam parameters. It is therefore crucial to have precise control of the source and injector parameters. As an example, in CTF3 the phase and amplitude of the RF power in structures of the injector are one of the most critical parameters. Any change of these two parameters alters capture efficiency and therefore bunch charge. This also translates into a phase error after the magnetic chicane. Phase and charge differences modify the final bunch energy and length. This leads to different orbit and beam losses. Finally, the RF power produced by power extraction structures [10] has different amplitudes and phases.

In general, any observed drift at the end of a beam line can be caused by any of a vast amount of upstream signals, and the specific source is normally difficult to determine. In order to follow the evolution of all the signals and to provide input for the stability analysis of such complex system, two dedicated monitoring applications have been developed for machine operation.

The first one is called ReferenceMonitor and it is fully described in [11]. It shows in real time most of the beam related signals acquired along the beam pulse (hereafter referred to as “traces”) together with earlier captured reference signals. Additionally, it displays the time evolution of their values averaged over the beam pulse and the χ^2 with respect to the reference. More importantly, it saves all beam related signals for further analysis. Since saving all traces for every pulse is not possible due to large amount of data, it saves the mean and χ^2 values instead. Full traces are saved periodically every 10 to 20 min.

For beam stabilisation in a given working point (the set of beam conditions along the machine), a change of the working point must be first effectively identified. An online watchdog application has been developed to quantify and determine the sources of the drifts. It compares the machine settings and the beam measurements to reference values. It shows the largest deviations measured by χ^2 in continuously updating fixed-displays. The signals are grouped by their type and are

sorted according to their location along the machine layout. For clarity, only the locations with a beam presence are shown. This allows for quick identification of the origin of a drift, or at least its approximate location, by pointing out the most upstream signal that is diverging. The signal and its time evolution can be then verified in detail using the ReferenceMonitor. This makes these applications crucial for stabilisation of the machine since operators can more quickly identify a problem, determine the origin and react appropriately.

3. Drift and correlation analysis

Due to the large amount of recorded signals, drifts and jitters are analysed offline to identify the source and quantify the effect. This in turn defines the requirements for an appropriate feedback, specifically: required accuracy of signal acquisition, averaging time and gain. A dedicated algorithm has been developed to study drifts and jitters using the sample correlations between signals in a sliding time window of chosen length (depending on which time scale correlated signals are to be found). Let r be the correlation coefficient of pairs of normally distributed observables x and y :

$$r = \frac{\sum_{i=1}^n (x_i - \bar{x})(y_i - \bar{y})}{\sqrt{\sum_{i=1}^n (x_i - \bar{x})^2} \sqrt{\sum_{i=1}^n (y_i - \bar{y})^2}}, \quad (1)$$

where n is a sample size, $\bar{x} = \sum_{i=1}^n x_i$ and $\bar{y} = \sum_{i=1}^n y_i$. The sample correlation coefficient r lies in the interval $(-1; 1)$. In order to easily work with significance levels, Fisher z-transform [12] is performed to obtain corresponding normally distributed quantity z and its uncertainty se :

$$z = \tanh^{-1} r = \frac{1}{2} \ln \left(\frac{1+r}{1-r} \right)$$

$$se = \sqrt{\frac{1}{n-3}}$$

The confidence interval $(r_-; r_+)$ for r (asymmetric in general) is obtained by back-transforming $z \pm se$. Nevertheless, this procedure would be biased, where n is small or r is close to ± 1 , because a finite sample of normal distribution follows the student t -distribution. The latter case is not important for drift detection since the resolution for high correlations is not needed. A correction for small sample size (given the requested confidence level) follows:

$$z \pm \sqrt{\frac{1}{n-3}} \cdot f(1-\alpha, n-2),$$

where f is inverse of cumulative student t -distribution function, given the confidence level α . We treat the correlation as non-significant if zero is within the back-transformed $(r_-; r_+)$ interval. It is practical to define a measure $R^2_{non-zero}$, which is similar to the coefficient of determination R^2 :

$$R^2_{non-zero} = \text{sgn}(r_+) \cdot \text{sgn}(r_-) \cdot \min(r_+^2, r_-^2), \quad (2)$$

which is positive only if the correlation coefficient is statistically inconsistent with zero at the chosen confidence level. R^2 quantifies the fraction of a signal B variation that can be explained by another signal A change. If $R^2_{non-zero}$ is positive, it directly implies lower estimate on a fraction of signal B variation explainable by signal A. This represents a robust measure, which can be used to filter a large amount of signal pairs in long data samples. This is especially important for a large-scale machine, such as CLIC. Typically the beam passes through periods of drift (signals strongly correlated with time) and periods of relative stability (the signal variations are dominated by noise). It is convenient to study the correlations at various fixed time scales, typically a few minutes to several hours. A drifting signal together with calculated sample correlation coefficients (with time) and respective $R^2_{non-zero}$ is shown in Fig. 2. We introduce a “movie” of a visualised matrix (devices vs devices) of $R^2_{non-zero}$ s over a sliding time interval. Sample frame of the matrix of lower limits on coefficients of determination is shown in Fig. 3.

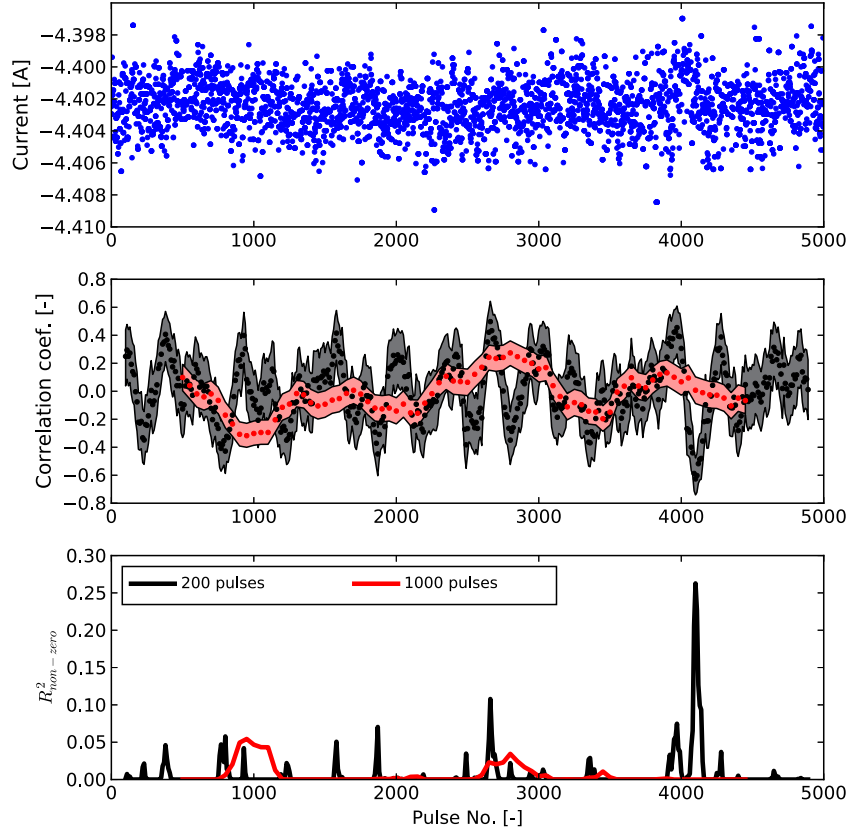


Fig. 2. In the top plot, a time evolution of a beam current signal is shown, its sample correlation coefficients with time over sliding time window (of two different lengths: 200 and 1000 pulses) is shown in the middle together with its confidence interval bands. In the bottom plot, the respective $R^2_{non-zero}$ is shown for given confidence level of two sets of correlation coefficients.

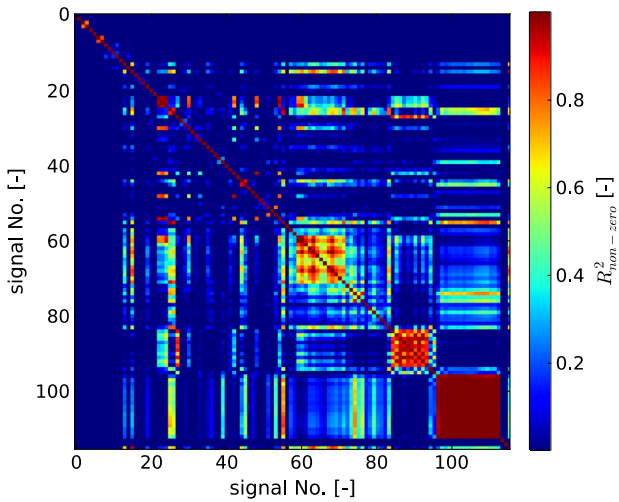


Fig. 3. Sample frame of the matrix of lower limits on coefficients of determination among devices along the beam line in a sliding time window.

A small subset of signals is shown in Fig. 4, demonstrating the changes of downstream observables caused by a beam current (signal No. 0) drift, i.e. high correlation with time (signal No. 14). Due to full beam loading in the linac, the beam energy changes (signal No. 10), while the beam phase is almost intact (signals No. 4 and 8). The consequent beam energy drift changes the extraction efficiency from CR, i.e. the beam current in TL2 and TBM (signals No. 12 and 13) is correlated to beam energy.

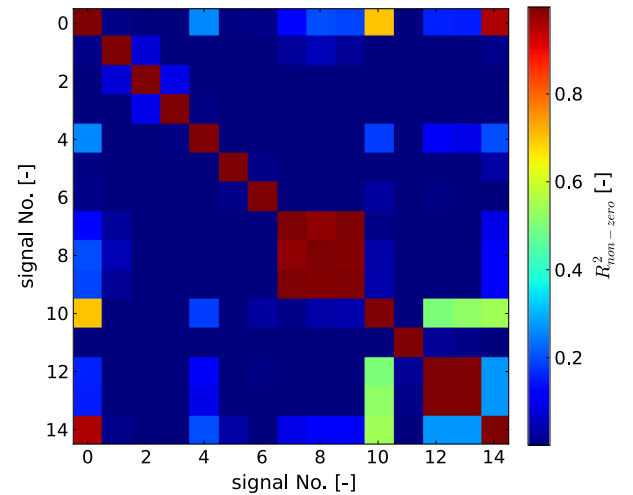


Fig. 4. Sample frame of the matrix of lower limits on coefficients of determination among a small subset of devices, directly corresponding to physical observables, in a sliding time window. A beam current (signal No. 0) drift, i.e. high correlation with time (signal No. 14), causes the downstream parameters to change. Due to full beam loading in the linac, the beam energy changes (signal No. 10), while the beam phase is almost intact (signals No. 4 and 8). The consequent beam energy drift changes the extraction efficiency from CR, i.e. the beam current in TL2 and TBM (signals No. 12 and 13) is correlated to beam energy.

4. Stabilisation systems

Direct observation of the recorded signals lead to the implementation of the following RF feedbacks:

- RF phase loops
- ambient temperature feedback in the RF pulse compression system
- RF power flattening feedback.

The RF feedbacks detailed above improved beam stability by more than one order of magnitude and are summarised in Table 1. To further improve beam stability, an extensive signal correlation study pointed out a need for additional beam-based feedback systems:

- gun current stabilisation feedback
- injector feedback, which stabilises the beam phase
- loading feedbacks, which mainly stabilise the phase and remove the correlation between the beam current and energy
- energy flattening feedback, which flattens the beam energy along the pulse.

These feedback systems are described below, together with the treatment of potential cross talks among different systems.

All the CTF3 feedback systems are designed in a fail-safe manner. They do not act unless all control parameters are within tolerances defined at the time of commissioning and calibration of the system. In particular, they are active only when sufficient beam current is confirmed by the first beam position monitor (BPM) downstream from the location of the signal that is being stabilised. Injector and loading feedbacks also check whether the RF power delivered by the associated klystrons is close enough to the reference value. Experience showed that reaching the reference working point is impossible when the difference is bigger than 1 MW and an attempt to compensate it by adjusting RF phases or gun current would result in significant beam losses.

The beam pulse length varies significantly in operation of CTF3 drive beam, as it consists of different beam setups and experiments. The feedbacks also follow changes of the beam pulse length and automatically adapt the reference ranges. For that reason, the feedbacks are always calibrated with the longest possible beam pulse. When the start or end time of a beam pulse is changed, the feedbacks recompute all the required variables using only the overlapping part of the actual beam pulse and the reference measurement. Therefore, neither recalibration nor a new reference measurement is needed. Thanks to this feature the feedbacks can be used to automatically restore the beam conditions during restart. They proved to be very efficient and even in cases of longer shutdowns, when the RF phases and the current of the gun drifted to basically random values, they were able to bring back the beam to the reference conditions within hundreds of pulses.

4.1. RF-feedbacks

The RF pulse compression [13–15], which increases the RF peak power in CTF3 linac, is very temperature sensitive. Even though the cooling water temperature of the RF compressors was stabilised to 0.05 °C, residual variations coming from the klystrons, waveguides and originating from ambient temperature changes in the klystron gallery influenced the shape of the compressed pulse. For this reason, a temperature feedback was implemented to dynamically correct the setpoint of the water-cooling station for each compressing cavity [16].

In order to further stabilise RF phase and power, additional feedback systems are implemented. The amplitude of the compressed RF pulse is controlled by RF phase at the input of the compressing cavity. It is derived with a non-trivial iterative algorithm [17]. A part of this algorithm was programmed into a feedback loop in order to preserve the pulse amplitude [18] (RF pulse flattening). It stabilises not only the mean power, reducing the mean beam energy drifts, but also the

amplitude along the pulse, stabilising the energy of the bunches along the train. The phase of the RF is stabilised using phase loops, which keep constant the RF phase measured after the pulse compressor [16]. They need to act fast enough to correct the phase errors introduced by the RF pulse flattening. Phase-locked loops are also implemented in the travelling wave tubes (TWTs) in the injector. However, the measurements used in the feedbacks are temperature sensitive as well. For example, day/night temperature variations are pronounced during summer, when air-conditioning capacity is insufficient to prevent the temperature raise.

This results in long-term variations of the phase working points, which need to be mitigated by beam-based feedbacks described below. Fig. 5 shows the CTF3 injector and linac layout including the beam-based feedback measurement locations and Table 2 summarises the control settings used to stabilise them.

4.2. Beam current and phase stabilisation

The beam current is stabilised using the BPM located at the end of injector because it offers much more accurate current measurement comparing to the devices installed upstream. At this location, the beam is fully relativistic, which allows use of an inductive wall current monitor. Such a device is much more reliable compared to the electrostatic devices installed within the injector, which suffer from a large droop and are heavily influenced by charging-up from the electrons scattered in the bunching cavities. The feed-back loop is closed on the gun pulser intensity knobs (fine and coarse), that regulate the grid voltage in the thermionic gun.

The beam phase is predominantly defined by the injector, where the electrons become ultra-relativistic. Further downstream, the beam phase is less influenced by accelerating RF, especially when the lattice is correctly tuned with the nominal $R_{56} = 0$ m. Two Beam Phase Reference (BPR) monitors are installed in the injector to measure bunch phase and length, see Fig. 5). The bunch length measurement is only relative because the signals have strong non-linear dependence on bunch charge and position. It is, therefore, important to monitor that these parameters are constant.

The injector feedback stabilises the longitudinal beam parameters as measured by the two BPRs. The main part of the feedback system is common for both 1.5 and 3 GHz bunch frequency modes. Different configurations were verified and the best performance is achieved when

- Phase of the klystron 3 is used to stabilise the bunch length signal of the downstream monitor (BPR0475).
- Simultaneous phase change of both klystrons 2 and 3 is used to stabilise phase signal of the upstream monitor (BPR0290). Such correction does not modify the bunch length at the downstream monitor because the relative phase between the cavities is left unchanged.

The second part of the feedback system acts only on the beam with 1.5 GHz bunching frequency and stabilises the phases of the travelling wave tubes (TWT) that power the SHBs. The system stabilises the RF power measured at the exit of SHB cavity in presence of the beam (i.e., beam loading measurement) and the BPR0290 bunch length measurement. As the proportionality ratios are subject to drifts it employs an automatic calibration procedure. In an optimised working point this feedback is linear in the first two phases and quadratic in the third. The feedback uses the acquired reference signals as a target for corrections using measured calibration factors. Both the reference signals and the calibration factors are beam-mode dependent.

As already mentioned, the bunch length measurement is sensitive to beam current (in principle proportional to beam current squared) and the deviation from the reference klystron phases with respect to the beam phase changes the amount of beam losses in the injector. This entangles the beam current and the beam phase. In order to avoid resonant cross-talks between the feedbacks, they work at different

Table 1
Measurements and steering knobs used in CTF3 RF feedback systems.

Feedback	Measurement	Knob
Phase-loops	Phase of compressed RF	Phase shifters
Ambient temperature	Pulse compressor temperatures	Temperature set point
RF flattening	Power amplitude of compressed RF	Waveform generator function

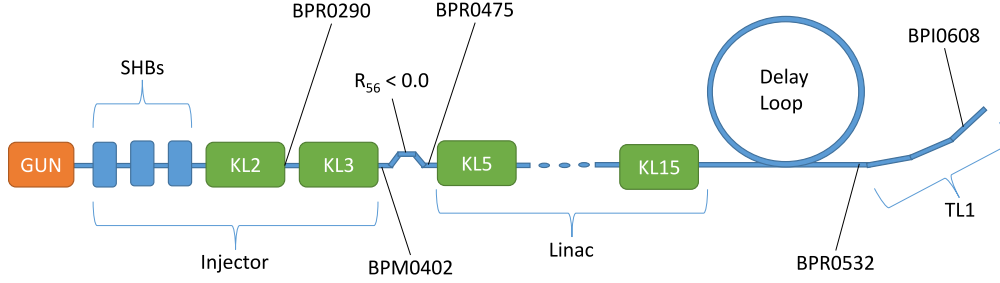


Fig. 5. Schematic view (not to scale) of the CTF3 injector and linac showing the locations of measurements, which are being stabilised, together with the knobs used to control them, listed in Table 2.

Table 2
Measurements and steering knobs used in CTF3 beam-based feedback systems. Their physical locations are shown in Fig. 5.

Feedback	Measurement	Knob
Gun current	BPM0402 — current	grid voltages of thermionic gun
Injector 3 GHz	BPR0290S BPR0475W	Klystron 2 phase Klystron 3 phase
Injector 1.5 GHz	TWT loadings BPR0290W	Phases of all three TWTs
Klystron Loading (5 to 15)	Accelerating structure loading	Klystron phase
Energy flattening	BPI0608H — dispersive BPI	Waveform klystron 15

time scales, i.e. integration times. Moreover, in case when the beam is restarted and the settings might have drifted away from references, the beam phase feedback is not acting for several pulses, waiting for the beam current being back at the reference value.

4.3. Beam energy stabilisation

After implementation of the RF power stabilisation system [18], the beam energy stability was improved to about 0.2% over several minutes, and over longer times up to about 2%. It was found that the remaining beam energy variations still caused beam intensity fluctuations through losses. The energy variations are mainly due to slow changes of sensitivity in RF phase and power measurements (e.g. temperature effects), upon which the phase loops and the RF power stabilisation feedback respectively rely. Further, any beam current variation affects the acceleration, for these reasons beam-based feedback systems are employed.

The CTF3 linac is operated close to fully loaded mode [4], therefore in most of the cavities the remaining power at the output port (referred to as loading) is measurable. A sample signal is shown in Fig. 6. This strongly depends on the phase between the electron bunches and the accelerating field. It is stabilised by loading feedbacks, which adjust the appropriate klystron phases. Loading feedbacks are implemented and commissioned for all the klystrons in the linac. The reference trace is an average of several traces acquired for a short period after the feedback is turned on. The construction of the penalty function is not trivial because simple difference or χ^2 , even in the simplest case, is neither linear nor monotonous as the working point is close to full beam loading, where the loading shapes are complex (Fig. 6).

The feedback minimises a linear combination of χ^2 from the reference measurement (trace along the beam pulse) and the slope of the

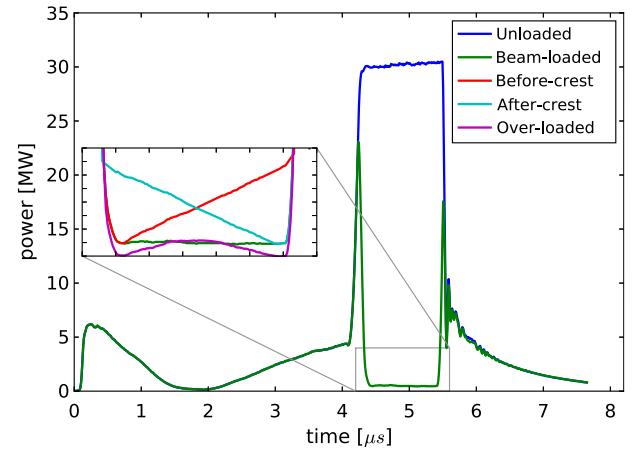


Fig. 6. The power measured at the exit of accelerating structure. In case of full beam loading the internal part of a pulse is close to zero. Sketches of different beam-loading patterns depending on relative phase and amplitudes between the RF and the beam-loading are shown in zoomed-in plot.

remaining power along the pulse:

$$p = \sum_{i=1}^n (x_{meas} - x_{ref})^2 + C \left(\sum_{i=n-10}^n (x_{meas} - x_{ref}) - \sum_{i=1}^{10} (x_{meas} - x_{ref}) \right),$$

where C is a klystron-specific free parameter to make the penalty function a monotonous function of klystron phase deviation. Since the minimisation without gain setting is relatively slow, a higher gain mode

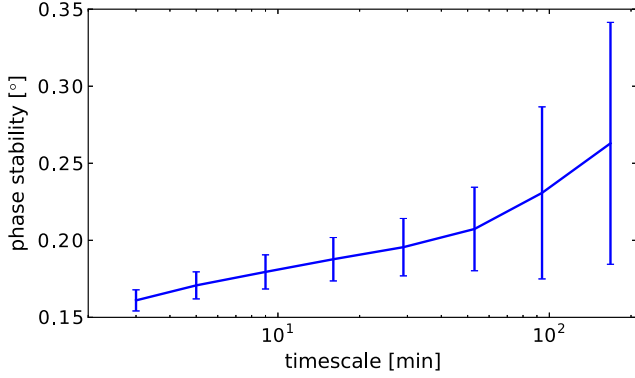


Fig. 7. Average beam phase stability measured at location BPR0532 as a function of the averaging time in the 3 GHz beam mode.

has been developed for more rapid drifts, i.e. when the beam condition gets further away from the reference, where it is not limited by noise. In such a case, the feedback measures the local penalty function derivative and performs a biased Newton iterative method minimisation. In other cases the feedbacks are limited by high noise and drifts of power measurements themselves, therefore they operate on scales of minutes rather than seconds.

In order to stabilise the beam energy along the pulse, which is disturbed by residual RF power variations added up through the acceleration, an energy flattening feedback was developed [9]. It is a variant of RF pulse flattening feedback that flattens the beam energy instead.

5. Beam stability

The CTF3 beam stability in various beam modes is quoted in this section in terms of drive beam phase, energy, current, and probe beam acceleration. Generally, we show the average stability (i.e. as opposed to best obtained stability) as a function of a time-scale (a period of time over which the stability is measured). The repetition time of CTF3 beam pulses is 1.2 s, thus stability over one hour means 3000 pulses.

The beam phase and energy variation is measured at BPR0532 and BPI0608 (see Fig. 5). The phase measurement is close to the upstream high-precision PFF phase monitors offering a resolution of 0.05° at 3 GHz [19]. At the location of BPI0608, there is a horizontal dispersion of 60 cm, therefore any change of energy is visible as a horizontal orbit change. It is verified with singular value decomposition of multiple BPMs that there is no significant dispersion upstream of the first bend that would modify the assumed value at BPI0608, and that incoming orbit and power supply jitters have negligible influence. Therefore, this signal represents well the beam energy.

The achieved beam phase stability is shown in Fig. 7 and is limited by the fluctuation of the phase measurements themselves. The fluctuations are likely caused by thermal effects in the distribution of a local oscillator signal for the mixers as a different levels of coupling between different measurements were observed. The relative mean energy variation is shown in Fig. 8. Both the phase stability and the relative mean energy variation of the uncombined beam are quoted in Table 3, together with relative energy variation along the pulse. The beam phase and energy stability is independent of the beam recombination factor. It remains unchanged further downstream in the machine due to absence of further acceleration and overall momentum compaction $R_{56} = 0$ m [20].

The current stability from the gun to the dump with a beam recombination factor 4 is shown in Fig. 9. Each blue line stands for a relative current stability (at a given BPM) over an hour of beam time with beam-based feedbacks running. Red lines stand for the same quantity without beam-based feedbacks. The green dashed line reflects the CLIC current stability goal. For the same period of time, we show

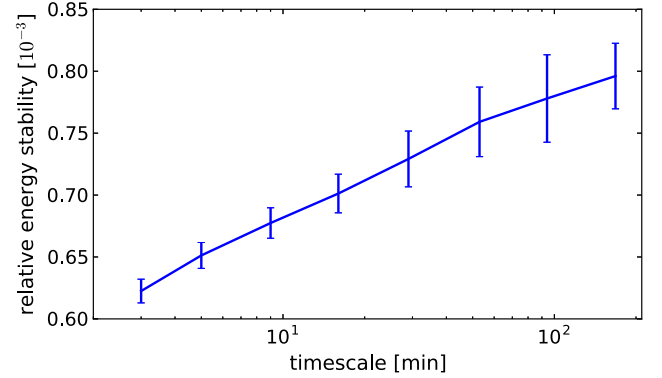


Fig. 8. Average relative beam energy stability measured at location BPI0608 as a function of the averaging time in the 3 GHz beam mode.

Table 3

Beam phase and energy stability over period of one hour.

Quantity	Stability over an hour
Phase [$^\circ$ @ 3 GHz]	0.2
Relative pulse-to-pulse energy [%]	0.07
Relative energy along the pulse [%]	0.08

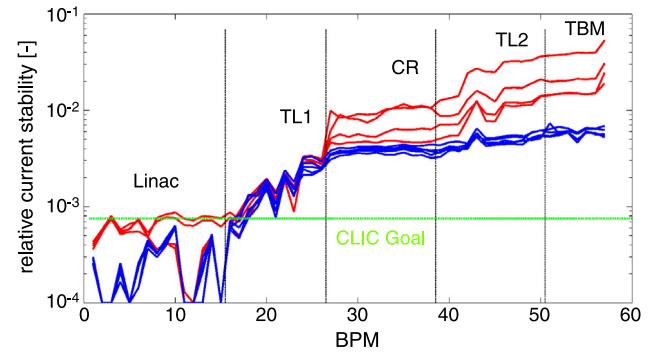


Fig. 9. Several sets of relative beam current stability measurement (combination factor 4) along the machine. Each line refers to stability over a period of one hour. In blue; beam-based feedbacks operating, in red: feedbacks turned off. The BPM noise is subtracted (in squares). The current variation in the linac is below the BPM resolution, causing the jagged structure of the lines. (For interpretation of the references to colour in this figure legend, the reader is referred to the web version of this article.)

in Fig. 10 the average relative beam current stability (in given a part of CTF3 with beam-based feedbacks operating) as a function of averaging time scale.

In the following we show the best average beam current stability in two typical operational modes:

- 3 GHz beam with multiplication factor 4 (not passing via Delay Loop) is shown in Fig. 11.
- 1.5 GHz beam with multiplication factor 8 is shown in Fig. 12.

In the first case, the beam has been well optimised and stability was limited by the resolution and stability of multiple measurements in the linac. For the 1.5 GHz beam, there were three main sources of difficulties:

- the time spent on optimisations and long stability studies of this beam was limited due to recurring failures of the TWTs
- the power supply of the septa magnet used for the injection to and extraction from the delay loop was jittering and could not be replaced with a better performing device

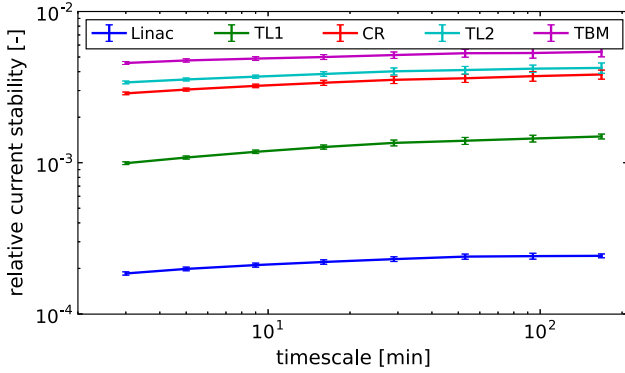


Fig. 10. Average beam current stability in different parts of the machine, as shown in Fig. 1, as a function of the averaging time for the very same data as in Fig. 9 (with beam-based feedbacks operating). For each machine part we use the average of several BPMs. The beam mode is 3 GHz beam with a recombination factor 4 in the combiner ring.

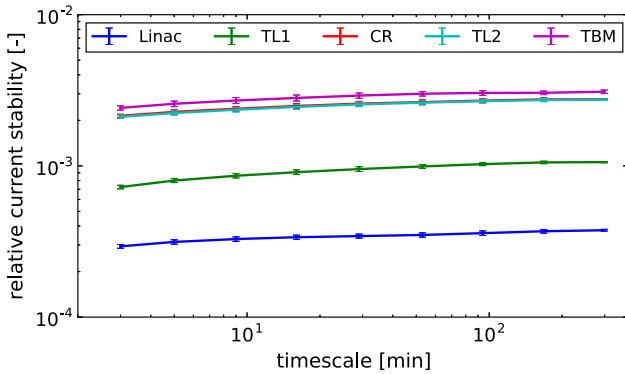


Fig. 11. Average beam current stability in different parts of the machine, as shown in Fig. 1, as a function of the averaging time. The beam mode is a recombination factor 4 in the combiner ring of 3 GHz beam.

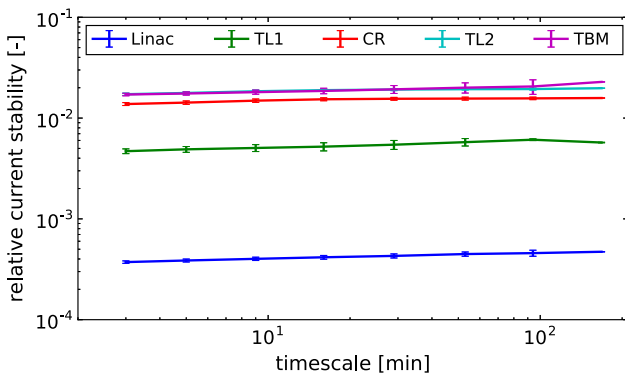


Fig. 12. Average beam current stability in different parts of the machine, as shown in Fig. 1, as a function of the delay averaging time. The beam mode is a recombination factor 8–2 in the delay loop and 4 in the combiner ring of 1.5 GHz beam.

- full transmission through the delay loop was not achieved since the strong isochronous optics of the delay loop limit momentum acceptance below the drive beam 0.6% r.m.s. energy spread. Unfortunately, due to the limited space in the pre-existing building, it was not possible to design weaker optics.

The main beam has been accelerated by the factor 8 combined drive-beam-generated RF power from the energy of 199 MeV to 242 MeV.

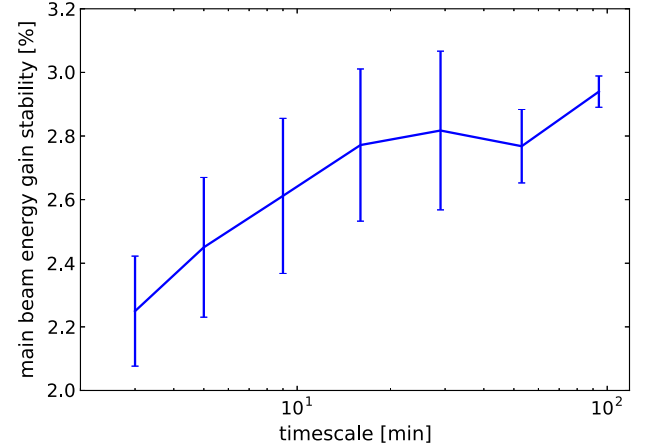


Fig. 13. The main beam energy gain stability while accelerated by RF coming from the factor 8 combined drive beam as a function of the averaging time.

Table 4

Achieved average drive beam stability compared to CLIC goals.

Quantity	Achieved	Goal
Phase [° @ 3 GHz]	0.2	0.2
Mean energy variation [%]	0.07	0.1
Energy variation along the pulse [%]	0.08	0.1
Current (linac) [%]	0.02–0.04	0.075
Current (after combination) [%]	0.2–1.8	0.075

The main beam energy was rather constant at the level of 1 MeV to be compared with typical spread of 0.6 MeV without the presence of drive-beam-generated RF power. The stability of the average energy gain of the main beam at different time scales is shown in Fig. 13. In the case of the factor 4 combined drive beam, the energy variation shows no increase (compared to case with no drive-beam-generated RF power). This shows that in such a case the drive-beam induced energy variation is much smaller than 0.6 MeV.

6. Conclusions and strategies for CLIC

In this paper, we focus on the beam stabilisation aspects of the CLIC drive beam complex. A novel analysis technique has been applied in detailed studies and allowed identification of the critical issues for beam stability. This algorithm, essential for the understanding of drifts and for latter implementation of feedback systems, is described in Section 3. Feedback systems to stabilise the drive beam have been designed and commissioned at CTF3. These feedback systems may also be useful in XFEL linacs, which operate in a similar mode to the CTF3 linac.

The achieved beam stability in CTF3 is summarised and compared to the CLIC drive beam stability goals in Table 4.

The CLIC goals have been reached in terms of beam phase (time of arrival), i.e. 0.2° at 3 GHz or 180 fs, before the final correction with the phase feed-forward (PFF) system. It must be noted that the PFF system showed a reduction of the incoming phase jitter to the final CLIC specifications (0.2° at 12 GHz, or 50 fs) thus validating the entire scheme [19]. Results below the CLIC requirements were also obtained for the mean beam pulse momentum stability and the momentum variations along the beam pulse. While the beam current in the linac was stabilised below the CLIC requirement as well, losses along the beam lines prevented this goal being reached for the combined beam, especially at its final destination in CLEX. There the average relative variation was 0.2%–1.8% depending on the beam mode, with the best stability being achieved for a combination factor 4 of the 3 GHz beam, the better known and used among the different operation modes. Given the much better beam size to aperture ratio of the CLIC beam lines with

respect to CTF3, the linac stability result constitute a reasonable proof-of-principle for the current stability in the overall drive beam complex of CLIC, where beam losses should be minimal.

The feedback systems developed at CTF3 are crucial for the CLIC drive beam stabilisation except for the RF pulse compression, which will not be used in CLIC. In the CLIC drive beam complex, the injector RF needs to be exceptionally stable. If possible, a solution like the one in CTF3, granting the same or better stability, should be implemented. This requires accurate beam instrumentation, especially for beam phase, current and acceleration cavity loading measurements. A general feedback framework needs to be embedded in the design of the machine and the control system, including the temperature measurements at all beam or RF related measurements. The monitoring application, together with the drift analysis framework need to be ready for the first beam commissioning in order to make the beam optimisation possible.

Acknowledgements

The authors would like to thank all CTF3 operators. We also would like to thank to Ewen Maclean for English language corrections.

References

- [1] M. Aichler, P. Burrows, M. Draper, T. Garvey, P. Lebrun, K. Peach, N. Phinney, H. Schmickler, D. Schulte, N. Toge (Eds.), *A Multi-TeV Linear Collider Based on CLIC Technology: CLIC Conceptual Design Report*, Technical Report CERN-12-007, CERN, Geneva, Switzerland, 2012.
- [2] G. Geshonke, A. Ghigo, *CTF3 Design Report*, Technical Report CERN-PS-2002-008-RF, CERN, Geneva, Switzerland, 2002.
- [3] D. Schulte, et al., Status of the CLIC phase and amplitude stabilisation concept, in: LINAC'10, Tsukuba, Japan, 2010, pp. 103–105.
- [4] R. Corsini, et al., First full beam loading operation with the CTF3 Linac, in: EPAC'04, Lucerne, Switzerland, 2004, pp. 39–41.
- [5] R.L.A. Cottrell, C.A. Logg, M.J. Browne, A feedback system for steering and correcting the energy of the SLAC beam in the beam switchyard, *Nucl. Instrum. Methods* 164 (1979) 405–409.
- [6] C. Schmidt, M.K. Bock, S. Pfeiffer, H. Schlarb, W. Koprek, W. Jalmuzna, Feedback strategies for bunch arrival time stabilization at FLASH towards 10 fs, in: FEL'11, Shanghai, China, 2011, pp. 531–534.
- [7] S. Pfeiffer, C. Schmidt, M.K. Bock, H. Schlarb, W. Jalmuzna, G. Lichtenberg, H. Werner, Fast feedback strategies for longitudinal beam stabilization, in: IPAC'12, New Orleans, USA, 2012, pp. 26–28.
- [8] S. Schulz, M.K. Czwalińska, M. Felber, P. Predki, S. Schefer, H. Schlarb, U. Wegner, Femtosecond-precision synchronization of the pump-probe optical laser for user experiments at FLASH, in: Proc SPIE 8778, Advances in X-ray Free-Electron Lasers II: Instrumentation, 87780R, Prague, Czech Republic, 2013.
- [9] L. Malina, R. Corsini, D. Gamba, T. Persson, P.K. Skowronski, Recent improvements in drive beam stability in CTF3, in: IPAC'16, Busan, Korea, 2016, pp. 2677–2679.
- [10] E. Adli, R. Ruber, V. Ziemann, R. Corsini, A. Dubrovskiy, I. Syratchev, X-band RF power production and deceleration in the two-beam test stand of the Compact Linear Collider test facility, *Phys. Rev. ST Accel. Beams* 14 (2011) 081001.
- [11] T. Persson, *Fighting Beam Instabilities At CTF3*, Chalmers University of Technology, 2011.
- [12] R.A. Fisher, Frequency distribution of the values of the correlation coefficient in samples from an indefinitely large population, *Biometrika* 10 (1915) 507–521.
- [13] J. Mournier, R. Bossart, J.-M. Nonglaton, I. Syratchev, L. Tanner, Low level RF including a sophisticated phase control system for CTF3, in: LINAC'04, Lübeck, Germany, 2004, pp. 748–750.
- [14] V.E. Balakin, I.V. Syrachev, Status of VLEPP RF power multiplier (VPM), in: EPAC'92, Berlin, Germany, 1992, pp. 1173–1175.
- [15] A. Fiebig, R. Hohbach, Study of peak power doublers with spherical resonators, *IEEE Trans. Nucl. Sci.* 30 (1983) 3563–3565.
- [16] A. Dubrovskiy, F. Tecker, RF pulse compression stabilization at the CTF3 CLIC Test Facility, in: IPAC'10, Kyoto, Japan, 2010, pp. 3774–3776.
- [17] S.H. Shaker, R. Corsini, P.K. Skowronski, I. Syratchev, F. Tecker, Phase modulator programming to get flat pulses with desired length and power from the CTF3 pulse compressors, in: IPAC'10, Kyoto, Japan, 2010, pp. 1425–1427.
- [18] T. Persson, P. Skowronski, R. Corsini, Drive beam stability studies and stabilization algorithms in CLIC test facility 3, *Nucl. Instrum. Methods Phys. Res. A* 735 (2014) 152–156.
- [19] J. Roberts, P. Skowronski, P.N. Burrows, G.B. Christian, R. Corsini, A. Ghigo, F. Marcellini, C. Perry, Stabilization of the arrival time of a relativistic electron beam to the 50 fs level, *Phys. Rev. Accel. Beams* 21 (2018) 011001.
- [20] E. Ikarios, A. Andersson, J. Barranco, B. Constance, R. Corsini, A. Gerbershagen, T. Persson, P.K. Skowronski, F. Tecker, The drive beam phase stability in CTF3 and its relation to the bunch compression factor, in: IPAC'13, Shanghai, China, 2013, pp. 1655–1657.

Paper VI:

Optics measurements in storage rings based on simultaneous 3-dimensional beam excitation

OPTICS MEASUREMENTS IN STORAGE RINGS BASED ON SIMULTANEOUS 3-DIMENSIONAL BEAM EXCITATION

L. Malina¹, J. Coello de Portugal, CERN, Geneva 23, Switzerland
¹ also at University of Oslo, 0316 Oslo, Norway

Abstract

Optics measurements in storage rings usually employ excitation in both transverse directions. This needs to be repeated at several different beam energies and is time-consuming. In this paper, we develop a new optics measurement technique, which excites the beam in all three spatial dimensions simultaneously. It allows measuring the linear optics and chromatic properties at the same time, leading to speed up of the optics measurements. The measurement method has been successfully demonstrated in the LHC using AC-dipoles and RF frequency modulation. Analysis methods have been derived for the 3-dimensional beam excitation case. We quantify the resolution of the measured optical quantities. The first results suggest that the added complexity does not deteriorate the resolution of the linear optics measurement. In the future, this method can serve as an operational tool to check the optics or even to correct it.

INTRODUCTION

One of the ways to perform optics measurements in a storage ring is to excite the beam and acquire turn-by-turn (TbT) beam position monitor (BPM) data showing the coherent betatron motion [1]. The beam is excited using either kickers or AC-dipoles [2]. AC-Dipoles can ramp up and down the oscillation adiabatically [3], i.e. without any measurable emittance growth. Typical optics measurement consist of several kicks at different beam energies, in order to measure the linear optics as well as the chromatic properties.

Based on the experience with optics measurements in the LHC, there are two main sources of delay during the measurements. First, the human intervention to change beam energy by adjusting the RF frequency and check other beam parameters for the new set of measurements usually takes up to 15 minutes. Second, the AC-dipole needs about 70 seconds to cool down after every single excitation. Addition of longitudinal excitation [4] can be used to speed up the measurement, when performed adiabatically.

BEAM EXCITATION

In the LHC, the beam is excited using AC-dipoles in both transverse directions simultaneously. This gives the BPM reading as shown in Figure 1, for one of the planes. Once the beam energy is changed the measurement is repeated. This time-consuming process can be avoided by fast modulation of RF-frequency. RF-frequency change is normally used to adjust the beam energy, or it is modulated in order to measure the chromaticity. However, the frequency of the modulation for the chromaticity measurement is typically

about 0.1 Hz, such that Base-Band Tune (BBQ) system can measure the tune.

We employ the same system at its maximal frequency of 5 Hz, which is still far from the natural synchrotron frequency of about 20 Hz. The RF-frequency modulation is ramped up before the actual AC-dipole excitation starts. Three periods of adiabatic energy variation (forced synchrotron oscillation) fit within 6600 turns acquired (with LHC's revolution frequency of 11.3 kHz). The sample TbT reading at dispersive BPM is shown in Figure 2.

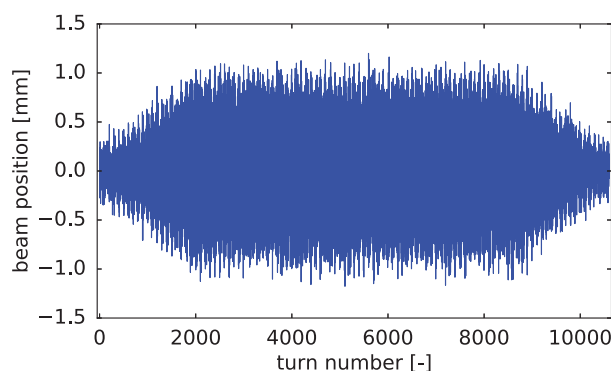


Figure 1: Sample BPM TbT data of beam excited by AC-dipole performing the driven coherent betatron oscillation. Note the ramp-up and ramp-down of the oscillation amplitude, which is important to avoid emittance growth [3] (in hadron machines).

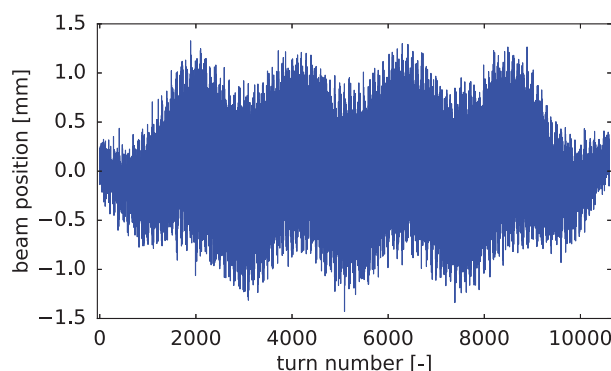


Figure 2: Sample of TbT data at dispersive BPM of beam excited by AC-dipole when the frequency of RF system has been simultaneously modulated. The beam performs the driven coherent betatron oscillations and the beam energy is adiabatically varied.

The adiabaticity of this mode of excitation has been experimentally demonstrated in the LHC, as it can be seen

from the beam size measurement from Beam Synchrotron Radiation Telescope (BSRT) during the 3-dimensional (3D) excitations shown in Figure 3.

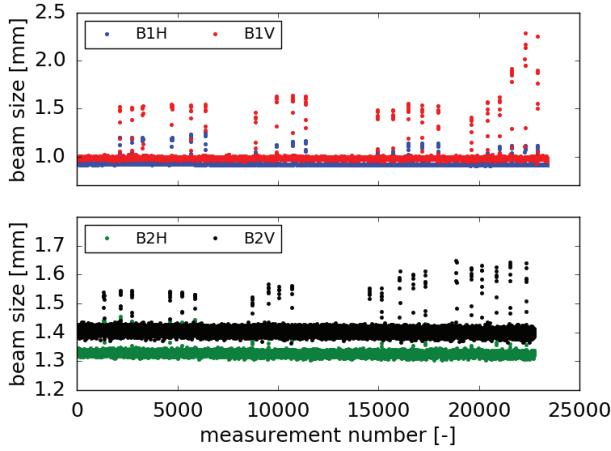


Figure 3: The beam size measurement using BSRT during the 3D excitations, in case the measurement is not fully adiabatic a step-like beam size increase would appear. The spikes refer to AC-dipole excitations.

CHROMATIC PROPERTIES ANALYSIS

The largest advantage of simultaneous 3D excitation is that the chromatic properties, such as normalized dispersion $D_x/\sqrt{\beta}$ [5] or the W-function [6] can be a ratio of certain spectral lines amplitudes. A new dedicated harmonic analysis framework [7] searches for resonances originating from all three spatial dimensions (x, y and s, namely, horizontal, vertical and longitudinal). The following notation of the driven spectral lines has been adopted, for example $H(2,0,1)$ being at frequency $2 \cdot Q_x^F + 0 \cdot Q_y^F + 1 \cdot Q_s^F$ in the horizontal plane ($Q_{x,y,s}^F$ denotes fractional forced tunes).

Relative Beam Momentum Change

Under the assumption of linear dispersion and of beam oscillation around stable orbit (closed orbit), the amplitude of relative beam momentum variation Δp_{amp} is measured. The closed orbit change in the arc BPMs (with larger dispersion) in the horizontal plane is used at the extremes of beam momentum variation. The extremes are identified from frequency and phase of synchrotron spectral line $H(0,0,1)$, i.e. where $|\cos(Q_s n_{turns} + \phi_s)| > 0.9$. A model dispersion is assumed in the calculation of relative beam momentum variation, for measurements in the LHC a variation of 10^{-4} is utilized.

Normalised Dispersion

Using the above-mentioned spectral line notation the normalised dispersion [5] is proportional to the ratio of spectral line amplitudes corresponding to dispersion and $\sqrt{\beta}$:

$$D/\sqrt{\beta} = C \frac{H(0,0,1)}{H(1,0,0)}, \quad (1)$$

where C is a global multiplication factor (related to excitation amplitudes) obtained as a ratio of average measured and average model normalised dispersions in the arc BPMs:

$$C = \frac{\sum_{arcBPMs} \frac{H(0,0,1)}{H(1,0,0)}}{\sum_{arcBPMs} \left(\frac{D}{\sqrt{\beta}} \right)_{model}}, \quad (2)$$

As the spectral line amplitude is always positive, we need to compare the phase of $H(0,0,1)$ at the given BPM with the average phase in the arc BPMs, i.e. if the phases are opposite the dispersion is negative.

OPTICS MEASUREMENT PRECISION

In this section, we compare the precision of the normalised dispersion and the linear optics measurements [8] using 3D and 2D driven beam excitation. The analysis of linear optics quantities is the same as in the 2D case, i.e. N-BPM method [9,10] is applied. In terms of driven motion, the TbT BPM data differs only in presence of spectral lines related to adiabatic energy variation. The normalised dispersion measurements in high β optics at injection energy (with fractional natural tunes of 0.305 and 0.315 in the horizontal and the vertical plane) were performed by the two methods, one right after the other. Their comparison is shown in Figure 4. In the 3D driven excitation based measurement, TbT data from 6 acquisitions are combined, while 11 acquisitions are combined in 2D case. The measurement error distributions are shown in Figure 5 including the mean errors. The residuals scaled by the errors of measurements combined in quadratures are shown in Figure 6. The mean value of such distribution close to zero demonstrates no systematic bias. The standard deviation shows the agreement within the measurement errors (i.e. smaller than 1). The two methods are in excellent agreement.

The agreement of linear optics quantities, measured the same way using both types of beam excitation (except for normalised dispersion) is summarized in Table 1. As a drift of betatron tunes and coupling was observed during the measurement, the linear coupling is not included. However, impact of tune drift on measured phase advances and β -functions is assumed to be negligible compared to measurement errors. No statistically significant bias, nor precision loss were observed in any of the quantities (phase advances, β -functions from phase and from amplitude, and already mentioned normalised dispersion).

In ESRF [11] the transverse 2D kicks were performed, however a residual synchrotron oscillation corresponding to a relative beam energy variation of $5 \cdot 10^{-5}$ was visible in the data. The normalised dispersion can also be measured by the 3D method from the residual synchrotron motion of bunch centroids using transverse kicks only. The obtained normalised dispersion, shown in Figure 7, is only 4 times less precise, even though the amplitude of residual synchrotron motion is only 3 % of relative beam energy changes of 0.16% applied for the standard measurement.

REFERENCES

- [1] R. Tomás, M. Aiba, A. Franchi, and U. Iriso, “Review of linear optics measurement and correction for charged particle accelerators”, *Phys. Rev. Accel. Beams*, vol. 20, p. 054801, 2017.
- [2] M. Bai *et al.*, “Experimental test of coherent betatron resonance excitations”, *Phys. Rev. E* vol. 56, p. 6002, 1997.
- [3] R. Tomás, “Adiabaticity of the ramping process of an ac dipole”, *Phys. Rev. ST Accel. Beams*, vol. 8, p. 024401, 2005.
- [4] G. Rumolo and R. Tomás, “Decoherence of a longitudinally kicked beam with chromaticity”, *Nucl. Instr. Meth. A*, vol. 528, p. 670-676, 2004.
- [5] R. Calaga, R. Tomás and F. Zimmermann, “BPM calibration independent LHC optics correction”, in *Proc. PAC’07*, Albuquerque, New Mexico, USA, Jun. 2007, paper THPAS091, pp. 3693-3695.
- [6] B. W. Montague. “Linear Optics for Improved Chromaticity Correction”, CERN, Geneva, Switzerland, Rep. CERN-LEP-NOTE-165, 1979.
- [7] L. Malina *et al.*, “Performance optimization of turn-by-turn beam position monitor data harmonic analysis”, presented at IPAC’18, Vancouver, Canada, May 2018, paper THPAF045, this conference.
- [8] T. Persson *et al.*, “LHC optics commissioning: A journey towards 1% optics control”, *Phys. Rev. Accel. Beams*, vol. 20, p. 061002, 2017.
- [9] A. Langner and R. Tomás, “Optics measurement algorithms and error analysis for the proton energy frontier”, *Phys. Rev. ST Accel. Beams*, vol. 18, p. 031002, 2015.
- [10] A. Wegscheider, A. Langner, R. Tomás and A. Franchi, “Analytical N-beam position monitor method”, *Phys. Rev. ST Accel. Beams*, vol. 20, p. 111002, 2017.
- [11] L. Malina *et al.*, “Improving the precision of linear optics measurements based on turn-by-turn beam position monitor data after a pulsed excitation in lepton storage rings”, *Phys. Rev. Accel. Beams*, vol. 20, p. 082802, 2017.

Paper VII:

Performance optimization of turn-by-turn beam position monitor data harmonic analysis

PERFORMANCE OPTIMISATION OF TURN-BY-TURN BEAM POSITION MONITOR DATA HARMONIC ANALYSIS

L. Malina¹, J. Coello de Portugal, J. Dilly, P.K. Skowroński, R. Tomás, M. Toplis
CERN, Geneva 23, Switzerland

¹ also at University of Oslo, 0316 Oslo, Norway

Abstract

Nowadays, turn-by-turn beam position monitor data is increasingly utilized in many accelerators, as it allows for fast and simultaneous measurement of various optics parameters. The accurate harmonic analysis of turn-by-turn data costs beam time when needed online. Generally, the electronic noise is avoided by cleaning of the data based on singular value decomposition. In this paper, we exploit the cleaning procedure to compress the data for the harmonic analysis. This way the harmonic analysis is sped up by an order of magnitude. The impact on measurement accuracy is discussed.

INTRODUCTION

Optics measurements in storage rings can be performed by exciting the beam and acquiring turn-by-turn (TbT) beam position monitor (BPM) data of the coherently oscillating beam [1]. In the analysis process, TbT BPM data is first cleaned, which reduces the amount of information. Later the harmonic analysis is performed on cleaned TbT data BPM by BPM. A framework presented here implements new methods to increase the speed of harmonic analysis. This framework replaces SUSSIX [2, 3] in optics measurements analysis software in the LHC. It also implements BPM by BPM harmonic analysis, further referred to as "bpm" method.

SINGULAR VALUE DECOMPOSITION

In order to improve analysis precision and accuracy, TbT data needs to be cleaned of the noise, for example BPM electronic noise. This is done using methods [4–6] based on Singular Value Decomposition (SVD). The SVD of a matrix A is given by

$$A = USV^T, \quad (1)$$

where columns of U and V are normalized eigenvectors of $A^T A$ (left-singular vectors) and AA^T (right-singular vectors), respectively. S is a positively definite diagonal matrix of singular values ordered in decreasing order. The TbT BPM data decomposition contains all temporal and spatial information about physical modes of beam motion. The noise floor removal is performed by keeping only the modes corresponding to the largest singular values, as shown in Figure 1. Table 1 presents the typical TbT matrix dimensions in the LHC, N_{BPMs} and N_{turns} , together with N_{modes} , number of singular values to be kept. This reduces the size of data and information. Matrix A with dimensions (500x6600) is approximated by USV^T matrices with dimensions: (500x12),

Table 1: Typical Parameters of TbT Data and its SVD Cleaning

N_{BPMs}	No. BPMs (per plane)	500
N_{turns}	No. turns acquired	6600
N_{modes}	No. singular values	12

(12x12) and (12x6600). In the second step, TbT data are re-composed by matrix multiplication of the reduced matrices. The size of the data after the recomposition is the same as the input one (500x6600), which is about a factor 40 larger than the reduced USV^T matrices. However, the amount of information is still reduced.

HARMONIC ANALYSIS

The actual lattice properties are contained in the frequency information of TbT BPM data. The Discrete Fourier Transform (DFT) is obtained performing Fast Fourier Transform (FFT) on the cleaned TbT data from a single BPM x_n :

$$X_k = \sum_{n=0}^{N-1} x_n e^{-i2\pi kn/N} \quad (2)$$

The equation has the form of inner product of x_n and $e^{-i2\pi kn/N}$, which means that X_k is a multiplicative complex coefficient of a signal with frequency k/N . In case of FFT k is an integer smaller than N . The refined frequency of the strongest signal is found using Jacobsen frequency interpolation with bias correction [7] based on 3 DFT peaks (the maximal amplitude $|X_{k_p}|$ and two neighbouring samples $X_{k_p \pm 1}$):

$$\delta = \frac{\tan(\pi/N)}{(\pi/N)} \text{Real} \left[\frac{(X_{k_p-1} - X_{k_p+1})}{(2X_{k_p} - X_{k_p-1} - X_{k_p+1})} \right], \quad (3)$$

where $\delta \in [-0.5, 0.5]$ is a correction to the frequency of DFT peak. The refined complex amplitude of the signal is obtained from the inner product of a unit signal with pure frequency $(k_p + \delta)/N$ with the TbT data:

$$X_{k_p+\delta} = \sum_{n=0}^{N-1} x_n e^{i2\pi n(k_p+\delta)/N} \quad (4)$$

This signal is subtracted from the TbT data and the whole procedure starting with FFT is repeated [8], in the LHC typically 300 times. As a result the TbT data is approximated by the sum of the 300 strongest harmonics $\sum_{j=0}^{299} h_j$. The basis forms a linear vector space.

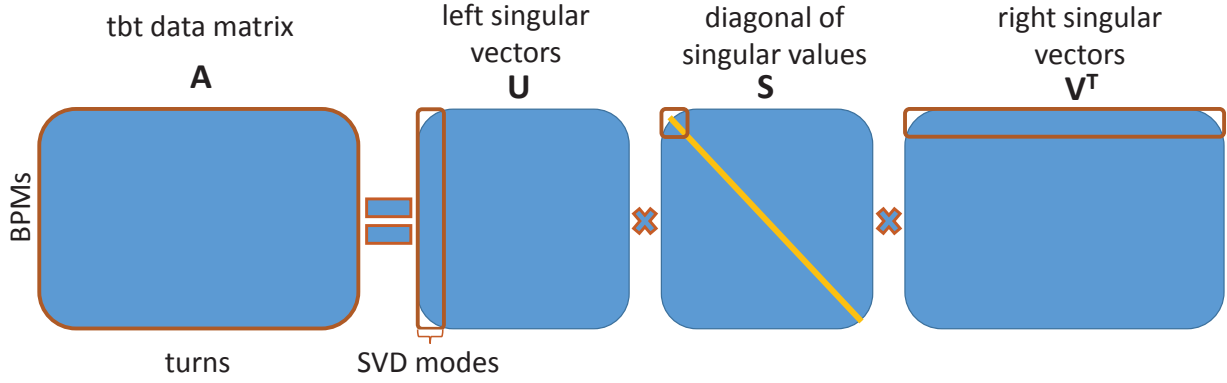


Figure 1: Sketch of the TbT data recomposition for noise floor removal. The decomposition of raw TbT data (in blue) gives full matrices, which are then reduced, as only several largest singular values are kept for the clean TbT data recomposition (in brown edges).

HARMONIC ANALYSIS OF DECOMPOSED DATA

As SVD and refined harmonic analysis are both linear operations, they can be combined. The cleaned TbT data (Equation (2)) can be reconstructed from SVD matrices elements:

$$x_{jn} = \sum_{l=0}^{N_{modes}-1} u_{jl} s_{ll} v_{nl}, \quad (5)$$

where j is the BPM number. The complex coefficients corresponding to an arbitrary frequency a/N are given by:

$$X_{ja} = \sum_{n=0}^{N-1} \sum_{l=0}^{N_{modes}-1} u_{jl} s_{ll} v_{nl} e^{i2\pi na/N} = \quad (6)$$

$$= \sum_{l=0}^{N_{modes}-1} u_{jl} \sum_{n=0}^{N-1} s_{ll} v_{nl} e^{i2\pi na/N}, \quad (7)$$

second summation represents the complex coefficient corresponding to frequency a/N in a l^{th} row of SV^T .

Putting all this together, we obtain complex coefficients corresponding to frequency a/N in cleaned TbT data from all BPMs as a linear combination of complex coefficients corresponding to the same frequency in the rows of SV^T with the multiplication factor being the rows of U . In order to measure the frequencies, two algorithms were developed, performing harmonic analysis on:

- the sum $\sum_{l=0}^{N_{modes}-1} s_{ll} v_{nl}$ of the rows of reduced SV^T giving a single set of frequencies, hereafter referred to as "fast" method
- each of the rows of reduced SV^T , giving a union of frequencies, found for every row, hereafter referred to as "svd" method

The complex coefficients, corresponding to such sets of frequencies, are calculated for each of the rows of reduced SV^T matrix by the inner product in time domain (last sum in Equation (7)). At this point the vectors in frequency domain are no longer orthogonal. The perturbation of the

orthogonality of the two vectors (in frequency domain) is influenced by two factors:

- the difference (in the time domain) between the vector under study and the vector the harmonic analysis was performed on
- the spectral response of a windowing function, that can be used to filter the signal in time domain

A rectangular window, which does not change the signal and has the best frequency resolution, is used in the following. On the other hand, the rectangular window has larger spectral response in other frequencies compared to other windowing functions [9], which should be kept in mind.

ACCURACY

The accuracy of the harmonic analysis performed on decomposed TbT data is studied in this section. TbT data matching the LHC lattice injection optics was simulated along with the betatron resonances of known frequency, phase and amplitude. Realistic noise of about 8 % amplitude compared to coherent betatron motion at focusing quadrupoles was added. Results of the afore-mentioned analysis corresponding to a given spectral line consist of its frequency $\in (0, 1)$, initial phase in units of 2π and its amplitude. The accuracy is estimated by the root mean square of the difference to the value defined in a simulation in a set of all BPMs. The two methods ("svd" and "fast") are compared to the original harmonic analysis the "bpm" method. The betatron tune is found in the spectra from all three methods. Accuracies of the frequency and phase of the found betatron tunes as a function of number of turns are shown in Figures 2 and 3.

Both "svd" and "fast" methods have comparable accuracy or slightly better accuracy in frequency and phase compared to the "bpm" method. An exception is the "svd" analysis performed on a low number of turns, where it shows less accurate results. The differences in relative amplitude accuracy are not shown as they are negligible. Generally, "svd" and "fast" methods seem to be better suited for larger number

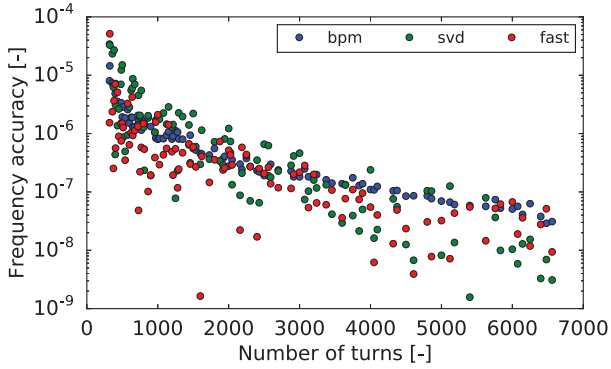


Figure 2: Accuracy of the betatron tune (the strongest spectral line) frequency as a function of number of turns.

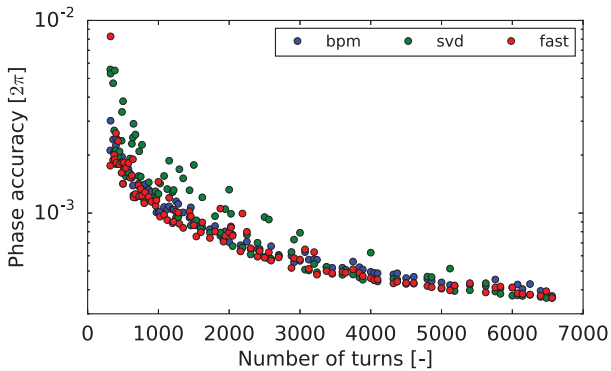


Figure 3: Accuracy of the betatron tune (the strongest spectral line) phase as a function of number of turns.

of turns and larger noise levels. For small number of turns or small noise levels, the situation is opposite. Additionally, a weaker spectral line with about 14 % amplitude at focusing BPMs and 0.01 away in frequency from the betatron tune was investigated. Here, the methods perform all similarly in terms of frequency accuracy, as shown in Figure 4. In terms of its phase accuracy, shown in Figure 5, the "bpm" method is better than the other two. The amplitude accuracy shows similar behaviour as the phase accuracy.

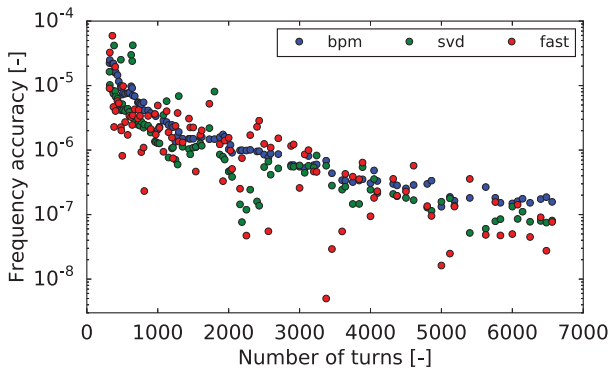


Figure 4: Frequency accuracy of weaker spectral line as a function of number of turns.

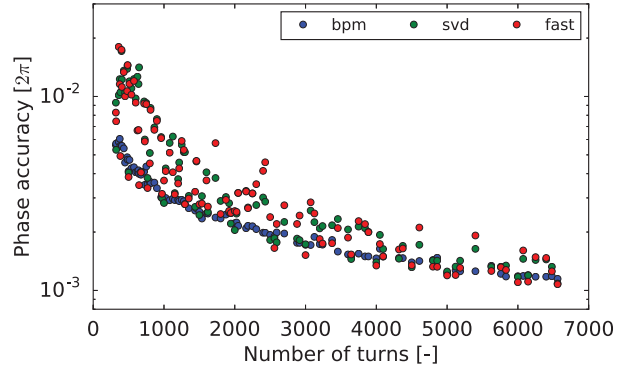


Figure 5: Phase accuracy of weaker spectral line as a function of number of turns.

SPEED UP

Harmonic analysis performed on decomposed TbT BPM data is faster by up to a factor of N_{BPM}/N_{modes} using the "svd" method and up to a factor of N_{BPM} in the "fast" method. Harmonic analysis by "fast" method of one set of LHC TbT BPM data takes about 2 seconds in a single thread compared to about 18 seconds in 32 threads in the "bpm" method.

CONCLUSIONS AND OUTLOOK

New techniques combining data cleaning together with harmonic analysis have been developed. Their usage results in a speed up by factor about 300 in the LHC. This is possible by analysing decomposed data directly instead of the recomposed data. The analysis is comparably or more accurate in terms of frequency. However currently, it is less accurate in terms of phase and amplitude of smaller spectral lines. This can be potentially overcome by the choice of a windowing function, addressing the orthogonality perturbation, which will be studied. It needs to be stressed, that both new algorithms are better suited for noisy data, compared to standard method.

REFERENCES

- [1] R. Tomás, M. Aiba, A. Franchi, and U. Iriso, "Review of linear optics measurement and correction for charged particle accelerators", *Phys. Rev. Accel. Beams*, vol. 20, p. 054801, 2017.
- [2] R. Bartolini and F. Schmidt, "A Computer Code for Frequency Analysis of Non-Linear Betatron Motion", CERN, Geneva, Switzerland, Rep. CERN-SL-NOTE-98-017-AP, 1998.
- [3] T. Bach and R. Tomás, "Improvements for Optics Measurements and Corrections Software", CERN, Geneva, Switzerland, Rep. CERN-ACC-NOTE-2013-0010, 2013.
- [4] J. Irwin et al., "Model-Independent Beam Dynamics Analysis", *Phys. Rev. Letters* Vol. 82, p. 1684, 1999.
- [5] R. Calaga and R. Tomás, "Statistical Analysis of RHIC beam position monitors performance", *Phys. Rev. ST Accel. Beams*, vol. 7, p. 042801, 2004.

- [6] X. Huang, S. Y. Lee, E. Prebys and R. Tomlin, "Application of independent component analysis to Fermilab Booster", *Phys. Rev. ST Accel. Beams*, vol. 8, p. 064001, 2005.
- [7] Ç. Candan, "A method For Fine Resolution Frequency Estimation From Three DFT Samples", *IEEE Signal Process. Lett.*, vol. 18, p. 351-354, 2011.
- [8] J. Laskar, "Frequency analysis for multi-dimensional systems. Global dynamics and diffusion", *Physica D* vol. 67, p. 257-281, 1993.
- [9] G. Heinzel, A. Rüdiger and R. Schilling, "Spectrum and spectral density estimation by the Discrete Fourier transform (DFT), including a comprehensive list of window functions and some new flat-top windows", 2002, <http://edoc.mpg.de/395068>